DISSERTATION

NUMERICAL MODELING OF RESERVOIR SEDIMENTATION AND FLUSHING

PROCESSES

Submitted by

Jungkyu Ahn

Department of Civil and Environmental Engineering

In partial fulfillment of the requirements

For the Degree of Doctor of Philosophy

Colorado State University

Fort Collins, Colorado

Fall 2011

Doctoral Committee:

Advisor: Chih Ted Yang

Pierre Y. Julien
Christopher I. Thornton
Ellen E. Wohl

ABSTRACT

NUMERICAL MODELING OF RESERVOIR SEDIMENTATION AND FLUSHING

PROCESSES

As rivers flow into reservoirs, part of the transported sediment will be deposited. Sedimentation in the reservoir may significantly reduce reservoir storage capacity. Reservoir capacity can be recovered by removing deposited sediment by dredging or flushing. Generally speaking, the latter is preferable to the former. An accurate estimation sedimentation volume and its removal are required for the development of a long term operation plan in the design stage.

One-dimensional, 1D, models are more suitable for a long term simulation of channel cross section change of a long study reach than two or three dimensional models. A 1D model, GSTARS3, was considered, because this study focuses on sedimentation and flushing in the entire reservoir over several years and GSTARS3 can predict channel geometry in a semi-two dimensional manner by using the stream tube concept. However, like all 1D numerical models, GSTARS3 is based on some simplified assumptions.

One of the major assumptions made for GSTARS3 is steady or quasi-steady flow condition, which is valid for most reservoir operation. If there is no significant flow change in a reservoir, such as rapid water surface drop during flushing, steady model can be applied. However, unsteady effect due to the flushing may not be ignored and should be considered for the numerical modeling of flushing processes. Not only flow characteristics but also properties of bed materials in reservoir regime may be different from those in a river regime. Both reservoir and river regimes should be considered for a drawdown flushing study. Flow in the upper part of a reservoir may become river flow during a drawdown flushing operation. A new model, GSTARS4 (Yang and Ahn, 2011) was developed for reservoir sedimentation and flushing simulations in this study. It has the capabilities of simulating unsteady flow and coexistence of river and reservoir regimes in the study area.

GSTARS4 was applied to the Xiaolangdi Reservoir, located on the main stream of the Yellow River. The sediment concentration in the reservoir is very high, 10 ~ 100 kg/m^3 for common operation and 100 ~ 300 kg/m^3 for flushing operation, with very fine materials about 20 ~ 70 % of clay. Stability criteria for computing sediment transport and channel geometric changes by using GSTARS4 model was derived and verified for the Xiaolangdi Reservoir sedimentation and flushing computations.

Han's (1980) non-equilibrium sediment transport equation and the modified unit stream power equation for hyper-concentrated sediment flows by Yang et al. (1996) were used. Both unsteady and quasi-steady simulations were conducted for 3.5 years with calibrated site-specific coefficients of the Xiaolangdi Reservoir. The computed thalweg elevation, channel cross section, bed material size, volume of reservoir sedimentation,

and gradation of flushed sediments were compared with the measured results. The unsteady computation results are closer to the measurements than those of the steady flow simulation results.

ACKNOWLEDGEMENTS

I would like to express my gratitude to Dr. Chih Ted Yang who supported my Ph.D. study and provided me with valuable suggestions and guidance to improve my understanding of sediment transport theories and engineering. His advices not only improved my academic development but also guided me to become a better engineer. It is a great honor for me to be his student. I also wish to acknowledge the contributions of my committee members, Dr. Pierre Julien, Dr. Christopher Thornton, and Dr. Ellen Wohl for their advices to complete my course work and dissertation.

I wish to express my appreciation to fellow civil engineering students at CSU who encouraged me during my studies. I am grateful to CSU faculty members who provided the needed academic background in classes.

I am grateful to my parents for their support and encouragement of my Ph.D. studies.

TABLE OF CONTENTS

LIST OF TABLES

LIST OF FIGURES

LIST OF SYMBOLS

A = cross section area,

A_d = ineffective cross sectional area,

b = a site-specific coefficient for the determination of relationship between discharge and sediment in transport,

$C_{1,k}$ = incoming sediment of the kth sediment size group from the upstream,

c_{es} = computational kinematic wave speed of bed changes with steady flow simulation,

c_{eu} = computational kinematic wave speed of bed changes with unsteady flow simulation,

c_k = kinematic wave speed of bed changes,

C_i = concentration of sediment in transportation at cross section i,

C_m = sediment concentration at the mouth of a tributary,

C_t = total sediment concentration,

$C_{t,i}$ = sediment transport capacity at cross section i,

C_v = suspended sediment concentration by volume, including wash load,

d = sediment particle diameter,

d_{50} = mean bed material size,

$d_{50,c}$ = computed mean bed material size,

$d_{50,m}$ = measured mean bed material size,

d_k = geometric mean diameter of sediment size group k,

$\overline{F}_e$ and $\overline{F}_w$ = variables to determine change of velocity head gradient,

Fr = Froude number,

g = gravitational acceleration,

H = elevation of the energy line above the datum,

h = water surface elevation,

h_m = tributary mouth bed elevation,

i = cross section index,

j = time index,

J = total number of data set,

K = total number of size fractions,

$\overline{K}_i$ = conveyance (m^3/s) at cross section i,

k = size fraction index,

n = Manning's roughness coefficient,

$\overline{Q}_i$ = time weighted discharges,

Q_s = volumetric sediment discharge,

$Q_{s,i}$ = sediment transport rate at cross section i,

$Q_{s,i,k}$ = computed volumetric sediment discharge for size k at cross section i,

q = discharge of flow per unit width,

q_{lat} = lateral inflow per unit length of channel,

q_{sl} = lateral sediment inflow,

S_f = friction slope,

T = the flow top width,

t = time,

t_j = time step j,

U^* = shear velocity,

V = flow velocity,

v_1 and v_2 = coefficients for the determination of volume of a tributary,

Vol = volume of water in a tributary,

$V_{R,c}$ = computed volume of sedimentation,

$V_{R,m}$ = measured volume of sedimentation,

VS = unit stream power,

x = length along the flow direction,

y = water depth,

z = bed elevation,

z_c = computed bed elevations,

z_m = measured bed elevations in meter,

α = recovery factor,

α_d = recovery factor for deposition,

α_k = recovery factor of sediment size group k,

α_s = recovery factor for scour,

γ_s = specific weights of sediment,

γ_m = specific weights of sediment-laden flow,

ΔQ = water discharge from a tributary to the reservoir,

ΔQ_s = sediment load from or into a tributary,

Δt = time step interval,

ΔVol = change of tributary volume due to the change of reservoir elevation in a time step,

Δx = distance between cross section,

Δx_i = distance between cross section i and $i+1$,

Δx_{river} = distance between cross sections for the river reach,

$\Delta x_{reservoir}$ = distance between cross sections for the reservoir reach,

Δz = change in bed elevation (positive for aggradation, negative for scour),

δ_i, φ_i, and σ_i = coefficients for the determination of flow area,

ε and ζ = coefficients for the determination of recovery factor,

η = volume of sediment in a unit bed layer volume (one minus porosity),

$\eta_{i,k}$ = volume of sediment in a unit bed layer for size k at cross section i,

κ = coefficient for the determination of Manning's n,

λ = velocity distribution coefficient,

ν = kinematic viscosity of clear water,

ν_m = kinematic viscosity in a sediment-laden flow,

Φ_1, Φ_2, and Φ_3 = weighting factors that must satisfy $\Phi_1 + \Phi_2 + \Phi_3 = 1$,

θ = a weight factor,

ρ = specific density of clear water,

ρ_m = specific density of sediment laden flow,

ρ_s = specific density of sediment particles,

ω = sediment particle fall velocities in clear water,

ω_k = fall velocity of sediment size k, and

ω_m = particle fall velocity in a sediment-laden flow.

CHAPTER 1. INTRODUCTION

1.1 Overview

The construction of dams and reservoirs can provide flood control, water supply, recreation, and navigation benefits. One of the significant changes on a river caused by a dam is the sedimentation in the reservoir. Reservoir sedimentation reduces its storage capacity and may have upstream and downstream impacts on a river. Therefore, sedimentation in a reservoir should be considered not only in the design phase but also in its operation phase. Sedimentation in reservoirs reduces water storage, flood control, and water supply capacities. The storage can be restored by several methods. The removal of sediment deposition can be done by dredging or by water flow flushing. In most cases flushing causes less adverse impacts on the disposal of the sediment. The sedimentation and sediment flushing in the Xiaolangdi Reservoir, where drawdown flushing was conducted every year, were used in this study.

1.2 General Description of Xiaolangdi Reservoir

Xiaolangdi Dam is located 40km north of Loyang, in Henan Province, China and is 128.42 km downstream of the Sanmenxia Dam on the main stem of the Yellow River. It

is a rock fill dam with inclined core. Its construction began in 1994 and was completed in 2000. The maximum height of the dam is 160 m and the crest length is 1667 m. Figs. 1.1 (a) and (b) show the layout at the dam site. Total storage of the Xiaolangdi Reservoir is about 13 billion m^3. The drainage basin area is about 7.0×10^5 km^2, and average flow at the dam site is 1.3×10^3 m^3/s. Sediment concentration in the reservoir is very high, 10 ~ 100 kg/m^3 for common operation and up to 100 ~ 300 kg/m^3 during some flushing operations. The bed material and sediment input from the upstream of the reservoir are very fine with about 20 ~ 70 % clay. The average annual sediment passage is 1.4×10^9 m^3. Sediment deposition in the Xiaolangdi Reservoir is controlled by drawdown flushing through three low-level outlets, usually between May and September each year. The flushing operation is shown in Fig. 1.1 (b).

There are more than 40 tributaries flowing into the Xiaolangdi Reservoir. Fig. 1.2 is the plan view of the Xiaolangdi Reservoir and 12 major tributaries with the approximate location of the "imaginary" tributary to account for the volume of all the smaller tributaries.

The study area is between Xiaolangdi Dam and Sanmenxia Dam which is located at about 120 km upstream. Sediment deposition in the Sanmenxia Reservoir is controlled by drawdown flushing. The incoming water and sediment from the upstream boundary of the study area is equal to those discharged from the upstream Sanmenxia Reservoir. Therefore, water and sediment input from flushing operation of the Sanmenxia Reservoir should be considered in this study.

(a) Common operation (no flushing)

(b) Flushing operation

Figure 1.1 Xiaolangdi Dam (Yellow River Conservancy Press, 2004)
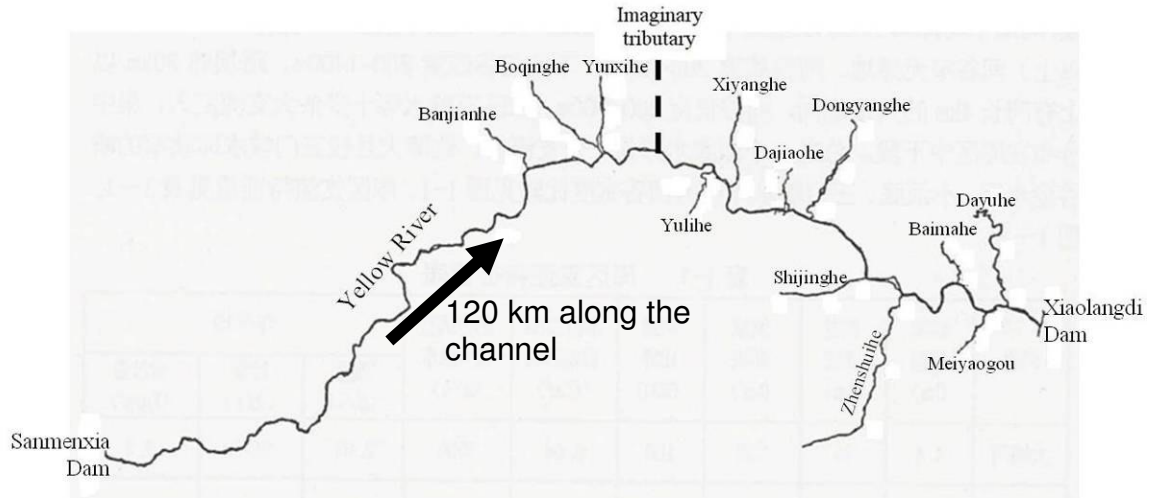
Figure 1.2 Plan views of the Xiaolangdi Reservoir and tributaries

1.3 Objectives

Evaluation of reservoir sedimentation and flushing processes are required for the development of an operation plan. Numerical modeling is considered for this study, which focuses on an entire reservoir over several years. The main objectives of this study are:

1) Development of a numerical model applicable to reservoir sedimentation and flushing processes.

2) Derivation of stability criteria for computing channel geometric change by using the new model and determination of time step and distance between cross sections for the simulation of the Xiaolangdi Reservoir sedimentation and flushing process.

3) Analysis of field data from the Xiaolangdi Reservoir to build input data for the numerical model and calibration of site-specific coefficients of the Xiaolangdi Reservoir.

4) Verification of the new model by comparisons between computed and field measurements of thalweg elevation, cross section geometry, bed material size, volume of sedimentation, and gradation of flushed sediments.

1.4 Study Methodology

Scour, transportation, and deposition of sediments are complicated processes. Mathematical equations for reservoir sedimentation have been derived based on simplified assumptions or empirical relationships. Numerical models are used to solve these equations. If the flow and sedimentation conditions in a reservoir are not far from those assumed in a numerical model, the numerical model may be applicable. For most reservoirs, some simplified assumption and empirical relationships are used. However, under complicated flow conditions, such as drawdown flushing with high sediment concentration, some commonly used assumptions may not be valid. If a numerical model is based on steady flow assumption, the model may not be applicable for flushing studies because sediment flushing is usually done by highly unsteady water surface drop for drawdown flushing.

In most cases, sediment concentration is not high enough to change physical properties of water, such as viscosity and density. Sediment transport in rivers is treated as sediment

transport in clear water. However, in the case of high concentration of fine materials, such as those in the Yellow River, more complex special considerations must be made. Therefore, sedimentation studies for sediment-laden reservoirs or rivers must be carried out carefully considering high sediment concentration flow mechanism. Yang et al. (1996) modified Yang's 1979 unit stream power formula for high-concentration sediment laden flow in the Yellow river. Yang's modified formula will be used in this study.

Simões and Yang (2006), Yang and Simões (2008) and Simões and Yang (2008) have shown that the Generalized Sediment Transport model for Alluvial River Simulation ver. 3.0 (GSTARS3) is suitable for most reservoir scouring and silting studies. GSTARS3 not only can simulate but can also predict morphologic changes of rivers and reservoirs based on the stream tube concept and the application of minimum stream power theory (Yang and Song, 1979). However, some of the simplified assumptions in GSTARS3 should be modified before they can be applied to reservoir sedimentation and drawdown flushing studies. A new model, GSTARS4, Generalizes Sediment Transport model for Alluvial River Simulation ver. 4.0 (Yang and Ahn, 2011), was developed. GSTARS4 is a truly unsteady model, while GSTARS3 is a quasi-steady flow model. The numerical scheme for GSTARS4 model is based on Sedimentation and River Hydraulics – One-dimension (SRH-1D), (Huang and Greimann, 2007). SRH-1D unsteady flow computational scheme was revised and used for GSTARS4.

Some other revisions were also made for GSTARS4 sediment transport and channel geometric adjustment routing modules.

For most cases, the rate of sediment transport or channel geometric change is not as significant as that in the Yellow River. For simulations of channel change, time steps of 1 ~ 24 hours, and distances between cross sections of 100 ~ 1000 m, are typical for river or reservoir sedimentation studies. However, typical time step and distance between cross sections used for most reservoirs may lead to numerical instability in this study, because the rate of sediment transport and channel bed change in the Yellow River and the Xiaolangdi Reservoir are very high. In this study, stability criteria for the channel geometric change were derived and applied for the determination of proper time step and distance between cross sections for the Xiaolangdi Reservoir sedimentation and flushing studies.

Field measurements were analyzed. Water surface elevation at the Xiaolangdi Dam and incoming water from Sanmenxia Reservoir were used as downstream and upstream boundary conditions, respectively. However, some of required data for the simulation, such as water temperature and density of bed material, were missing, and assumptions were made.

Thalweg elevation, channel geometry, size distribution of bed materials, volume of sedimentation, and gradation of flushed sediment were measured several times between May 2003 and October 2006. Both unsteady and steady flow simulations using GSTARS4 were conducted for 3.5 years and the results were compared with surveyed results. The goodness-of-fit between computed, for steady and unsteady simulations, and surveyed results was evaluated by statistical parameters in this study.

CHAPTER 2. LITERATURE REVIEW

Walling (1984) summarized regional sedimentation rates world wide. Chinese reservoirs have an average of 22 years of estimated reservoir half-life expectancy, which is the shortest in the world. The average half-life for North America and Europe is more than 250 years. Compared to North American and European reservoirs, Chinese reservoirs have a very short life expectancy due to high sediment concentration such as that in the Yellow River. Prediction of sedimentation and operation for sediment management in reservoirs are critical for Chinese reservoirs. This section presents a literature review of reservoir sedimentation and sediment control, focusing on drawdown flushing and numerical models.

2.1 General Reservoir Sedimentation Process

As a natural stream enters a reservoir, the flow depth increases, the flow velocity decreases, and friction slope becomes milder. In other words, unit stream power, VS, decreases in a reservoir. This reduces the sediment transport capacity and causes siltation to form a delta, as shown in Fig. 2.1. Sediment carried into a reservoir will be deposited, causing bed aggradation and reduction of storage. The deposition generally begins with delta formation near the reservoir headwater area. Morris and Fan (1997) divided the sediment deposition into three zones; topset, foreset, and bottomset, as shown in Fig. 2.1.

The topset of the delta consists of relatively coarse materials, while the bottomset is formed with finer materials. Aggradation in the upstream channel may occur over a long distance above the reservoir. Fan and Morris (1992a) noted the following basic characteristics of reservoir deltas:

1. There is an abrupt change between the slope of the topset and foreset deposits.

2. Sediment particles on the topset bed are coarser than those on the foreset bed, and there is an abrupt change in particle diameter between topset and foreset deposits.

3. The elevation of the transition zone from the topset to the foreset bed depends on the reservoir operating rule and pool elevation.
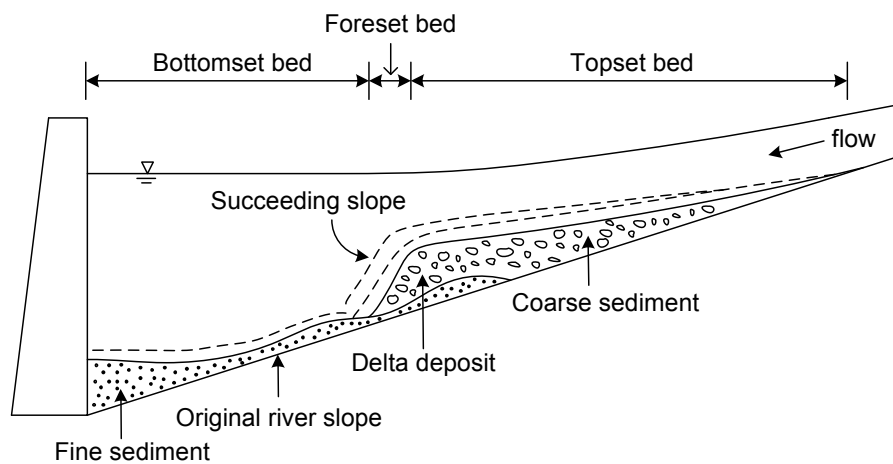
Figure 2.1 Typical formation of delta in a reservoir (Morris and Fan, 1997)

Reservoir sedimentation processes vary with complex conditions over the entire basin such as watershed sediment production, rate of sediment transport, flood frequency, geometry of river, sediment properties, land use, dam operation and so forth. Morris and Fan (1997) classified reservoir sedimentation into four general types, as shown in Fig. 2.2.

9
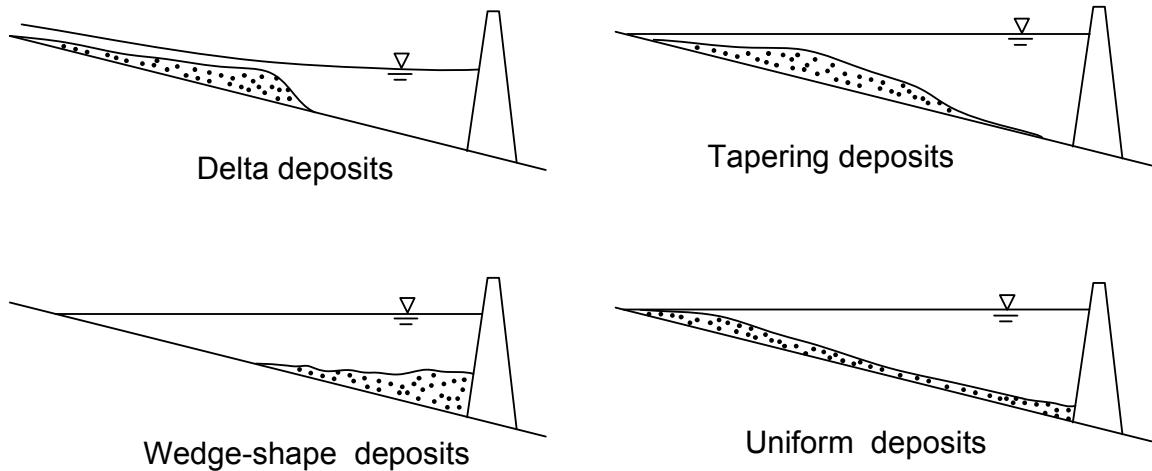
Figure 2.2 Basic type of deposition (Morris and Fan, 1997)

2.2 Reservoir Sedimentation Control Methods

Three strategies can be used to control reservoir sedimentation (Fan and Morris, 1992b).

First, the sediment delivered from the basin can be reduced by erosion control or upstream traps. This strategy may reduce long term sediment input. However, it cannot be the solution for already reduced reservoir storage.

Second, dredging can recover the reservoir storage. However, this is not practical, due to high cost and the environmental consequences.

Third, sediment can be removed by the water flow, a hydraulic method. Fan and Morris (1992b) classified hydraulic methods used in China to manage reservoir sediment deposition as:

1. Sediment routing during floods.

2. Venting density current.

3. Emptying and flushing.

4. Drawdown flushing.

Sediment flushing reduces the hydraulic detention time of high sediment concentration in reservoirs. In northern China, 80 ~ 90 % of the annual sediment load carried by rivers is discharged in July and August, whereas 25 ~ 50 % of the annual runoff occurs in the same period (Fan and Morris, 1992b). In summer seasons, an increase of discharge from the reservoirs may reduce the detention time and deposition rate. White (2001) differentiated flushing from sluicing. Flushing is scouring deposited sediments and passing the sediment laden flow through the dam, while sluicing is passing sediment laden water through the reservoir during the flood and it is applicable to silt and clay.

Venting a density current can discharge muddy flow carried by the density current through low level outlets. This method has been applied to the Sanmenxia Reservoir with 18 ~ 36 % venting efficiency, which is the ratio between in and outflow of silt during a flood (Fan, 1986).

Emptying and flushing should be used when deposition and erosion cannot be balanced by flushing. This method has been useful with small reservoirs (Fan and Morris, 1992b).

The drawdown flushing method scours sediment deposition by dropping water surface elevation to increase flushing efficiency. Flushing can be done with a full drawdown of the reservoir or with an partial drawdown of the water level. With respect to water surface elevation, White (2001) presented three stages of flushing, as shown in Fig. 2.3. Mahmood (1987), White and Bettess (1984) and Atkinson (1996) stated that reservoir water level should be close to the bed elevation to maximize the flushing efficiency, but partial drawdown can still increases flow velocities at the head water area where the reservoir delta has formed. In the case of partial drawdown or no drawdown, high flow velocities at the outlets are localized. Partial drawdown has been conducted for the

11

Xiaolangdi Reservoir. Significant scour of the reservoir delta at the head water area and localized scour pattern near the low level outlet were observed in the Xiaolangdi Reservoir.
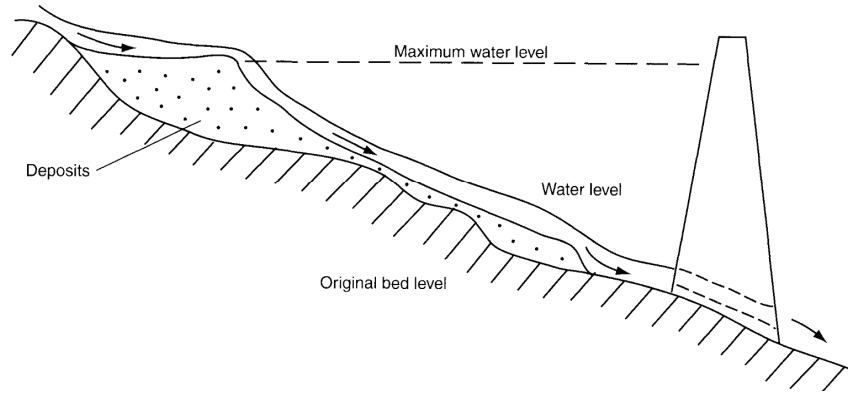
(a) Flushing with full drawdown
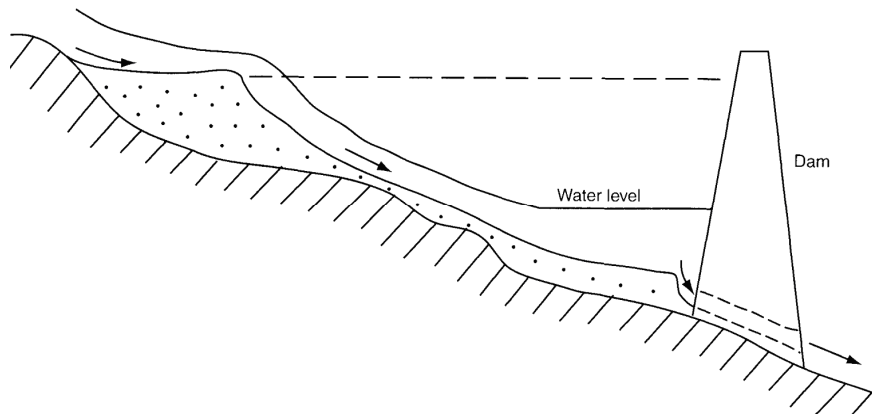
(b) Flushing with intermediate drawdown
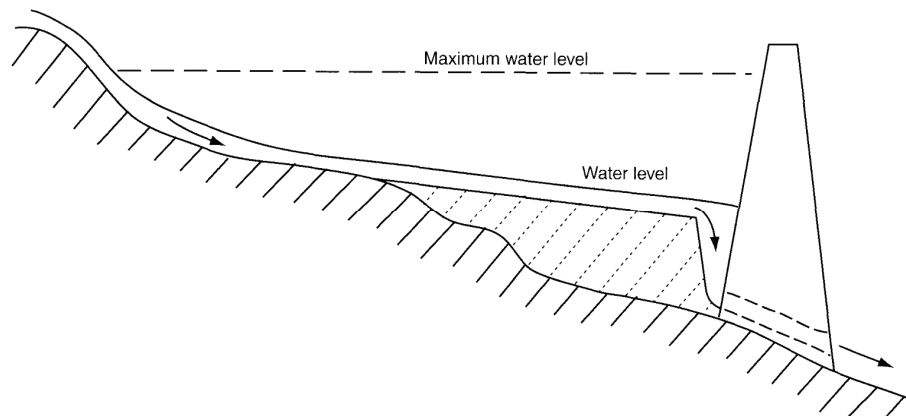
(c) Final condition after a long period of flushing with intermediate drawdown

Figure 2.3 Longitudinal bed profile of reservoir during flushing

Fig 2.4 shows the progress of retrogressive erosion (Morris and Fan, 1997). It shows a zone of high slope and rapid erosion, moving upstream along a channel and having a lower slope and erosion rate. The maximum erosion rate occurs along the steep slope at the downstream end of the reservoir delta, causing the maximum erosion area to migrate upstream through a head cutting process.
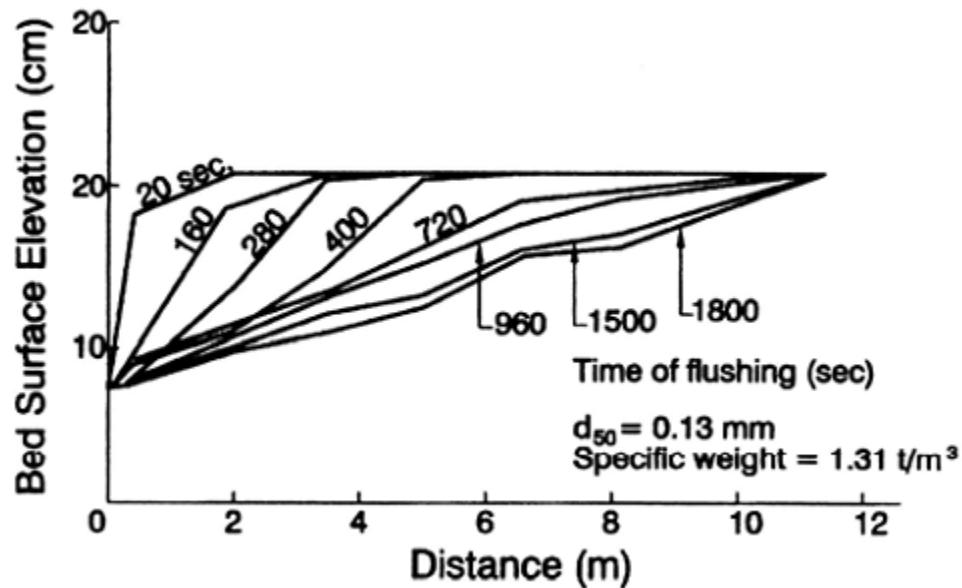
Figure 2.4 Longitudinal profile of retrogressive erosion from flume tests

(Morris and Fan, 1997)

2.3 Previous Studies of Reservoir Sedimentation and Flushing

Julien (1998) showed some field measurements of the Tarbela Reservoir in Pakistan. The life expectancy of that reservoir is about 100 years. Yang and Simões (2002) used GSTARS3 model to compute the Tarbela Reservoir geometric change over 21 years, from 1975 to 1996. The simulated bed profile using GSTARS3 is in good agreement with the measured profile. White (2001) did a similar numerical model study of sedimentation in the Tarbela Reservoir. His model predicted more deposition than the measurement.

Yang and Marsooli (2010) applied GSTARS3 to sedimentation studies of the Ekbatan Reservoir and Kardeh Reservoir in Iran. The computed bed profiles with calibrated coefficients are generally in good agreement with the measurements.

Chang et al. (1996) evaluated the efficiency of sediment-pass-through for low level outlets in reservoirs on the North Fork Feather River using Fluvial-12 (Chang, 1988). The Fluvial-12 simulation indicated that the sediment-pass-through operation is feasible to maintain sediment equilibrium for the river/reservoir system, and sediment released from the reservoir would not have adverse impacts on fish habitat in the river.

Morris and Hu (1992) simulated sediment flushing in the Loíza Reservoir in Puerto Rico using a one-dimensional model HEC-6 (U.S Army, 1991). The reservoir was assumed as one-dimensional, because the lateral variation of the channel was not significant.

Flushing with intermediate water surface drawdown has been conducted for the Jensanpei Reservoir (Hwang, 1985). The storage capacity was reduced due to sedimentation in the first 15 years of operation. After 15 years of operation, flushing with intermediate water surface drawdown was conducted once a year, and no further reduction of storage capacity was observed. The operation rule in a year consists of flushing, refilling, and deliveries from the storage. With respect to the reservoir operation, water surface changes are shown in Fig. 2.5. The operation rule applied in the Jensanpei Reservoir is similar to that of the Xiaolangdi Reservoir.
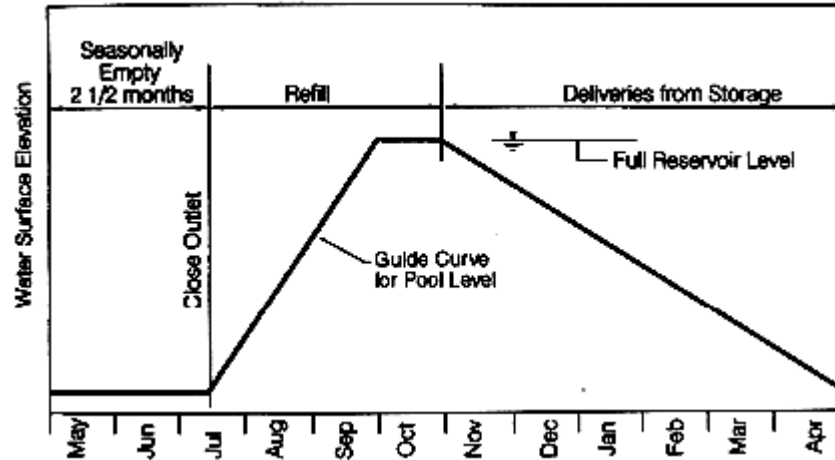
Figure 2.5 Operation rule in Jensanpei Reservoir (Hwang, 1985)

White (2001) summarized 22 case studies of flushing based on field measurements. Most of them were successful, but some of them were not successful due to downstream constraints. Morris and Fan (1997) indicated some limitations of flushing. First, there should be sufficient water to be used for flushing. Second, flushing causes a sudden release of higher sediment concentration than occurs naturally in the river. High sediment concentration may create unacceptable downstream impacts, such as clogging of channel due to deposition and damaging fish habitat.

2.4 Numerical Modeling (1D, 2D, and 3D)

Numerical models are classified as one-dimensional (1D), two-dimensional (2D), and three-dimensional (3D) models. Most numerical modeling uses a 1D model, which is more robust than 2D and 3D models (Morris and Fan 1997). White (2001), and Molinas and Yang (1986) noted that a 1D model is suitable for long-term simulation of reservoir sedimentation, while 2D or 3D models require much more field data for calibration. Complicated 2D and 3D models can be used to assess localized impact of flushing near a

low level outlet. Generally speaking, a 1D model is suitable for long-term simulation of a long reach of river or reservoir with elongated channel geometry. 1D model requires the least amount of data for calibration and verification and their numerical solutions are relatively simple and stable. 2D or 3D models are suitable for short-term simulations of localized phenomena of a short reach of a river or reservoir. 2D or 3D models require large amounts of data for calibration and verification, and their numerical solutions are complex. Yang (2010) suggested that a quasai-2D model for hydraulic simulation and prediction and a qusai-3D simulation and prediction of channel geometry and profile adjustment is more suitable for long-term simulation and prediction of morphologic changes of a long reach of a river and reservoir with limited field data for engineering purposes.

2.5 Previous Numerical Models

Most commonly used numerical sediment transport models were originally developed for movable bed rivers (Morris and Fan 1997). Two numerical models are considered in this study.

GSTARS3 is a numerical model for simulating the flow of water and sediment transport in alluvial rivers and reservoirs. GSTARS3 was developed as a generalized water and sediment-routing computer model that could be used to solve river and reservoir sedimentation engineering problems. It has the capability of computing not only water surface profiles in the subcritical, supercritical, and mixed flow regimes, but also sediment movement in longitudinal and lateral directions. One important feature of the

16

GSTARS3 model is the use of the stream tube concept for sediment routing computations. The adoption of this concept allows the simulation of lateral movement of sediments. The position and width of each stream tube may change after each time step of computation. The scour or deposition computed in each stream tube gives the variation of channel geometry in the vertical and lateral directions.

GSTAR-1D (Yang et al., 2005) (Generalized Sediment Transport for Alluvial Rivers – One dimension) is a one-dimensional hydraulic and sediment transport model. It is a mobile boundary model with the ability to simulate steady and unsteady flows, internal boundary conditions, and looped river networks. GSTAR-1D has been revised and improved, and the latest version has been named SRH-1D. SRH-1D is more robust than GSTAR-1D for unsteady flow simulation.

GSTAR-1D and its latest version SRH-1D have the capability to simulate unsteady flow conditions. SRH-1D can simulate unsteady flow characteristics more accurately than GSTARS3, which uses quasi-steady approximation. GSTARS3 uses the stream tube concept, which can simulate lateral sediment movement in a semi-two-dimensional manner. SRH-1D is a one-dimensional model. Thus, GSTARS3 is more appropriate for the simulation of semi-two dimensional sediment movement than SRH-1D if the flow is not highly unsteady.

CHAPTER 3. THEORETICAL BACKGROUND OF GSTARS4

All GSTARS models employ an uncoupled approach for flow and sediment routing. This means that flow properties, such as flow velocity and water stages, are computed first, followed by the sediment routing and bed changes. In this type of uncoupled method, it is assumed that the computed hydraulic parameters are fixed during a time step of sediment routing computation. This section explains governing equations and numerical schemes that are used in the GSTARS4 model.

3.1 Hydraulic Computation of GSTARS4

3.1.1 Quasi-steady Flow Computation

GSTARS4 uses the same equation and numerical scheme of GSTARS3 for the computation of steady or quasi-steady flow simulation. The equations shown in this section are also found in the User's Manual of GSTARS3 (Yang and Simões, 2002)

GSTARS4 uses the energy equation to compute the flow in the case of subcritical flow. Although GSTARS4 can handle supercritical flow computations, there is no critical or supercritical flow in the Xiaolangdi Reservoir.
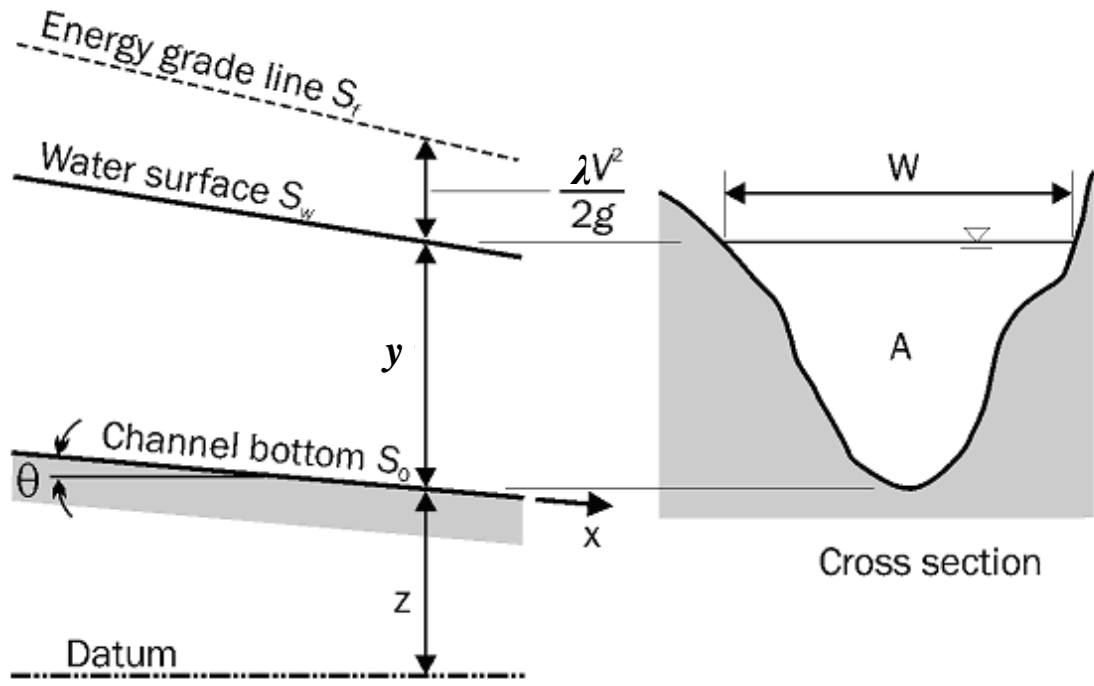
Figure 3.1 Definition of variables (Yang and Simões, 2002)

Using the notation defined in Fig. 3.1, the energy equation is written as

$$z + y + \lambda \frac{V^2}{2g} = H \qquad (3.1)$$

where z = bed elevation; y = water depth; V = flow velocity; λ = velocity distribution coefficient; H = elevation of the energy line above the datum; and g = gravitational acceleration.

The energy equation is solved using the standard step method (Henderson, 1966) for a given duration of time and discharge. For quasi-steady simulation, GSTARS3 and GSTARS4 models assume bursts of constant discharge with finite duration, as shown in Fig. 3.2.
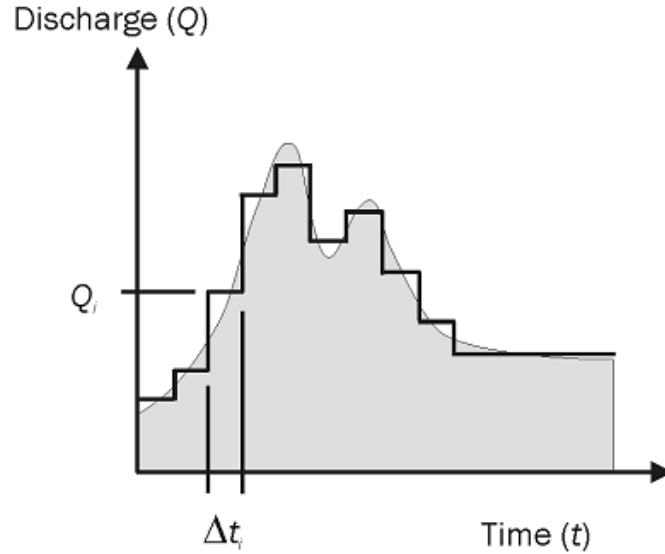
Figure 3.2 Representation of a hydrograph by a series of steps with constant discharge

and finite duration (Yang and Simões, 2002)

3.1.2 Unsteady Flow Computation

GSTARS4 has the capability to simulate unsteady flows. The theoretical background used for the development of GSTARS4 unsteady flow scheme is based on SRH-1D with some revisions. Equations used in this section can also be found in the user's manual of SRH-1D (Huang and Greimann, 2007).

The continuity equation of one-dimensional flow is

$$\frac{\partial (A + A_d)}{\partial t} + \frac{\partial Q}{\partial x} = q_{lat} \tag{3.2}$$

The momentum equation of one-dimensional flow is

$$\frac{\partial Q}{\partial t} + \frac{\partial (\lambda Q^2 / A)}{\partial x} + gA \frac{\partial z}{\partial x} = -gAS_f \tag{3.3}$$

where A = cross section area; A_d = ineffective cross section area; q_{lat} = lateral inflow per unit length of channel; S_f = friction slope; t = time; and x = length along the flow direction.

The discretization of the continuity equation is made with one area point and two discharge points as

$$A_i^j + A_{di}^j - A_i^{j-1} - A_{di}^{j-1} = -\frac{\Delta t}{\Delta x_i}\left(\overline{Q}_{i+1} - \overline{Q}_i\right) \qquad (3.4)$$

where i = cross section index; j = time index; and $\overline{Q}_i$ = time weighted discharges.

Eq. (3.4) can be written with weighting factor θ as

$$\overline{Q}_i = \theta Q_i^j + (1-\theta)Q_i^{j-1} \qquad (3.5)$$

Eq. (3.4) can be written in an iteration form, with m, the iteration number

$$\Delta A_i^m = \varphi_i \Delta Q_i^m + \delta_i \Delta Q_{i+1}^m + \sigma_i \qquad (3.6)$$

where the coefficients are

$$\varphi_i = \frac{\theta \Delta t}{\Delta x_i} \qquad (3.6a)$$

$$\delta_i = -\frac{\theta \Delta t}{\Delta x_i} \qquad (3.6b)$$

$$\sigma_i = -A_i^j - A_{di}^j + A_i^{j-1} + A_{di}^{j-1} + \left(\overline{Q}_i - \overline{Q}_{i+1}\right)\frac{\Delta t}{\Delta x_i} \qquad (3.6c)$$

The discrete form of the momentum equation is made with two area points and three discharge points with a weighting factor θ as

$$Q_i^j - Q_i^{j-1} + \frac{\Delta t}{\Delta x_i}\left(\overline{F}_e - \overline{F}_w\right) = \Delta t g \frac{\overline{A}_i + \overline{A}_{i-1}}{2}\left(\frac{\overline{z}_i + \overline{z}_{i-1}}{\Delta x_i} - \overline{S}_{fi}\right) \qquad (3.7)$$

where $\overline{F}_e = \lambda \dfrac{\left(\overline{Q}_i + \overline{Q}_{i+1}\right)^2}{4\overline{A}_i}$ (3.7a)

$\overline{F}_w = \lambda \dfrac{\left(\overline{Q}_i + \overline{Q}_{i-1}\right)^2}{4\overline{A}_{i-1}}$ (3.7b)

$S_{fi} = \dfrac{4\overline{Q}_i \left|\overline{Q}_i\right|}{\left(\overline{K}_i + \overline{K}_{i-1}\right)^2}$ (3.7c)

where $\overline{K}_i$ = conveyance (m^3/s) at cross section i.

GSTARS4 and SRH-1D provide various options for the treatment of the convective terms and detailed information can be found in the user's manual of SRH-1D (Huang and Greimann, 2007).

Using a weighting factor θ, Eq. (3.7) can be written in iteration form

$$
\begin{aligned}
\Delta Q_i^m + \theta \frac{\Delta t}{\Delta x_i} & \left(\begin{array}{l} \dfrac{\partial \overline{F}_e}{\partial Q_i^j}\Delta Q_i^m + \dfrac{\partial \overline{F}_e}{\partial Q_{i+1}^j}\Delta Q_{i+1}^m + \dfrac{\partial \overline{F}_e}{\partial A_i^j}\Delta A_i^m \\[2mm] -\dfrac{\partial \overline{F}_w}{\partial Q_i^j}\Delta Q_i^m - \dfrac{\partial \overline{F}_w}{\partial Q_{i-1}^j}\Delta Q_{i-1}^m - \dfrac{\partial \overline{F}_e}{\partial A_{i-1}^j}\Delta A_{i-1}^m \end{array} \right) \\[3mm]
& - \theta \Delta t g \frac{\Delta A_i^m + \Delta A_{i-1}^m}{2}\left(\frac{z_{i-1}^{j+1} - z_i^{j+1}}{\Delta x_i} - S_{fi}^{j+1}\right) \\[3mm]
& - \theta \Delta t g \frac{\overline{A}_i + \overline{A}_{i-1}}{2}\left(\begin{array}{l} \dfrac{\Delta A_{i-1}^m}{T_{i-1}^{j+1}\Delta x_i} - \dfrac{\Delta A_i^m}{T_i^{j+1}\Delta x_i} - \dfrac{\partial \overline{S}_{fi}}{\partial A_i^j}\Delta A_i^m \\[2mm] -\dfrac{\partial \overline{S}_{fi}}{\partial A_{i-1}^j}\Delta A_{i-1}^m - \dfrac{\partial \overline{S}_{fi}}{\partial Q_i^j}\Delta Q_i^m \end{array} \right) \\[3mm]
& = -Q_i^j + Q_i^{j-1} - \frac{\Delta t}{\Delta x_i}\left(\overline{F}_e - \overline{F}_w\right) + \Delta t g \frac{\overline{A}_i + \overline{A}_{i-1}}{2}\left(\frac{\overline{z}_{i-1} + \overline{z}_i}{\Delta x_i} - \overline{S}_{fi}\right)
\end{aligned}
$$ (3.8)

Substituting Eq. (3.6) into Eq. (3.8), results in

$a_i \Delta Q_{i-1}^m + b_i \Delta Q_i^m + c_i \Delta Q_{i+1}^m = d_i$ (3.9)

where the coefficients are

$$
\begin{aligned}
a_i &= \theta \frac{\Delta t}{\Delta x_i} \left(-\frac{\partial \overline{F}_w}{\partial Q_{i-1}^j} - \frac{\partial \overline{F}_w}{\partial A_{i-1}^j} \varphi_{i-1} \right) \\
&\quad - \frac{\theta \varphi_{i-1} \Delta t g}{2} \left[\frac{z_{i-1}^{j+1} - z_i^{j+1}}{\Delta x_i} - S_{fi} + \left(\frac{\overline{A}_i + \overline{A}_{i-1}}{2} \right) \left(\frac{1}{T_{i-1}^j \Delta x_i} - \frac{\partial \overline{S}_{fi}}{\partial A_{i-1}^j} \right) \right]
\end{aligned}
\tag{3.9a}
$$

$$
\begin{aligned}
b_i &= 1 + \theta \frac{\Delta t}{\Delta x_i} \left(\frac{\partial \overline{F}_e}{\partial Q_i^j} + \frac{\partial \overline{F}_e}{\partial A_i^j} \varphi_i - \frac{\partial \overline{F}_w}{\partial Q_i^j} - \frac{\partial \overline{F}_w}{\partial A_{i-1}^j} \delta_{i-1} \right) \\
&\quad - \theta \frac{\Delta t g}{2} (\varphi_i + \delta_{i-1}) \left(\frac{z_{i-1}^j - z_i^j}{\Delta x_i} - S_{fi} \right) \\
&\quad - \theta \frac{\Delta t g}{2} \left(\overline{A}_i + \overline{A}_{i-1} \right) \left[\begin{array}{c} \delta_{i-1} \left(\dfrac{1}{T_{i-1}^j \Delta x_i} - \dfrac{\partial \overline{S}_{fi}}{\partial A_{i-1}^j} \right) \\[2mm] + \varphi_i \left(\dfrac{-1}{T_i^j \Delta x_i} - \dfrac{\partial \overline{S}_{fi}}{\partial A_i^j} \right) - \dfrac{\partial \overline{S}_{fi}}{\partial Q_i^j} \end{array} \right]
\end{aligned}
\tag{3.9b}
$$

$$
\begin{aligned}
c_i &= \theta \frac{\Delta t}{\Delta x_i} \left(\frac{\partial \overline{F}_e}{\partial Q_{i+1}^j} + \frac{\partial \overline{F}_e}{\partial A_i^j} \delta \right) \\
&\quad - \theta \frac{\delta_i \Delta t g}{2} \left[\left(\frac{z_{i-1}^j - z_i^j}{\Delta x_i} - S_{fi} \right) + \frac{\overline{A}_i + \overline{A}_{i-1}}{2} \left(\frac{-1}{T_i \Delta x_i} - \frac{\partial S_{fi}}{\partial A_i} \right) \right]
\end{aligned}
\tag{3.9c}
$$

$$
\begin{aligned}
d_i &= Q_i^{j-1} - Q_i^j \\
&\quad + \frac{\Delta t}{\Delta x_i} \left(\overline{F}_w - \overline{F}_e - \theta \sigma_i \frac{\partial \overline{F}_e}{\partial A_i^j} + \theta \sigma_{i-1} \frac{\partial \overline{F}_w}{\partial A_{i-1}^j} \right) \\
&\quad + \frac{\Delta t g}{2} \left(\overline{A}_i + \overline{A}_{i-1} + \theta \sigma_i + \theta \sigma_{i-1} \right) \left(\frac{\overline{z}_{i-1}^j - \overline{z}_i^j}{\Delta x_i} - \overline{S}_{fi} \right) \\
&\quad + \theta \frac{\Delta t g}{2} \left(\overline{A}_i + \overline{A}_{i-1} \right) \left[\sigma_{i-1} \left(\frac{1}{T_{i-1}^j \Delta x_i} - \frac{\partial \overline{S}_{fi}}{\partial A_{i-1}^j} \right) + \sigma_i \left(\frac{1}{T_i^j \Delta x_i} - \frac{\partial \overline{S}_{fi}}{\partial A_i^j} \right) \right]
\end{aligned}
\tag{3.9d}
$$

where T = the flow top width.

For a single channel with $N+1$ cross sections, there are $N+2$ unknowns and N equations from Eqs. (3.9) to (3.9d). The upstream and downstream boundary conditions provide two more equations. Therefore, all unknown variables can be solved.

3.2 Sediment Routing and Channel Adjustment of GSTARS4

GSTARS4 computes the flow either as quasi-steady or unsteady to simulate sediment transport and channel adjustments.

3.2.1 Governing Equation and Numerical Scheme for Channel Adjustment

The basis for sediment routing computation in GSTARS4 is the equation of sediment mass conservation, which is the same as that used in GSTARS3 (Yang and Simões, 2002). GSTARS3 and GSTARS4 also have the same numerical schemes used for the computation of sediment mass conservation.

$$\eta \frac{\partial A_d}{\partial t} + \frac{dQ_s}{dx} = q_{sl} \tag{3.10}$$

where Q_s = volumetric sediment discharge; η = volume of sediment in a unit bed layer volume (one minus porosity); and q_{sl} = lateral sediment inflow.

The first derivative term in Eq. (3.10) is approximated by

$$\frac{\partial A_d}{\partial t} = \frac{(\Phi_1 T_{i-1} + \Phi_2 T_i + \Phi_3 T_{i+1})\Delta z_i}{\Delta t} \tag{3.11}$$

where Δt = time step interval; Δz = change in bed elevation (positive for aggradation, negative for scour); and Φ_1, Φ_2, and Φ_3 = weighting factors that must satisfy $\Phi_1 + \Phi_2 + \Phi_3 = 1$.

There are many possible choices for the values of Φ_1, Φ_2, and Φ_3. $\Phi_1 = \Phi_3 = 0$ and $\Phi_2 = 1$ assumes that the wetted perimeter at station i represents the perimeter for the entire reach. $\Phi_2 = \Phi_3 = 0.5$, and $\Phi_1 = 0$ emphasizes the downstream end of the study reach. The standard values used in GSTARS4 are $\Phi_1 = \Phi_3 = 0.25$, $\Phi_2 = 0.5$, but other combinations can also be used. The choice of different combinations of these parameters reflects a trade-off between accuracy and numerical stability. The other derivative term of Eq. (3.10) is approximated by

$$\frac{dQ_s}{dx} = \frac{Q_{s,i} - Q_{s,i-1}}{(\Delta x_i + \Delta x_{i-1})/2} \tag{3.12}$$

where $\Delta x_i = $ distance between cross section i and $i+1$; and $Q_{s,i} = $ sediment transport rate at cross section i.

Sediment routing is computed for each stream tube in a 1D manner. The bed elevation change in each sediment size fraction within each stream tube is given by

$$\Delta z_{i,k} = \frac{\Delta t}{\eta_{i,k}} \frac{q_{sl}(\Delta x_i + \Delta x_{i-1}) + 2(Q_{s,i-1,k} - Q_{s,i,k})}{(aT_{i-1} + bT_i + cT_{i+1})(\Delta x_i + \Delta x_{i-1})} \tag{3.13}$$

where $k = $ size fraction index; $\eta_{i,k} = $ volume of sediment in a unit bed layer for size k at cross section i; and $Q_{s,i,k} = $ computed volumetric sediment discharge for size k at cross section i.

The total bed elevation change for each stream tube at cross section i is computed taking into account the contributions of all the size fractions, i.e.,

25

$$\Delta z_i = \sum_{k=1}^{K} \Delta z_{i,k}$$

<div align="right">(3.14)</div>

where K = total number of size fractions present in cross section i.

The new channel cross section at station i, to be used at the next time iteration, is determined by adding the bed elevation change to the old bed elevation. The particle size is assumed fully mixed across a given stream tube, but can vary among different stream tubes.

3.2.2 Sediment Transport Equations

The sediment transport capacity for each cross section is calculated by using one of the sediment transport equations shown in Table 3.1.

Table 3.1 Sediment transport equations used for GSTARS3 and GSTARS4

Equation	Type
DuBoys(1879)	Bed Load
Meyer-Peter and Müller(1948)	Bed Load
Laursen(1958)	Bed-Material Load
Laursen modified by Madden(1993)	Bed-Material Load
Toffaleti(1969)	Bed-Material Load
Engelund and Hansen(1972)	Bed-Material Load
Ackers and White(1973)	Bed-Material Load
Yang(1973) + Yang(1984)	Bed-Material Load
Yang(1979) + Yang(1984)	Bed-Material Load
Parker(1990)	Bed Load
Yang et al.(1996) modified	Bed-Material Load
Ashida and Michiue(1972)	Bed-Material Load
Tsinghua University(IRTCES,1985)	Bed-Material Load

In this study, sediment transport capacity was calculated using the Yang et al. (1996) modified unit stream power equation, which is applicable to high sediment concentration flow in the Yellow River.

$$\log C_t = 5.165 - 0.153 \log \frac{\omega_m d}{\nu_m} - 0.297 \log \frac{U^*}{\omega_m}$$
$$+ \left(1.780 - 0.360 \log \frac{\omega_m d}{\nu_m} - 0.480 \log \frac{U^*}{\omega_m} \right) \log \left(\frac{\gamma_m}{\gamma_s - \gamma_m} \frac{VS}{\omega_m} \right)$$

(3.15)

where C_t = total sediment concentration ; ω_m = particle fall velocity in a sediment-laden flow; d = sediment particle diameter; ν_m = kinematic viscosity in a sediment-laden flow; U^* = shear velocity; γ_s and γ_m = specific weights of sediment and sediment-laden flow, respectively; and VS = unit stream power.

Particle fall velocity in the Yellow River can be computed from

$$\omega_m = \omega(1 - C_v)^7$$

(3.16)

where ω = sediment particle fall velocities in clear water; and C_v = suspended sediment concentration by volume, including wash load.

The kinematic viscosity of the sediment-laden Yellow River is

$$\nu_m = \frac{\rho}{\rho_m} e^{5.06 C_v} \nu$$

(3.17)

where ρ and ρ_m = specific densities of clear water and sediment laden flow, respectively; and ν = kinematic viscosity of clear water.

The specific density of sediment laden flow is

$$\rho_m = \rho + (\rho_s - \rho) C_v$$

(3.18)

where ρ_s = specific density of sediment particles.

A unique characteristic of the Yellow River is that when the sediment inflow from upstream is very high, scour instead of deposition may occur. This phenomenon can be explained by the last term of Eq. (3.15). As sediment concentration increases, $(\gamma_s - \gamma_m)$ becomes smaller, so the dimensionless unit stream power for sediment-laden flow, $\dfrac{\gamma_m}{\gamma_s - \gamma_m}\dfrac{VS}{\omega_m}$, becomes very large. Thus, the Yellow River can transport a huge amount of sediment under sediment-laden flow conditions. More details of the theoretical analyses and comparisons with field data from the Yellow River are given in Yang (1996 and 2003).

3.2.3 Non-equilibrium Sediment Transport

It is usually assumed that the bed-material load discharge is equal to the sediment transport capacity of the flow; i.e., the bed-material load is transported in an equilibrium mode. In other words, the exchange of sediment between the bed and sediment in transport is instantaneous. However, there are circumstances in which the spatial-delay and/or time-delay effects are important. For example, reservoir sedimentation processes are essentially non-equilibrium processes. In the laboratory, it has been observed that it may take a significant distance for a clear water inflow to reach its saturation sediment concentration (Yang and Simões, 2002). To model these effects, GSTARS3 and GSTARS4 use the method developed by Han (1980). Using Han's technique, the non-equilibrium sediment transport rate can be computed from

$$C_i = C_{t,i} + \left(C_{i-1} - C_{t,i-1}\right)\exp\left[-\frac{\alpha\omega_m\Delta x}{q}\right] + \left(C_{t,i-1} - C_{t,i}\right)\left[\frac{q}{\alpha\omega_m\Delta x}\right]\left[1 - \exp\left(-\frac{\alpha\omega_m\Delta x}{q}\right)\right] \quad (3.19)$$

where C_i = concentration of sediment in transportation at cross section i; $C_{t,i}$ = sediment transport capacity at cross section i computed from Eq. (3.15) when using Yang et al. (1996) sediment transport formulas; q = discharge of flow per unit width; Δx = distance between cross section; and α = recovery factor.

For coarse particles, the second term and third term on the right hand side of Eq. (3.19) are small or negligible due to relatively fast fall velocities, sediment in transport is close to sediment transport capacity, $C_i \cong C_{t,i}$. On the other hand, when these terms are not negligible for small particles, then the determination of recovery factor becomes critical.

Han and He (1990) recommended an α value of 0.25 for deposition and 1.0 for entrainment. Different recovery factors have been suggested in the literature, either from a theoretical or from a practical point of view, by Zhang (1980), Zhou and Lin (1995), Zhou, et al. (1997), Zhou and Lin (1998), Han (2006), and by Yang and Marsooli (2010). There is no consensus on the best value and a modeler should use under different flow and sediment conditions. None of the recommended values listed above provide reasonable results in the Xiaolangdi Reservoir sedimentation and flushing simulations. Detailed explanations of the recovery factor and its relationship between other flow or sediment properties are described in section 4.2.2.

CHAPTER 4. NEW CAPABILITIES OF GSTARS4

The development of GSTARS4 was divided into two phases. The first phase of development was the inclusion of a fully unsteady flow computation. GSTARS3 uses a quasi-steady flow concept, which assumes that water discharge hydrographs are approximated by bursts of constant discharge as shown in Fig. 3.2. Consequently, GSTARS3 is not intended for truly unsteady flow computations. Thus, the GSTARS3 model may not be accurate for truly unsteady conditions, such as the flushing of water and sediment from a reservoir with sudden water surface drawdown and increase of water discharge from the upstream boundary. One of the main reasons for the development of GSTARS4 is the addition of truly unsteady flow simulation. The unsteady scheme was adopted from SRH-1D flow module and added to GSTARS4. The development of GSTARS4 started with the simulation of the Xiaolangdi Reservoir sedimentation and drawdown flushing.

The second phase of development was to modify sediment transport and channel adjustment computation scheme. Density of bed material may vary with respect to cross section location because texture of the deposited sediment varies with respect to the flow condition. GSTARS4 has the added capability of simulating spatial variation of bed

material density while previous versions of GSTARS models use the assumption that there is no spatial variation of density.

The Xiaolangdi Reservoir has one of the most complicated sedimentation and flushing mechanisms in the world. Thus, if a numerical model is applicable to the Xiaolangdi Reservoir sedimentation and flushing studies, the model may also be applicable to other reservoir studies.

4.1 Addition of Unsteady Flow Simulation

Removal of sediment deposition in the Xiaolangdi Reservoir has been done by drawdown flushing. Most reservoir operation can be approximated by a steady or quasi-steady scheme as shown in Fig. 3.2. However, truly unsteady simulation may be required to model drawdown flushing with rapid water surface drop in a reservoir.

The format of input file for the GSTARS4 model is based on GSTARS3. The GSTARS4 input file is almost same as that of GSTARS3 except for the data format for properties of unsteady flow. GSTARS4 has additional option to read unsteady flow data in the input file.

The numerical scheme for the unsteady flow is described in section 3.1.2, which is adopted from SRH-1D unsteady module with revisions. The flow chart of the GSTARS4 model is shown in Fig. 4.1. Unsteady flow computation modules adopted from SRH-1D cannot be used for GSTARS4 directly due to the difference in formats of the variables used for the two models. The performance of the SRH-1D unsteady flow module has already been tested. Consequently, it is better not to change the reliable SRH-1D modules.

31

Therefore, all the GSTARS4 variables used for unsteady flow simulations are converted into the format of SRH-1D first and the results from the SRH-1D module are then converted into GSTARS4 format again.
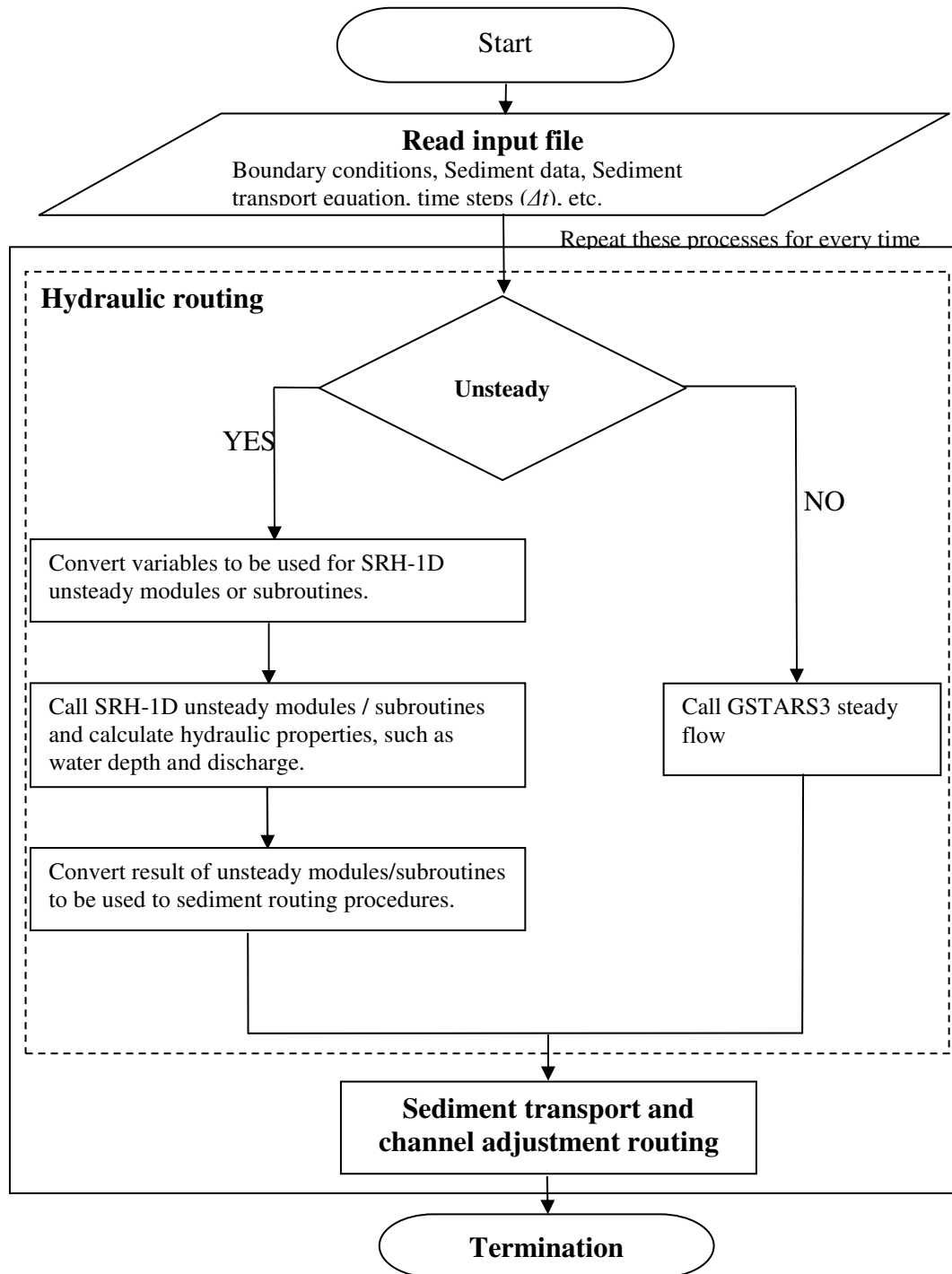
Figure 4.1 Flow chart of GSTARS4 model

4.2 Revision of Sediment Transport and Channel Adjustment

The Xiaolangdi Reservoir sedimentation and flushing processes are very complicated due to high sediment concentration with very fine materials of silt and clay. GSTARS3 sediment transport and channel adjustment computations should be revised for the development of GSTARS4 to simulate sedimentation and flushing processes in reservoirs. This was done by adding more options of functional relationships in GSTARS3. The upgraded capabilities of GSTARS4 are summarized and compared with GSTARS3, as shown in Table 4.1. Derivations for the new capabilities of sediment routing or channel adjustment computation are explained in the following sections.

Table 4.1 Upgraded capabilities of GSTARS4 sediment routing

Variables	Functions for variables		Remarks
	GSTARS3	GSTARS4	
Tributary inflow (both water and sediment)	f(time)	f(time) or f(water stage)	
Recovery factor, α	f(cross section location)	f(sediment size, cross section location)	
Deposited sediment density	f(sediment size)	f(sediment size, cross section location)	Density in river and reservoir may be different
Incoming sediment size distribution	f(discharge)	f(discharge, time)	
Wash load percentage	constant	f(time)	Required when using Yang et al. (1996) equation

4.2.1 Influence of Tributaries

GSTARS3 can simulate water and sediment inflow from tributaries. In addition to water and sediment inflow, the volume of tributaries should also be considered as part of the

33

total reservoir storage. The Xiaolangdi Reservoir has complex terrain features, as shown in Fig. 1.2, with more than 40 tributaries. The inflows of water and sediment from tributaries are very small, compared to those in the reservoir, and may be ignored for the simulation. However, the total volume of all the tributaries with reservoir water surface elevation between 230 m and 260 m is about 40% of the total reservoir volume and cannot be ignored. The "level pool" concept as shown in Fig. 4.2 is used to determine the reservoir volume and water and sediment discharge of tributaries.
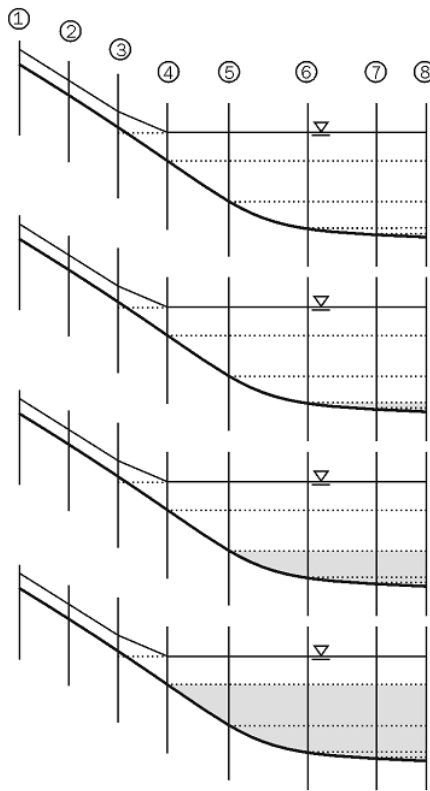
Figure 4.2 Delineation of volumes to build the capacity table for tributaries

(Yang and Simões, 2002)

During the water surface rising stage in the Xiaolangdi Reservoir, water flows from the main reservoir to the tributaries. In other words, the direction of lateral flow is from the

reservoir to the tributaries. On the other hand, when the water surface draws down, water discharge into the reservoir increases because the direction of flow is from the tributaries to the reservoir.

GSTARS3 requires water and sediment inflow from the tributaries with respect to time in the form of a hydrograph. It cannot simulate water and sediment discharge into tributaries. For the Xiaolangdi Reservoir routing, the important aspect is to consider water and sediment interchange between the main reservoir and tributaries. Therefore, tributary impact should be considered with respect to water stage change.

The following assumptions were used for the GSTARS4 model to simulate the influence of tributaries:

1. The tributary mouth bed elevation is the same as that of the reservoir at the mouth of the tributary.

2. The sediment concentration and size distribution of a tributary are the same as those in the reservoir at the mouth of the tributary.

3. During the flushing period or reservoir water surface elevation falling stage, tributary water and sediment will be discharged into the reservoir.

4. During the sedimentation or silting stage when the reservoir water surface elevation is rising, water and sediment will flow into tributaries.

5. The reservoir and tributary water surface is horizontal and the discharge of water and sediment into the reservoir from a tributary is

$$\Delta Q = -\Delta Vol / \Delta t \tag{4.1}$$

where ΔQ = water discharge from a tributary to the reservoir; ΔVol = change of tributary volume due to the change of reservoir elevation in a time step, Δt.

The volume of a tributary depends on water stage and bed elevation at the mouth. Therefore, the volume can be computed from

$$Vol = v_1 (h - h_m)^{v_2} \tag{4.2}$$

where Vol = volume of water in a tributary; h = water surface elevation; h_m = tributary mouth bed elevation; and v_1 and v_2 = coefficients of a tributary.

The value of ΔQ is positive when the water of a tributary is discharged into the reservoir during the flushing or water surface elevation falling period. The value of ΔQ is negative when water is discharged from the reservoir into a tributary during the sedimentation or reservoir refilling period when the reservoir water elevation is rising. Sediment load to and from a tributary is

$$\Delta Q_s = \Delta Q C_m \tag{4.3}$$

where ΔQ_s = sediment load from or into a tributary; and C_m = sediment concentration at the mouth of a tributary.

To compute ΔQ, water surface elevation at the mouth must be determined first. Computation of water surface elevation in the main reservoir should be carried out first to determine the water surface elevation and sediment concentration at the mouth of each tributary without considering the volume of the tributaries. Using water surface

elevations at the mouth of each tributary, ΔQ and ΔQ_s are calculated. After these processes, the main reservoir computation must be redone to calculate sediment transport and channel geometry adjustment in the main reservoir using ΔQ and ΔQ_s. This procedure of tributary inflow and outflow computation scheme, which is not included in the previous GSTARS3, has been added for GSTARS4.

4.2.2 Recovery Factor

The non-equilibrium sediment transport equation, Eq. (3.19), should be applied to simulate the delay effect of sediment scour, transport, and deposition in a reservoir. The delay effect is significant in the case of very fine material and rapid flow changes. The bed material and sediment inflow in the study area consist of about 60 ~ 95 % clay and silt and there are rapid flow changes due to drawdown flushing. Therefore, there is a significant delay effect in the Xiaolangdi Reservoir and the determination of the recovery factor is very important.

Different recovery factors have been suggested in the literature, either from an experimental or from a practical point of view. They include but are not limited to those by Zhang (1980), Armanini and Di Silvio (1988), Zhou and Lin (1995), Wang (1999), Zhou and Lin (1998), Zhou, et al. (1997), Han (2006), Chen et al. (2010), and Yang and Marsooli (2010). There is no consensus on method for the determination of the recovery factor. These studies indicated that the recovery factor is related to flow characteristics and sediment size. Han (2003) proposed that the recovery factor is a function of sediment fall velocity, shear velocity, and mean flow velocity, i.e.,

$$\alpha_k = f\left(\frac{V}{U^*}, \frac{\omega_k}{U^*}\right) \tag{4.4}$$

where α_k and ω_k = the recovery factor and fall velocity of sediment size group k, respectively; It should be noted that fall velocity is directly related to sediment particle size.

Wang (1999) conducted laboratory experiments by changing sediment size and flow characteristics. He computed "river bed inertia", related to the recovery factor and dry specific weight of the bed material, fall velocity, and discharge. The recovery factor for each experimental case was computed in this research. Fig. 4.3 (a) shows relationship between recovery factor and shear velocity. The recovery factor decreases with increasing shear velocity. However, the recovery factor varies significantly for almost the same shear velocity due to the steepness of the curve. Fig. 4.3 (b) shows close relationship between the recovery factor and fall velocity. A close relationship between recovery factor and ω_s/U^* is found in Fig. 4.3 (c). Therefore, the recovery factor is related to ω_s and ω_s/U^*. However, the flow condition and sediment size of his experiments are not the same as those in the Xiaolangdi Reservoir. It was assumed that the relationship found in Fig. 4.3 is basically valid for the Xiaolangdi Reservoir, because there is no measurement of recovery factor in the reservoir. Major factors for the fall velocity are water temperature and particle size. Because reservoir water temperature was not measured but assumed for the Xiaolangdi Reservoir, sediment particle size was assumed to be the major factor for the fall velocity and used for the calibration of recovery factor.
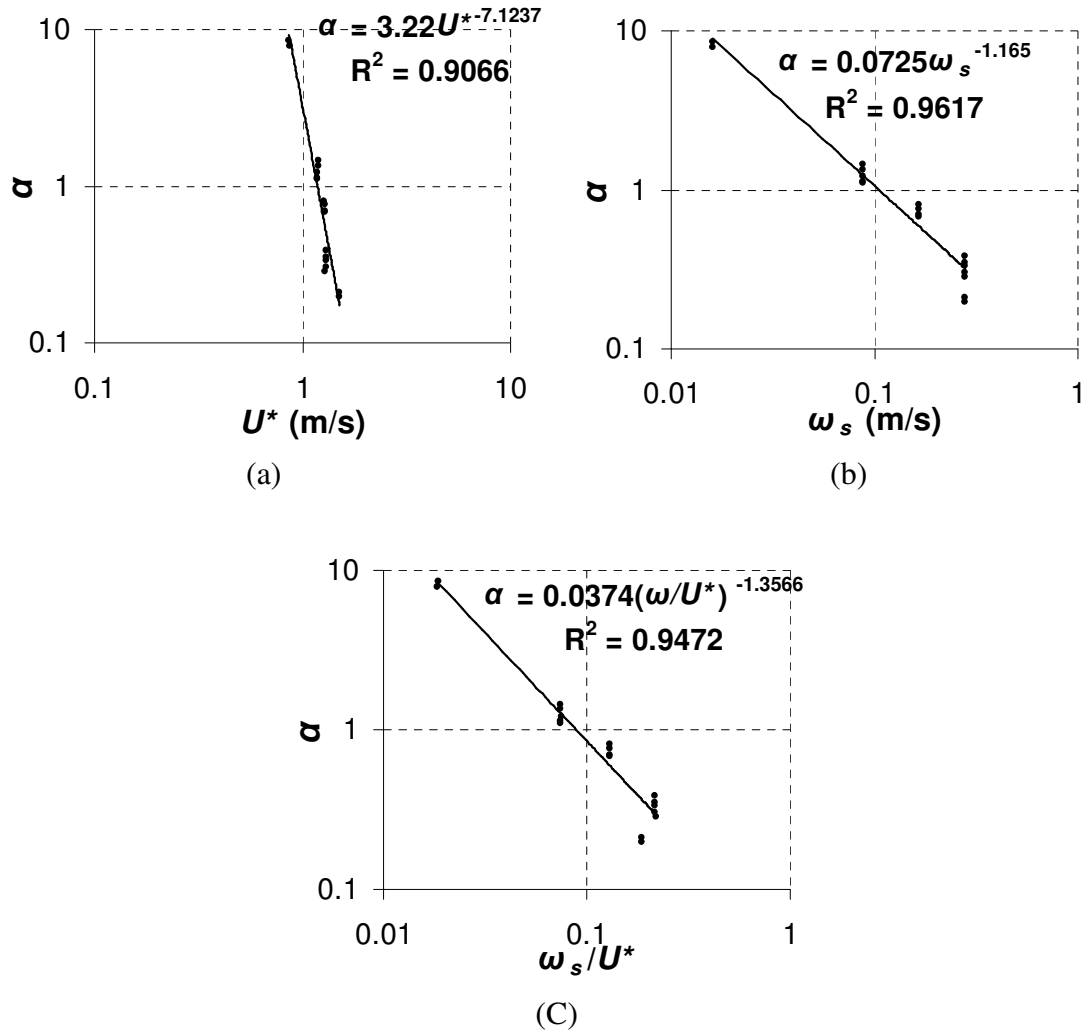
Figure 4.3 Relationship between recovery factor and (a) shear velocity, (b) sediment fall

velocity, and (c) ω_s/U^*

Due to the variation of sediment particle size along the reservoir, the recovery factor α

may be assumed as a function of cross section location i in GSTARS3, i.e.

$$\alpha = f(i) \tag{4.5}$$

Because the shear velocity and flow velocity may change with respect to time and cross

section location, the recovery factor with respect to each particle size, time step, and

cross section location should be considered. Thus the recovery factor may be expressed by a general function

$$\alpha_k = f\left(d_k, i, t_j \cdots\right) \tag{4.6}$$

where d_k = geometric mean diameter of sediment size group k; and t_j = time step j.

The relationship between recovery factor and these three factors was investigated for the Xiaolangdi Reservoir. More than 200 combinations were tested to find a general trend of bed profile change with respect to the recovery factor as a function of cross section location and time. The cross section location is divided into river and reservoir regimes, because flow characteristics are different in these two regimes. The routing is divided according to reservoir operation schemes, i.e., drawdown, rapid rise of water surface for reservoir refilling, and stagnant stages. However, there is no general trend of the variation of recovery factor as a function of location and time. An example is shown in Fig. 4.4 using recovery factors shown in Table 4.2. Therefore, it was assumed that sediment fall velocity or particle size is the dominant parameter for the calibration of the recovery factor, as shown in Fig. 4.3 (b). A relationship between recovery and sediment size is assumed as

$$\alpha_k = \frac{\varepsilon}{d_k^{\xi}} \tag{4.7}$$

where ε, and ξ = site-specific coefficients.

The assumed relation, Eq. (4.7), was used for this study and the two site-specific coefficients were calibrated for the Xiaolangdi Reservoir. The calibration of recovery factor is described in section 6.3.2.

Table 4.2 Combination of recovery factors

	Recovery factor	Drawdown flushing	Reservoir refilling	Stagnant water surface
Reservoir Reaches	α_d (deposition)	0.01	0.1	0.5
	α_s (scour)	1.0	0.5	0.7
River Reaches	α_d (deposition)	0.002	0.004	0.003
	α_s (scour)	1.0	1.0	1.0

(a) October 2004

(b) May 2004

(c) October 2003
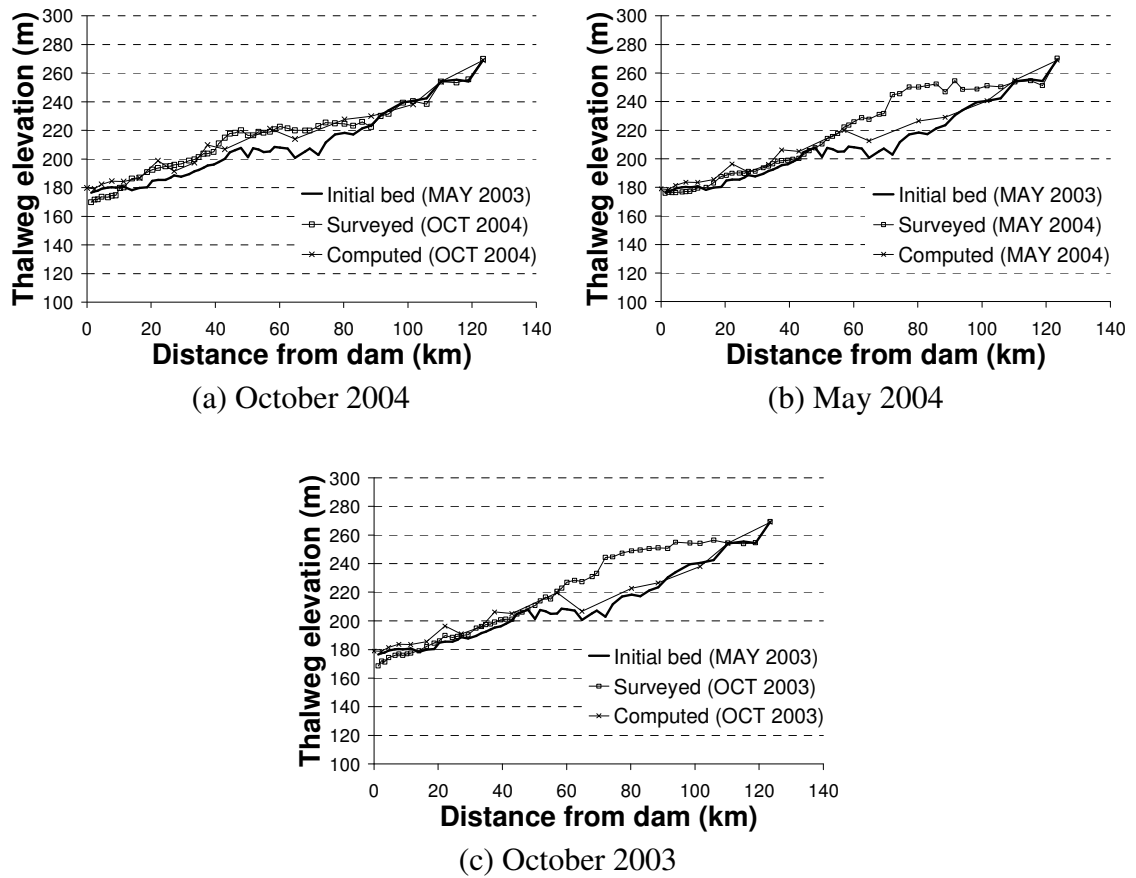
Figure 4.4 Comparison between measured and simulated bed profiles, using recovery

factor as a function of time and location

41

4.2.3 Variation of Deposited Sediment Density

Deposited sediment density is needed for sedimentation volume computation, or to convert the amount of sedimentation from weight to volume. Basic factors influencing the density of sediment deposition in a reservoir are reservoir operation, the texture and size of deposited sediment particles, and the compaction rate or consolidation rate (Yang, 1996 and 2003). GSTARS3 and GSTARS4 require dry specific mass, which is the dry mass per unit volume of deposited sediment (kg/m^3), for each sediment size group. Deposited sediment density may also vary with respect to cross section location, because texture and size of deposited sediment may vary with respect to river and reservoir regimes. If the variation is negligible, using only one set of deposited sediment densities may be reasonable. However, if flow characteristics vary in the study area, such as the existence of river and reservoir regimes, density of deposited sediment may not be the same in the two regimes. In the Xiaolangdi Reservoir sedimentation studies, both river and reservoir regimes exist in the study area. GSTARS3 can use only one set of deposited sediment density, while GSTARS4 is capable of simulating various sediment densities with respect to location.

4.2.4 Size Distribution of Incoming Sediment from Upstream Boundary

Most of the numerical models, including GSTARS models, require not only the quantity of incoming sediment from the upstream boundary, but also its size distribution at the upstream boundary. GSTARS3 requires incoming sediment size distribution as a function of water discharge at the upstream boundary as

$$C_{1,k} = f(Q) \tag{4.8}$$

where $C_{1,k}$ = incoming sediment of the kth sediment size.

However, if incoming sediment is controlled by the upstream reservoir operation, such as flushing of the upstream reservoir, gradation of incoming sediment should vary with respect to the upstream operation. For the Xiaolangdi Reservoir, incoming sediment is controlled by flushing from the upstream Sanmenxia Reservoir. Usually, flushed sediment becomes coarser. Sanmenxia Reservoir flushing started in June 2003 and ended in August 2003. The flushed sediment became coarser during the flushing operation. In other words, incoming sediment size distribution from the upstream boundary is not only a function of discharge but also a function of time of operation of the upstream reservoir, i.e.,

$$C_{1,k} = f(Q,t) \tag{4.9}$$

The sediment size distribution from the upstream boundary should be expressed by Eq. (4.9), which is a new capability of GSTARS4.
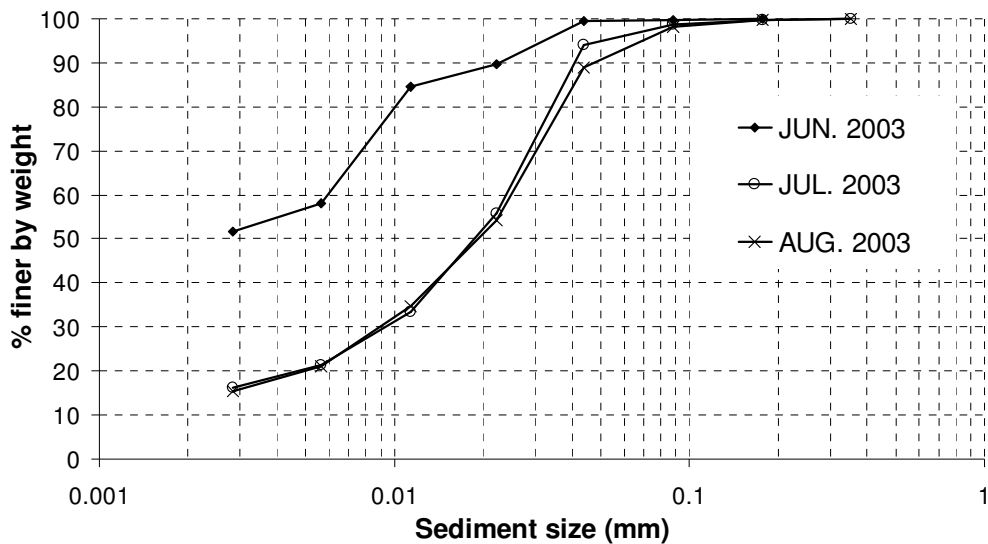
Figure 4.5 Measured size distribution of flushed sediment from the Sanmenxia Reservoir

4.2.5 Percentage of Wash Load

The Yang et al. (1996) sediment transport equation, developed for high concentration sediment laden flow in the Yellow River, was used for the simulation of the Xiaolangdi Reservoir sedimentation processes. Information on the percentage of wash load should be provided. If the gradation of sediment inflow does not change significantly, it may be reasonable to assume that the wash load percentage is constant, which is the assumption used for GSTARS3. However, because incoming sediment size distribution varies with respect to time due to flushing in the upstream reservoir, the percentage of wash load also varies. When relatively coarse materials are flushed out from the upstream reservoir, the wash load percentage may be small. When fine material is released from the upstream reservoir, the percentage of wash load may be relatively high. Therefore, the wash load percentage should be provided as a function of time. GSTARS4 has the capability of using various wash load percentages with respect to time. Variation of wash load percentage is required only when the Yang et al. (1996) sediment transport equation is used.

CHAPTER 5. NUMERICAL STABILITY CRITERIA FOR

CHANNEL ADJUSTMENT

The stability of uncoupled schemes for movable bed routing depends not only on the stability of the hydrodynamic scheme but also on the stability of sediment transport computation (Julien 2002). Numerical stability criteria of GSTARS4 channel aggradation and degradation routing are derived and explained in this chapter. Stability criteria were derived for steady and unsteady flow simulations. The derivations assumed that the channel was wide and rectangular with a constant width without lateral inflow of water and sediment.

5.1 Derivation of Kinematic Wave Speed of Bed Change for Steady Flow Simulation

The governing equation of the water flow used for steady state is Eq. (3.1). Assuming that velocity distribution coefficient is 1, $\lambda = 1$, it can be rewritten as

$$S_f + \frac{\partial z}{\partial x} + \frac{\partial y}{\partial x} + \frac{V}{g}\frac{\partial V}{\partial x} = 0 \tag{5.1}$$

The unit discharge at a given time t can be expressed as

$$q(t) = V \cdot y \tag{5.2}$$

For wide rectangular channel with constant widths and no lateral sediment inflow, the sediment continuity equation for sediment routing, Eq. (3.10), becomes

$$\eta \frac{\partial z}{\partial t} + \frac{\partial q_s}{\partial x} = 0 \tag{5.3}$$

The sediment transport rate at a given time t can be calculated from

$$q_s(t) = q(t) \cdot C_v(t) \tag{5.4}$$

Similar to the derivation of stability criteria by De Vries (1971), Eqs (5.1) ~ (5.4) can be rearranged to determine the stability criteria.

Derivative of Eq. (5.2) with respect to x is

$$y \frac{\partial V}{\partial x} + V \frac{\partial y}{\partial x} = \frac{\partial q}{\partial x} \tag{5.5a}$$

For steady state, the right hand side of Eq. (5.5a) is zero, then

$$y \frac{\partial V}{\partial x} + V \frac{\partial y}{\partial x} = 0 \tag{5.5b}$$

Eq. (5.5b) can be rewritten as

$$\frac{\partial y}{\partial x} = -\frac{y}{V} \frac{\partial V}{\partial x} \tag{5.5c}$$

Substitute Eq. (5.5c) into Eq. (5.1) gives

$$\frac{\partial V}{\partial x} = -\frac{S_f + \dfrac{\partial z}{\partial x}}{\dfrac{V}{g} - \dfrac{y}{V}} \tag{5.6}$$

Substituting Eq. (5.4) into the sediment routing equation Eq. (5.3) yields

$$\eta \frac{\partial z}{\partial t} + \frac{\partial (q C_v)}{\partial x} = 0 \tag{5.7a}$$

Because the unit discharge for steady state is a constant with respect to x, then Eq. (5.7a) can be rewritten as

$$\eta \frac{\partial z}{\partial t} + q \frac{\partial C_v}{\partial x} = 0 \tag{5.7b}$$

In Eq. (5.7b) the second term can be rewritten as

$$\eta \frac{\partial z}{\partial t} + q \frac{dC_v}{dV} \frac{\partial V}{\partial x} = 0 \tag{5.7c}$$

Substitute Eq. (5.6) into Eq. (5.7c) gives

$$\eta \frac{\partial z}{\partial t} - q \frac{dC_v}{dV} \frac{S_f + \dfrac{\partial z}{\partial x}}{\dfrac{V}{g} - \dfrac{y}{V}} = 0 \tag{5.8a}$$

Eq. (5.8a) can be rewritten as

$$\frac{\partial z}{\partial t} + c_{es} \frac{\partial z}{\partial x} = -c_{es} S_f \tag{5.9}$$

where $c_{es} = -\dfrac{1}{\eta} \dfrac{q}{\dfrac{V}{g} - \dfrac{y}{V}} \dfrac{dC_v}{dV}$ $\tag{5.10a}$

c_{es} can be rewritten using Froude number, Fr.

$$c_{es} = \frac{1}{\eta} \frac{V^2}{q} \frac{1}{1 - Fr^2} \frac{dq_s}{dV} \tag{5.10b}$$

De Vries (1971) indicated that

$$\frac{dq_s}{dV} = \frac{bq_s}{V} \tag{5.10c}$$

where b is a site specific value. His measurements indicated that $3<b<7$.

Then Eq. (5.10b) becomes

$$c_{es} = \frac{bV}{\eta} \frac{q_s}{q} \frac{1}{1 - Fr^2} \tag{5.10d}$$

Substituting Eq. (5.4) into Eq. (5.10d) gives

$$c_{es} = \frac{bVC_v}{\eta} \frac{1}{1 - Fr^2} \tag{5.10e}$$

Eq. (5.9a) is in the form of a wave equation with the damping term on the right hand side. Ignoring the damping term Eq. (5.9) can be approximated as

$$\frac{\partial z}{\partial t} + c_{es} \frac{\partial z}{\partial x} = 0 \qquad (5.11)$$

In Eq. (5.11), the kinematic wave speed of the bed change is $|c_{es}|$. However, due to the damping term in Eq. (5.9), the kinematic wave speed of the bed change for steady simulation is smaller than $|c_{es}|$, i.e.,

$$c_k \leq |c_{es}| \qquad (5.12)$$

where c_k = the kinematic wave speed of the bed changes.

GSTARS models uses an explicit method to solve the sediment routing and the stability criteria given by Yang and Simões (2002) as

$$c_k \frac{\Delta t}{\Delta x} \leq 1 \qquad (5.13)$$

Combination of Eq. (5.12) and (5.13) gives

$$|c_{es}| \frac{\Delta t}{\Delta x} \leq 1 \qquad (5.14)$$

The above stability criteria for steady flow satisfy Eq. (5.13) automatically.

5.2 Derivation of Kinematic Wave Speed of Bed Change for Unsteady Flow Simulation

The governing equations of unsteady flow are Eqs. (3.2) and (3.3). By assuming that velocity distribution coefficient is 1, it can be shown that

$$S_f + \frac{\partial z}{\partial x} + \frac{\partial y}{\partial x} + \frac{V}{g} \frac{\partial V}{\partial x} + \frac{1}{g} \frac{\partial V}{\partial t} = 0 \qquad (5.15)$$

48

The other equations for unsteady flow - sediment transport and the channel adjustment equations - are the same as those used for steady flow. In other words, Eq. (5.2), (5.3), and (5.4) are also valid for sediment routing with unsteady flow.

From Julien (2002),

$$\frac{\partial V}{\partial t} = -\beta V \frac{\partial V}{\partial x}$$ (5.16a)

$$\frac{\partial y}{\partial x} = \frac{y}{(\beta-1)V}\frac{\partial V}{\partial x}$$ (5.16b)

$$\frac{\partial q}{\partial x} = \frac{\beta q}{(\beta-1)V}\frac{\partial V}{\partial x}$$ (5.16c)

$$\frac{\partial y}{\partial V} = \frac{y}{(\beta-1)V}$$ (5.16d)

where $\beta = \dfrac{5}{3}$ when using Manning's equation (5.16e)

Substituting Eq. (5.16a) and (5.16b) into (5.15) gives

$$\frac{\partial V}{\partial x} = -\frac{S_f + \dfrac{\partial z}{\partial x}}{\dfrac{y}{(\beta-1)V} + \dfrac{V}{g} - \dfrac{\beta V}{g}}$$ (5.17)

On the other hand, the sediment load equation, Eq. (5.4), can be written in derivative form as

$$\frac{\partial q_s}{\partial x} = q\frac{\partial C_v}{\partial x} + C_v\frac{\partial q}{\partial x}$$ (5.18a)

Substituting Eq. (5.18a) into the channel adjustment equation, Eq. (5.3), gives

$$\eta\frac{\partial z}{\partial t} + q\frac{\partial C_v}{\partial x} + C_v\frac{\partial q}{\partial x} = 0$$ (5.18b)

Substituting Eq. (5.16c) into Eq. (5.18b) gives,

$$\eta \frac{\partial z}{\partial t} + q \frac{\partial C_v}{\partial V} \frac{\partial V}{\partial x} + \frac{\beta q C_v}{(\beta - 1)V} \frac{\partial V}{\partial x} = 0 \qquad (5.19a)$$

Eq. (5.19a) can be rewritten as

$$\eta \frac{\partial z}{\partial t} + \left[q \frac{\partial C_v}{\partial V} + \frac{\beta q C_v}{(\beta - 1)V} \right] \frac{\partial V}{\partial x} = 0 \qquad (5.19b)$$

Substituting Eq. (5.17) into Eq. (5.18b) gives,

$$\eta \frac{\partial z}{\partial t} - \frac{q \dfrac{\partial C_v}{\partial V} + \dfrac{\beta q C_v}{(\beta - 1)V}}{\dfrac{y}{(\beta - 1)V} + \dfrac{V}{g} - \dfrac{\beta V}{g}} \frac{\partial z}{\partial x} = S_f \frac{q \dfrac{\partial C_v}{\partial V} + \dfrac{\beta q C_v}{(\beta - 1)V}}{\dfrac{y}{(\beta - 1)V} + \dfrac{V}{g} - \dfrac{\beta V}{g}} \qquad (5.20)$$

Eq. (5.20) can be simplified by introducing, c_{eu}

$$\frac{\partial z}{\partial t} + c_{eu} \frac{\partial z}{\partial x} = -c_{eu} S_f \qquad (5.21)$$

where $c_{eu} = -\dfrac{1}{\eta} \dfrac{q \dfrac{\partial C_v}{\partial V} + \dfrac{\beta q C_v}{(\beta - 1)V}}{\dfrac{y}{(\beta - 1)V} + \dfrac{V}{g} - \dfrac{\beta V}{g}} \qquad (5.22)$

c_{eu} can be rearranged not to have the derivative form, as shown below.

Substituting Eq. (5.10c) into Eq. (5.18a) gives,

$$\frac{\partial C_v}{\partial V} = \frac{b C_v}{V} - \frac{C_v}{q} \frac{\partial q}{\partial V} \qquad (5.23a)$$

Eq. (5.2) can be used for the second term on the right hand side and Eq. (5.23a) becomes,

$$\frac{\partial C_v}{\partial V} = \frac{b C_v}{V} - \frac{C_v}{V} - \frac{C_v}{y} \frac{\partial y}{\partial V} \qquad (5.23b)$$

Substituting Eq. (5.16d) into Eq. (5.23b) gives

$$\frac{\partial C_v}{\partial V} = \left(b - 1 - \frac{1}{\beta - 1} \right) \frac{C_v}{V} \qquad (5.23c)$$

Substituting (5.23c) into Eq. (5.22) gives,

$$c_{eu} = -\frac{1}{\eta} \frac{q\left(b-1-\dfrac{1}{\beta-1}\right)\dfrac{C_v}{V} + \dfrac{\beta q C_v}{(\beta-1)V}}{\dfrac{y}{(\beta-1)V} + \dfrac{V}{g} - \dfrac{\beta V}{g}} \qquad (5.24a)$$

Multiplying the numerator and denominator by V/y and using Eq. (5.2) gives,

$$c_{eu} = -\frac{1}{\eta} \frac{\left(b-1-\dfrac{1}{\beta-1}\right)VC_v + \dfrac{\beta V C_v}{(\beta-1)}}{\dfrac{1}{(\beta-1)} + \dfrac{V^2}{gy} - \dfrac{\beta V^2}{gy}} \qquad (5.24b)$$

Using Froude number, Fr, Eq. (5.24b) can be rearranged as

$$c_{eu} = -\frac{bVC_v}{\eta} \times \frac{(\beta-1)}{1-(\beta-1)^2 Fr^2} \qquad (5.24c)$$

Eq. (5.21) is similar to the steady state formula, Eq. (5.9). Determination of the stability criteria for unsteady state is similar to that for the steady case shown in Eq. (5.14). By using c_{eu} instead of c_{es}, the stability criteria for unsteady flow is

$$\left|c_{eu}\right|\frac{\Delta t}{\Delta x} \le 1 \qquad (5.25)$$

CHAPTER 6. APPLICATION OF GSTARS4 TO XIAOLANGDI

RESERVOIR SEDIMENTATION AND FLUSHING

GSTARS4 model was applied to the Xiaolangdi Reservoir sedimentation and flushing processes. Simulations were conducted from May 2003 to October 2006. Both quasi-steady and unsteady flow simulations were performed and the computed results were compared to the surveyed results. The procedures and results of the application of GSTARS4 to the Xiaolangdi Reservoir are explained in this section.

6.1 Xiaolangdi Reservoir Data Analysis

The Xiaolangdi Reservoir data, such as hydrograph, channel geometry, and gradation of bed material, are available for 3.5 years, between May 2003 and October 2006. Analyses and evaluations of field data for their accuracy and relevance are necessary before they are applied to a numerical model. GSTARS4 requires input data in the proper formats. Each required data set was analyzed and some assumptions were made because some of the data were not available or not appropriate for modeling.

6.1.1 Hydrograph and Sediment Inflow Data

Fig. 6.1 shows the incoming discharge from the upstream boundary and water surface elevation at the Xiaolangdi Dam. Annual peak incoming flow usually occurs between

May and September. The water surface changes periodically, because of a sequence of flushing and refilling operations that repeat every year. Usually from May to August, the water surface drops due to drawdown flushing. After drawdown, the water surface rapidly rises to refill the reservoir and then the water surface does not change significantly before the next drawdown. The water surface variation cycle can be divided into three stages, i.e., drawdown, rapid rise and stagnant stage.

Fig. 6.2 shows incoming sediment discharge and water surface elevation at the Xiaolangdi Dam. Sediment discharge is very high when the upstream reservoir flushes its deposited sediments. The annual peak of sediment load coincides with the peak draw down stage. Incoming water and sediment are high between May and September every year.
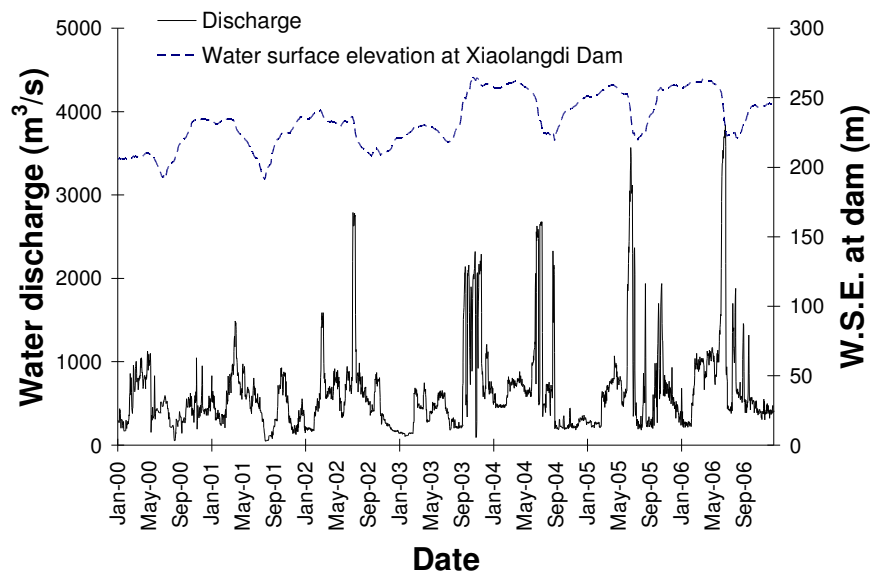
Figure 6.1 Hydrology and operation data of the Xiaolangdi Reservoir
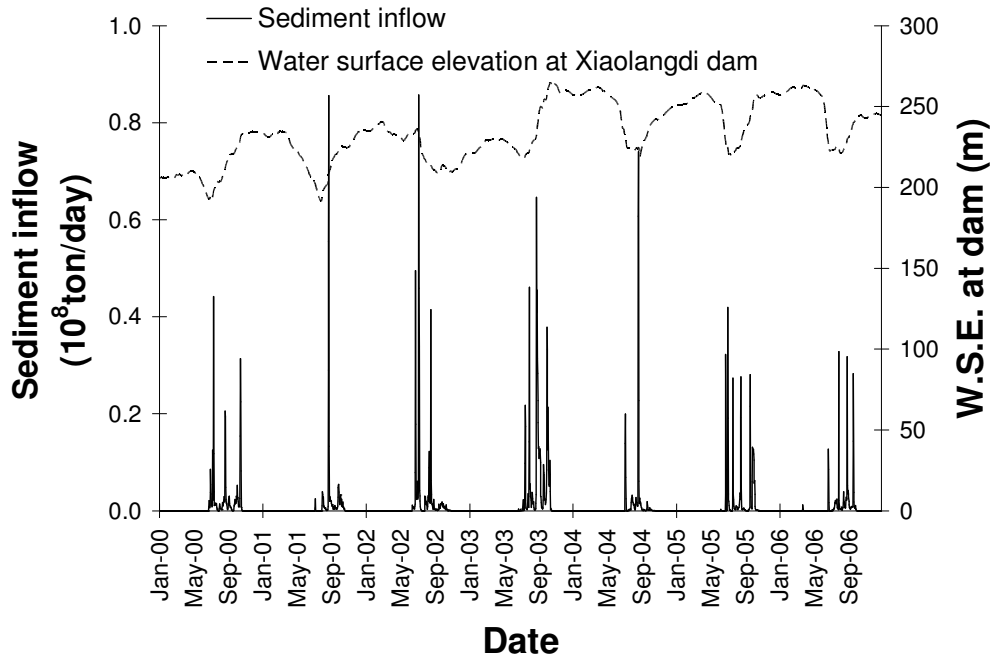
Figure 6.2 Sediment load and water surface elevation data

6.1.2 Sediment Size Distribution Data

The sediment size distribution in the Xiaolangdi Reservoir is divided into 9 groups. For

GSTARS4 modeling, both bed material and incoming sediment size distributions are

required. Dry specific weight of each size group is necessary for the model to convert

from weight to volume. The dry specific weights published in the literature (Yang 1996

and 2003) are used, because there are no field measurements for these values.

(1) Bed Material Size Distribution

Size distribution of bed material was surveyed several times from 2002 to 2006 in the

main reservoir and some major tributaries. Seven sets of measurement data of bed

material, which were measured in June 2002, October ~ November 2003, May 2004,

October 2004, April 2005, and November 2005, were available. Fig. 6.3 shows bed

material size distribution surveyed in June 2002. From Xiaolangdi Dam to about 60 km

54

above it, size distributions are similar to each other. From 64.8 km to 98.4 km, the distribution changes significantly. Upstream from 60.1 km, bed materials are much coarser than those in the downstream sections. The bed material size variation near 60.1 km has the typical basic characteristics of reservoir deltas (Fan and Morris, 1992a). The Xiaolangdi Reservoir delta is located at around 65 km above the dam. The cross section at 64.8 km is at the topset of the delta.

Fig. 6.4 compares mean bed material size, d_{50}, between May and October 2004. Fig. 6.4 shows that bed material is coarser in May than in October, because drawdown flushing scoured more fine sediment than coarse sediment in the reservoir. Immediately after flushing operations, bed material will become coarser because finer materials are eroded faster than coarser ones. Fig. 6.4 shows that bed material size decreases in the downstream direction, but variation at the end of the upstream reach does not have a stable general trend, because the upstream end is directly controlled by upstream dam operation.

Flushing starts usually in May or June and ends in August or September each year. If bed materials were surveyed in August or September, this might show that the size of bed material is coarser than in May. Bed material size was usually measured after reservoir refilling in October or November. After flushing, the water surface rises rapidly to fill the reservoir and the bed material becomes finer due to deposition. The trend of bed material size change follows the periodic change of the water surface elevation according to the reservoir operational plan.

Fig. 6.5 shows the variation of bed material size measured between 2002 and 2005. In the Xiaolangdi Reservoir, the reservoir delta is located at about 60 ~ 80km above the dam. Bed materials are coarser on the delta than those in other reservoir reaches. There is very little change of bed material sizes at the beginning stages of flushing each year.
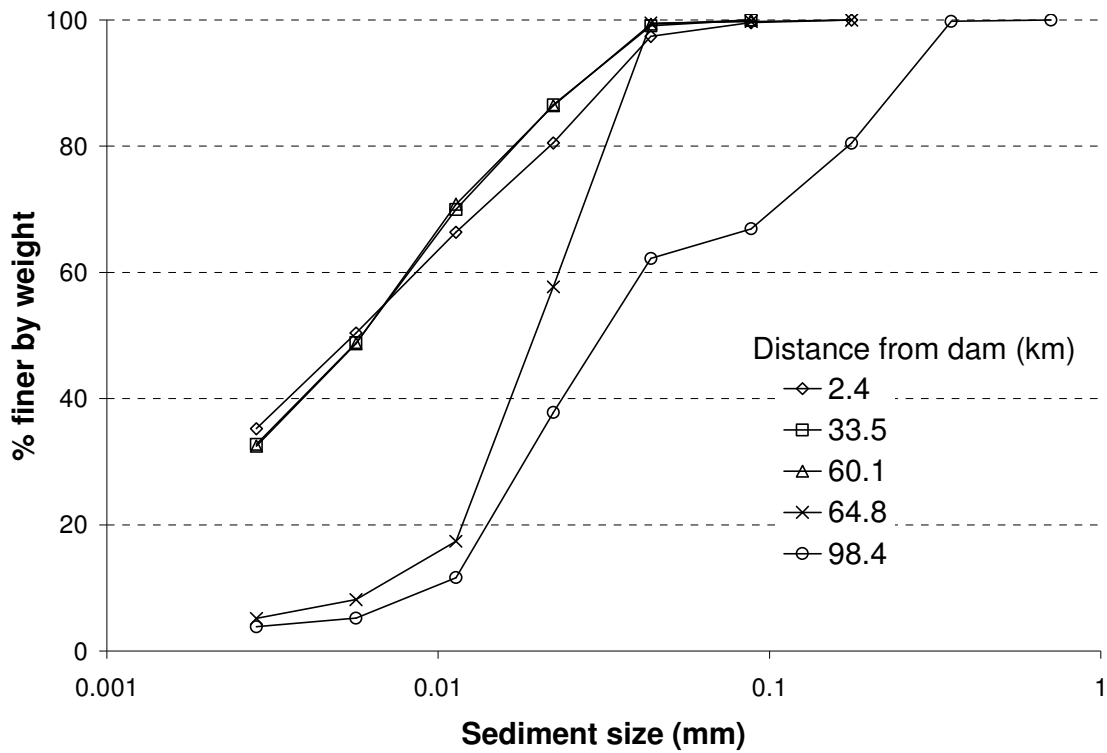
Figure 6.3 Bed material size distribution surveyed between 10 ~ 13 June 2002
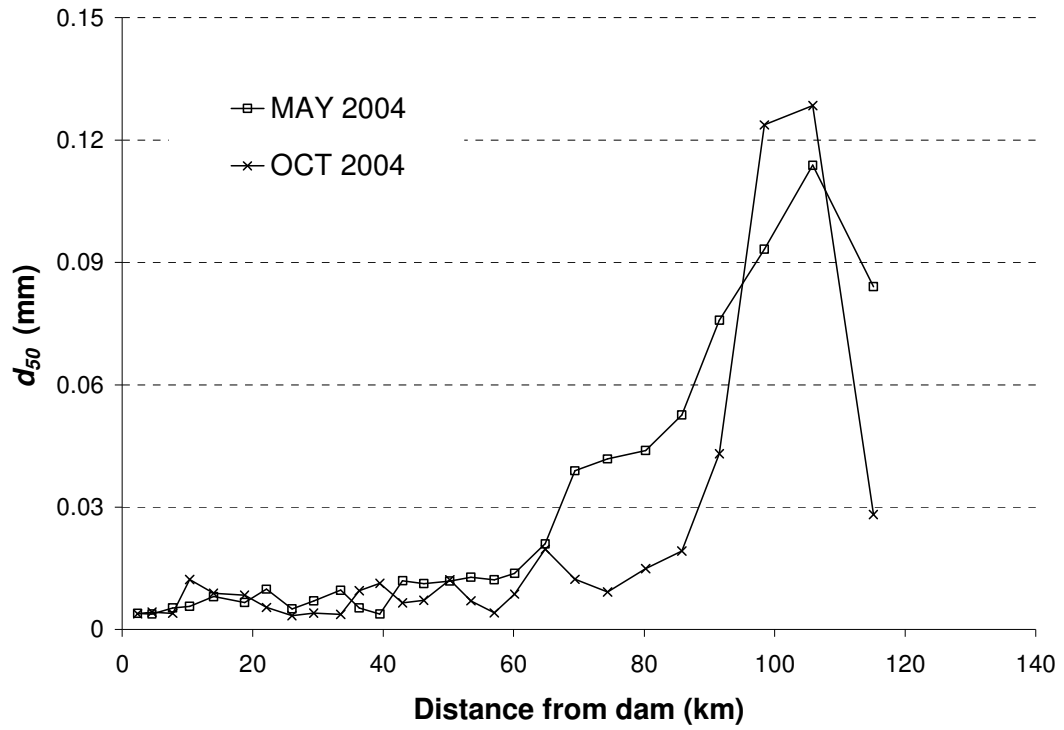
Figure 6.4 Bed material size distributions in 2004
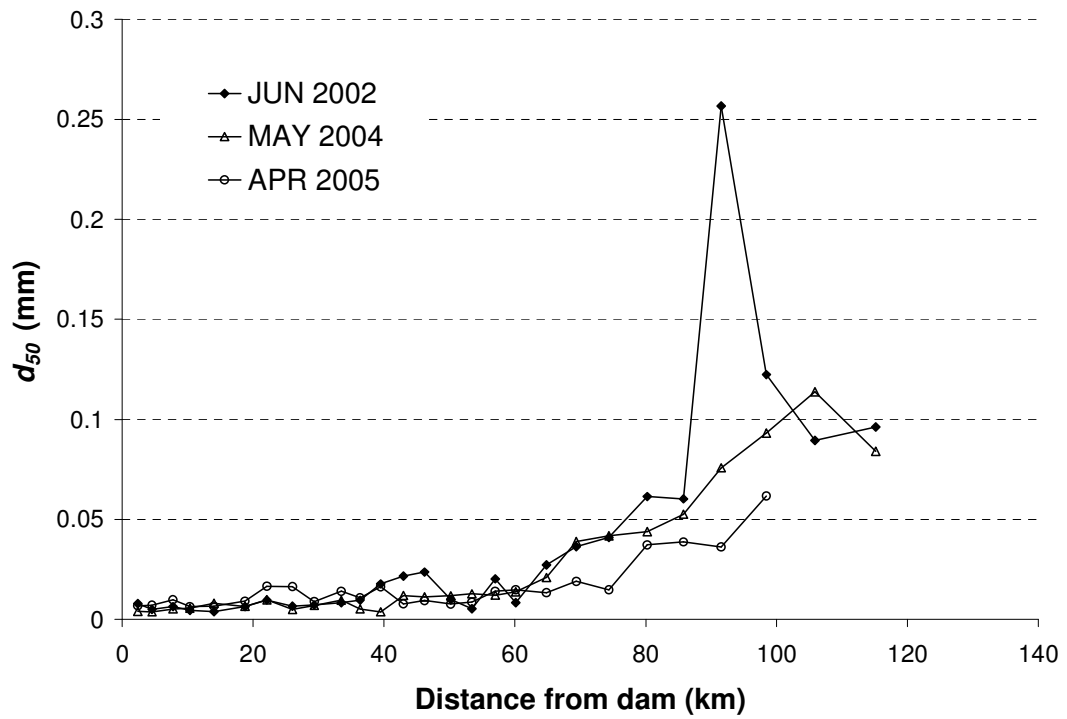
Figure 6.5 Surveyed d_{50} before flushing in year 2002, 2004, and 2005

(2) Incoming Sediment Quantity and Size Distribution

GSTARS models require not only the quantity of incoming sediment from the upstream boundary, but also the size distribution. Daily or monthly incoming sediment data are needed for GSTARS4 simulation.

The Yang et al. (1996) sediment transport equation, developed for high concentration sediment laden flow in the Yellow River, was used for this study. To use this method, information on the percentage of wash load is required. The percentage of wash load depends on field conditions. It is desirable to have surveyed bed material and suspended material sediment size distributions to determine the percentage of fine material transported as wash load.

Because the wash load fraction was not available, it was assumed that sediment size less than 0.01 mm was the wash load (Yang, 1996 and 2003) of total incoming sediment. Yang (1996 and 2003) found that even if the initially assumed wash load percentage is not accurate, the Yang et al. (1996) method can still give fairly good estimation of bed-material load in the Yellow River with high concentration of wash load. Therefore, bed-material load computation using the Yang et al. (1996) method is valid for this study.

Daily incoming sediment size distributions were available and monthly averaged values were used for GSTARS4 modeling because the variation in a month was small.

(3) Density of Deposited Sediment

Because dry specific weight or mass of bed materials in the Xiaolangdi Reservoir was not available, these values were estimated using the method recommended by Yang (1996 and 2003). There are usually four types of reservoir (U.S. Bureau of Reclamation, 1987) with different densities of deposited sediment. Classification of reservoir operation and dry specific mass of bed material are shown in Table 6.1 and 6.2, respectively.

The study reach is from Xiaolangdi Dam to Sanmenxia Dam. This study reach has a length of about 120km long and consists of both reservoir and river regimes. Density of deposited sediment in the reservoir regime can be classified as operation number 2, while that in the river regime should be operation number 4, "Riverbed sediments". The flow characteristics in the study reach should be divided into reservoir and river regimes. In the downstream reach, the flow is very slow and deep due to backwater effect. This reach can be classified as a reservoir regime. In the upper reach, upstream of the backwater, it is classified as a river reach. Therefore, sediment density in the reservoir reach has to be operation number 2 and that in river reach should be operation number 4. In other words, different sets of deposited sediment density must be used for computation. In this study, a combination operation number 2 for reservoir regime and number 4 for river regime was used for the simulation. However, simulations with operation number 1 for reservoir and number 4 for river were conducted for comparison.

As shown in Table 6.2, density variation of clay is significant, whereas for coarser materials of silt and sand the density is fairly constant regardless of the operation number. It is assumed that consolidation effect is negligible in this study due to annual flushing

operations. Generally speaking, the density of bed sediments may change with respect to time due to consolidation. For fine materials, such as clay and silt, these effects are important for the determination of deposited sediment volume in a reservoir. Consolidation is not considered in this study because a large portion of deposited sediment is scoured out during drawdown flushing each year. Sediment deposited in the Xiaolangdi Reservoir does not have enough time to be consolidated because of annual drawdown flushing.

Table 6.1 Four types of reservoir operation

Operation	Reservoir operation
1	Sediment always submerged or nearly submerged
2	Normally moderated to considerable reservoir drawdown
3	Reservoir normally empty
4	Riverbed sediments

Table 6.2 Initial dry specific mass with respect to operation number

Operation	Initial dry specific mass (kg/m^3)		
	Clay	Silt	Sand
1	416	1120	1550
2	561	1140	1550
3	641	1150	1550
4	961	1170	1550

6.1.3 Cross Section Geometry Data

Cross section geometry of the Xiaolangdi Reservoir and its tributaries were surveyed six times, i.e., January 2000, May and October 2003, May and October 2004, and October 2006. Fig. 6.6 shows the surveyed thalweg profiles of the study reach. In the first three years of operation, from January 2000 to May 2003, deposition occurred significantly and rapidly in the reservoir reach, from the dam to about 60 km. After the first three years, deposition also occurs in the reservoir reach but less than occurred in the first three years. There are 56 sets of cross sectional data with about 2 km spacing between cross sections. GSTARS4 simulation cannot be conducted using all 56 cross sections because 2 km spacing does not satisfy the stability criteria of the numerical simulation and the results are unstable. Determination of spacing is explained in section 6.2.
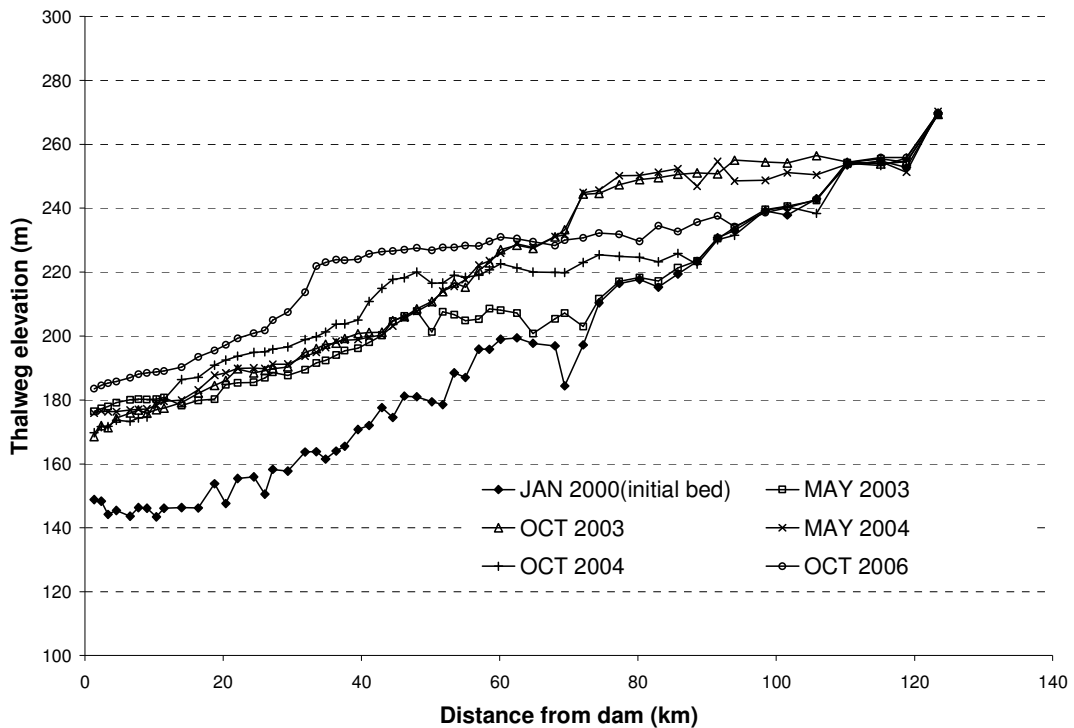
Figure 6.6 Measured thalweg elevation

61

6.1.4 Water Temperature Data

Water viscosity, density, and sediment fall velocity are all affected by water temperature. It is necessary to use accurate water temperature data for the GSTARS4 simulation. However, there is no water temperature data for the Xiaolangdi Reservoir. Therefore, water temperature was assumed for each month. Table 6.3 shows assumed water temperature.

Table 6.3 Water temperature of Xiaolangdi Reservoir (assumed values)

Month	Jan	Feb	Mar	Apr	May	Jun	Jul	Aug	Sep	Oct	Nov	Dec
Temperature ($^\circ$C)	5	5	5	8	8	10	10	16	10	8	5	5

6.1.5 Tributary Volume Data

There are more than 40 tributaries flowing into the Xiaolangdi Reservoir. Twelve of them were considered as major tributaries and the total volume of the small tributaries were combined into an "imaginary tributary" with the location shown in Fig. 1.2. Twelve major tributaries plus the imaginary tributary were considered in this study. The relationship between water surface elevation and volume of tributaries can be computed by Eq. (4.2). The parameters used in Eq. (4.2) are summarized in Table 6.4.

Table 6.4 Water stage and tributary volume relationships

Name of Tributaries	Location of the Mouth (m, distance from Xiaolangdi dam)	v_1	v_2	h_m
Simengou	600	666.99	2.5337	154.66
Dayuhe	4225	4404.6	2.4357	149.90
Meiyaogou	6350	102.89	2.9786	159.80
Baimahe	10355	187.71	2.7099	169.70
Zhenshuihe	17030	4545.2	2.6260	154.40
Shijinghe	21680	3177.5	2.4643	160.40
Donyanghe	29100	126.94	3.1193	171.40
Xiyanghe	39380	4659.1	2.3461	179.50
Ruicunhe	42410	6043.5	2.1970	178.20
Imaginary Tributary	52000	2286.8	2.9175	182.69
Yunxihe	54570	39380	2.0472	196.10
Boqinghe	56950	6803.6	2.3956	216.10
Banjianhe	61590	4158.2	2.2154	208.40

6.2 Determination of Time Step and Distance between Cross Sections

GSTARS models use a finite difference uncoupled scheme, which means that hydraulic properties are calculated first. Sediment routes and bed changes are computed after the hydraulic computation, keeping all the hydraulic parameters fixed during the calculation (Yang and Simões, 2002). During a time step Δt, hydraulic properties and channel boundary changes should be small because the channel boundary is assumed to be fixed during the hydraulic property calculation.

GSTARS3 model calculates the change of cross sections due to scour or deposition using Eq. (3.13). From Eq. (3.13), it is clear that the bed elevation change is related to Δt. When the bed elevation change during Δt is small compared to flow depth, the assumption of rigid boundary is valid for hydraulic property calculation, and the aggradation-degradation calculation can be performed by the uncoupled scheme (Julien, 2002).

In this study, the simulations were carried out from May 2003 to October 2006 when surveyed cross section geometry data were available for comparison; Δt = 3 minutes, 6 minutes, and 10 minutes were tested. Fig. 6.7 shows the simulated results using different Δt values. In the circled area near the reservoir delta with data of October 2006, the result of Δt = 3 minutes agrees best with the surveyed data. In other areas, Δt = 3 minutes and Δt = 6 minutes give similar results. Because the rate of scour or deposition near the reservoir delta is important, simulation with Δt = 3 minutes was used in this study.
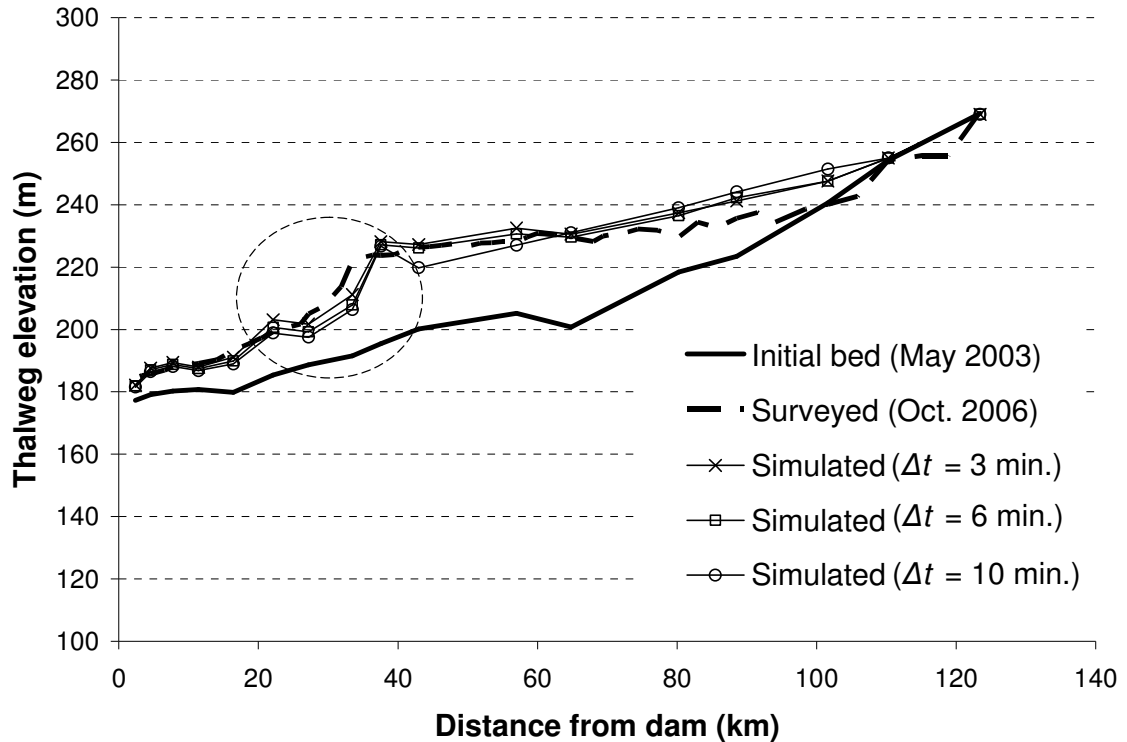
Figure 6.7 Comparison of longitudinal profiles using different time steps

(Δt = 3, 6, and 10 minutes)

Stability criteria for sediment transport and channel adjustment were derived in section 5.1 and 5.2 with the assumptions of a wide rectangular channel with constant width. Time step and distance between cross sections should satisfy Eq. (5.14) and Eq. (5.25) for quasi-steady and unsteady simulations, respectively.

For the Xiaolangdi Reservoir sediment and bed change computation,

$$\frac{1}{1-Fr^2} \cong 1 \tag{6.1a}$$

$$\frac{(\beta-1)}{1-(\beta-1)^2 Fr^2} \cong \beta-1 \tag{6.1b}$$

If the Manning's equation is used, $\beta = 5/3$

$$5 < b < 5.5, \quad b = 5.3 \quad \text{is used} \tag{6.1c}$$

$$0.3 < \eta < 0.55 \text{ in river regime, } \eta = 0.4 \text{ is used} \tag{6.1d}$$

V and C_v are the mean flow velocity and sediment transport capacity, respectively. These values depend on the flow condition, which is a function of time and cross section location. The bed change in the upstream reach is faster than that in the downstream reach. Therefore, values for the upstream reach should be used. For this study, V and C_v values in the upstream reach, at 110 km above Xiaolangdi Dam and about 10 km below Sanmenxia Dam, were considered.

To satisfy the stability criteria, the following maximum value should be used.

$$MAX[VC_v] \cong 3.0 \text{ (m/s)} \tag{6.1e}$$

This maximum value occurred in August 2004.

Eq. (5.14) and (5.25) give the stability criteria for the Xiaolangi Reservoir sedimentation routing in the upstream reach, for steady and unsteady simulations, respectively. The condition for stable computational results with an explicit scheme can be determined by substituting Eqs. (6.1a) ~ (6.1e) to Eqs. (5.14) and (5.25).

The condition of the stable solution for a steady simulation is

$$\frac{\Delta x}{\Delta t} \geq 39.8 \ \text{(in m/s)} \tag{6.2a}$$

Similarly, the condition for an unsteady simulation is

$$\frac{\Delta x}{\Delta t} \geq 26.5 \ \text{(in m/s)} \tag{6.2b}$$

For the same Δt, Eqs. (6.2a) and (6.2b) reveal that steady simulation requires a longer Δx than that of unsteady simulation.

With Δt = 3 minute (180 second), then $\Delta x \geq$ 7200 m and 4800 m for steady and unsteady simulations, respectively. To satisfy Eq. (6.2a) in river regime, from Sanmenxia dam to about 55 km above Xiaolangdi dam, $\Delta x >$ 7200 m.

VC_v values vary with respect to location. The upstream reach has larger values than the downstream reach, because the downstream reach is in the reservoir regime and the upstream reach is in the river regime. Therefore,

$$\Delta x_{river} \geq \Delta x_{reservoir} \tag{6.3}$$

where Δx_{river} and $\Delta x_{reservoir}$ = distance between cross sections for the river and reservoir reaches, respectively.

Shorter Δx values were tried for the downstream reservoir reach, and the simulated results did not show any numerical instability. In this study, Δt, Δx_{river}, and $\Delta x_{reservoir}$ are the same

for steady and unsteady simulations. Fig. 6.8 (b) shows unstable mean bed material size, d_{50}, in the upper reach using 56 cross sections in August 2008 when Eq. (6.1e) is used. Therefore, $\varDelta x_{river} > 7200$ m was selected for this study.
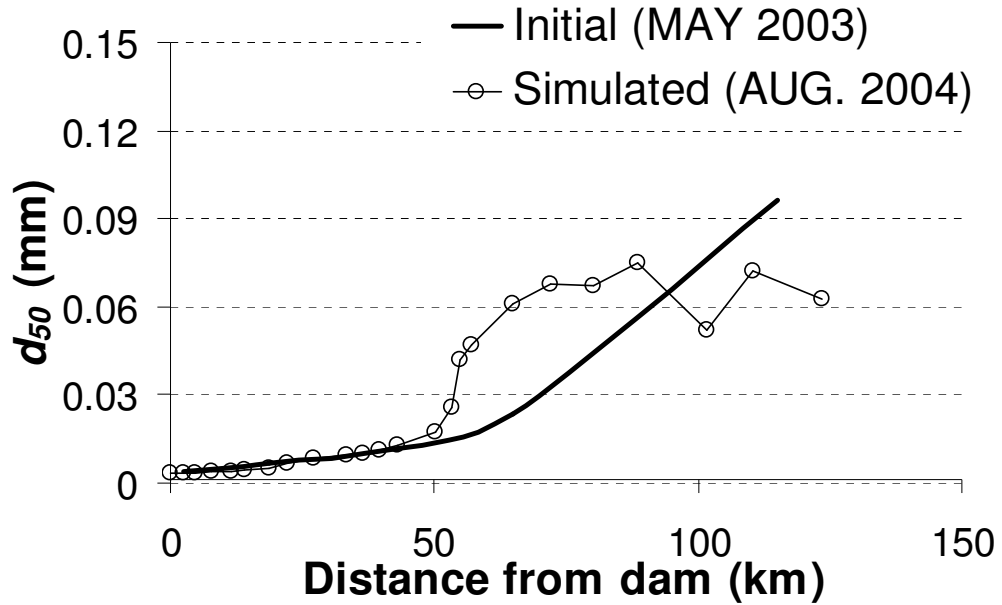
(a) 24 Cross sections ($\varDelta x_{river} > 7200$ m)
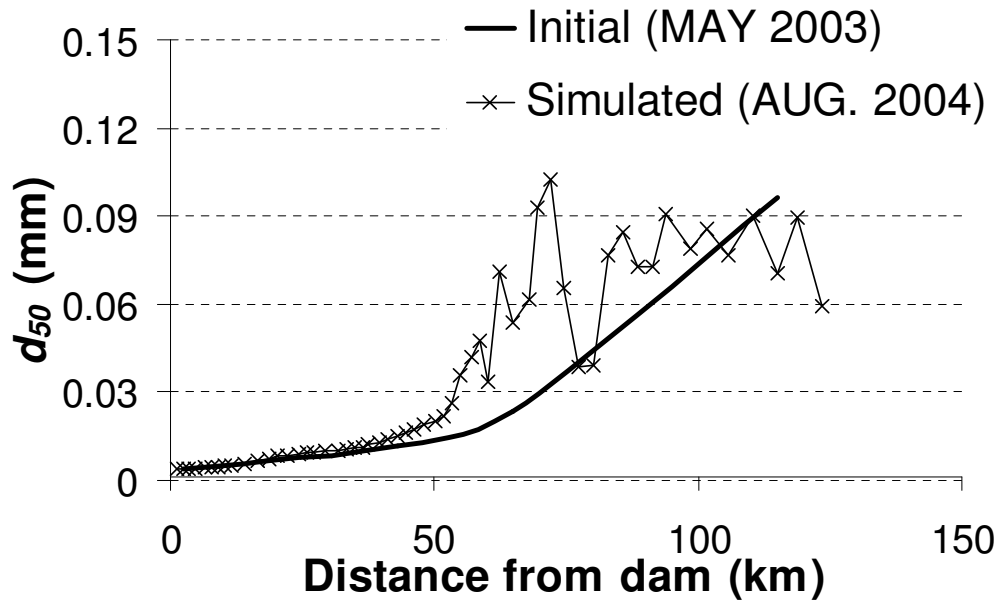
(b) 56 Cross sections ($\varDelta x_{river} < 7200$ m)

Figure 6.8 Bed material size profile with steady simulation using 24 and 56 cross sections

6.3 Calibration of Coefficients

6.3.1 Roughness Coefficient (Manning's *n*)

Manning's *n* values vary along the study reach with respect to time. However, it is very difficult to find a functional relationship between the roughness coefficient and time. It is assumed that Manning's *n* is a function of cross section location and man particle diameter.

Determination of the variation of the roughness coefficient along the main reservoir is important for the numerical model. It is reasonable to assume that Manning's *n* decreases in the downstream direction due to the decrease of sediment particle size. Manning's *n* value for each cross section could be determined as a function of d_{50}. Six sets of surveyed data on bed material size distributions, i.e., June 2002, October 2003, May and October 2004, and April and November 2005, were provided. Bed material sizes surveyed in those years are similar to each other. The measured results at about 95 km in June 2002 shown in Fig. 6.5 are unusually high. This is because the upstream reach is directly controlled by discharged sediment from the Sanmenxia reservoir. The sediment size profile for 2002 was used to determine Manning's *n* value.

Fig. 6.9 shows d_{50} variation along the study reach. The relationship between d_{50} and location can be divided into two regimes, i.e., reservoir and river regimes. The relationship between d_{50}, in mm, and distance from Sanmenxia Dam is

$$d_{50} = 0.0051 \times e^{0.0171x} \quad \text{for reservoir regime, below 60 km from the dam} \quad \text{(6.4a)}$$

$$d_{50} = 0.0061 \times e^{0.0262x} \quad \text{for river reaches, above 60 km from the dam} \quad \text{(6.4b)}$$

Eqs. (6.4a) and (6.4b) were used initially to determine Manning's n values for the study area.

The final Manning's n values for all cross sections were derived using the following relationship.

$$n \propto d_{50}^{1/6}, \quad n = \kappa \cdot d_{50}^{1/6} \quad (d_{50} \text{ in mm}) \tag{6.5}$$

where $\kappa = $ a coefficient.

Two separate κ values are required for river and reservoir regimes, respectively, as shown in Fig. 6.9. κ values of 0.063 and 0.022 were used for river and reservoir regimes, respectively. These relationships are

$$n = 0.063 d_{50}^{1/6}, \text{ in river regime} \tag{6.6a}$$

$$n = 0.022 d_{50}^{1/6}, \text{ in reservoir regime} \tag{6.6b}$$

Fig. 6.10 (a) Manning's n suddenly increases around 60 km ~ 61 km. Fig. 6.10 (a) indicates that n value suddenly increases around 60 ~ 61 km without a gradual transition between 50 ~ 90 km where the reservoir regime gradually changed to the river regime. The variation of n value along the study reach with a transition between reservoir and river reaches shown in Fig. 6.10 (b) was used for this study.
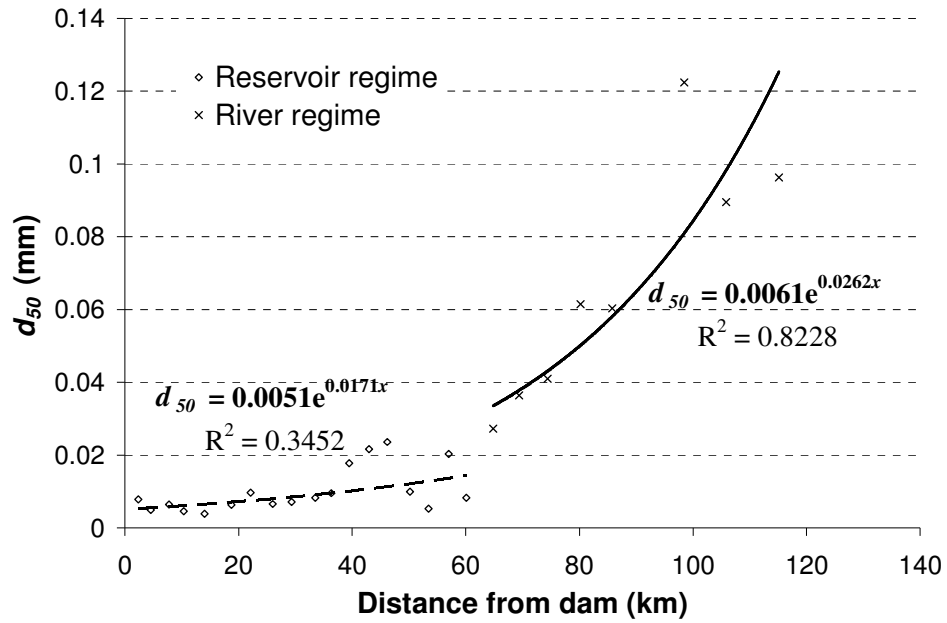
Figure 6.9 Measured d_{50} along the main reservoir reach in June 2002
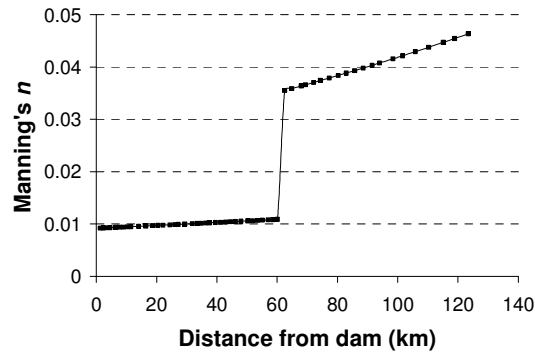
(a) Manning's n values using Eqs. (6.6a) and (6.6b)
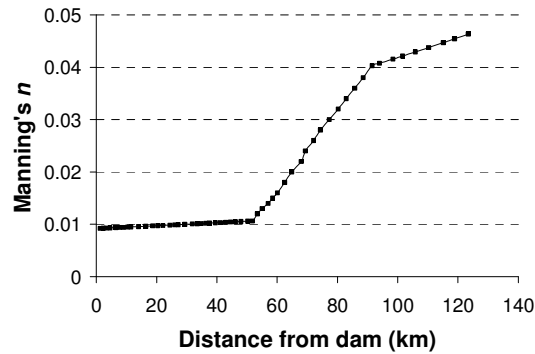
(b) Manning's n values for this study (gradual variation around the transient)

Figure 6.10 Variation of Manning's n values used for the simulation

6.3.2 Recovery Factor

Sediment size is divided into nine groups in this study. Each group has a lower and an upper limit of diameter and the representative size for each group is the geometric mean value of the limits, as shown in Table 6.5. In Eq. (4.7), two coefficients are required to determine the recovery factor α. Combinations of coefficients in Eq. (4.7) were calibrated by trial-and-error method with steady simulations. The duration of simulations for the calibration was 3.5 years from May 2003 to October 2006. The calibration process was carried out by comparing simulated thalweg profiles to measured ones. The goodness-of-fit of thalweg elevations was evaluated by two statistical parameters, the root-mean-square (RMS) and the average geometric deviation (AGD). Two parameters are computed as follows.

(1) RMS

$$\text{RMS} = \left[\sum_{j=1}^{J} \left(z_{cj} - z_{mj} \right)^2 / J \right]^{1/2} \tag{6.7}$$

where z_c and z_m = computed and measured elevations in meter, respectively; j = index of data set; and J = total number of data set. The unit of RMS for bed elevation is in meter.

(2) AGD

$$\text{AGD} = \left[\prod_{j=1}^{J} R_j \right]^{1/J} , \quad R_j = \begin{bmatrix} z_{cj} / z_{mj} & \text{for } z_{cj} \geq z_{mj} \\ z_{mj} / z_{cj} & \text{for } z_{cj} < z_{mj} \end{bmatrix} \tag{6.8}$$

where R_j = special discrepancy ratio. AGD is a dimensionless parameter.

Computed RMS and AGD for some of combinations of ε and ξ were summarized in Table 6.6 (a) and (b), respectively. The calibrated values of ε and ξ were 0.17 and 0.3,

respectively, because the combination provides the lowest RMS and AGD for the every comparison only except October 2004. Each coefficient has the same value for scour and deposition. The need to consider using different coefficient values for scour and deposition, suggested by Han and He (1990), was not found for the Xiaolangdi Reservoir study. This conclusion seems reasonable because the difference between scour and deposition reflects the change of the bed material size gradation. Recovery factors, which vary from 0.189 to 0.988, with calibrated coefficients are shown in Table 6.7. Calibration of two coefficients may be required for other reservoir sedimentation.

Table 6.5 Sediment size group for this study

Group	Lower bound (mm)	Upper bound (mm)	Geometric mean (mm)
1	0.002	0.004	0.00283
2	0.004	0.008	0.00563
3	0.008	0.016	0.0113
4	0.016	0.031	0.0223
5	0.031	0.062	0.0438
6	0.062	0.125	0.0880
7	0.125	0.25	0.1768
8	0.25	0.5	0.3536
9	0.5	1	0.7071

Table 6.6 (a) Calibration of recovery factor, RMS of thalweg elevation

ε	ξ	RMS (m)						Remarks
		Time					Average	
		OCT. 2003	MAY 2004	OCT. 2004	NOV. 2005	OCT. 2006		
0.5	0.1	5.93	5.39	6.18	5.02	7.32	5.97	
0.1	0.1	10.62	7.24	5.70	4.53	7.95	7.21	
0.3	0.2	5.77	5.31	5.82	4.78	7.25	5.79	
0.1	0.2	9.01	5.04	5.77	4.26	7.42	6.30	
0.1	0.3	7.23	4.71	5.87	4.26	6.42	5.70	
0.17	0.3	4.99	4.15	6.42	3.83	4.55	4.79	Lowest
0.2	0.3	5.66	5.16	5.42	3.84	5.74	5.16	
0.05	0.4	9.60	5.23	5.68	4.19	7.10	6.36	
0.1	0.4	6.05	4.63	5.44	3.92	5.45	5.10	
0.05	0.5	7.61	4.45	5.80	4.19	6.23	5.66	
0.02	0.5	13.19	9.59	8.57	5.87	6.03	8.65	
Han and He (1990)		6.92	5.25	5.83	4.13	7.32	5.89	

72

Table 6.6 (b) Calibration of recovery factor, AGD of thalweg elevation

ε	ξ	AGD						Remarks
		Time					Average	
		OCT. 2003	MAY 2004	OCT. 2004	NOV. 2005	OCT. 2006		
0.5	0.1	1.022	1.020	1.026	1.019	1.028	1.022	
0.1	0.1	1.029	1.021	1.024	1.018	1.030	1.029	
0.3	0.2	1.022	1.020	1.026	1.018	1.029	1.022	
0.1	0.2	1.026	1.017	1.024	1.016	1.027	1.026	
0.1	0.3	1.024	1.016	1.025	1.016	1.024	1.024	
0.17	0.3	1.020	1.016	1.027	1.016	1.018	1.020	Lowest
0.2	0.3	1.022	1.019	1.022	1.014	1.021	1.022	
0.05	0.4	1.027	1.017	1.024	1.016	1.026	1.027	
0.1	0.4	1.022	1.017	1.022	1.015	1.020	1.022	
0.05	0.5	1.023	1.015	1.024	1.016	1.022	1.023	
0.02	0.5	1.034	1.024	1.028	1.018	1.021	1.034	
Han and He (1990)		6.92	1.024	1.018	1.025	1.016	1.027	

Table 6.7 Calibrated recovery factor for both scour and deposition

Size group	Lower bound (mm)	Upper bound (mm)	Geometric mean (mm)	Recovery factor
1	0.002	0.004	Coarse clay	0.989
2	0.004	0.008	Very fine silt	0.803
3	0.008	0.016	Fine silt	0.652
4	0.016	0.031	Medium silt	0.532
5	0.031	0.062	Coarse silt	0.434
6	0.062	0.125	Very fine sand	0.352
7	0.125	0.25	Fine sand	0.286
8	0.25	0.5	Medium sand	0.232
9	0.5	1	Coarse sand	0.189

6.4 Xiaolangdi Reservoir Sedimentation and Flushing Simulation Results

Simulations from May 2003 to October 2006 were carried out to verify the capabilities of GSTARS4 for quasi-steady and truly unsteady flows. A total of four cases of simulations, shown in Table 6.8, were compared in this section.

All the simulations were carried out using $\Delta t = 3$ minutes and the Yang et al. (1996) sediment transport equation with the recovery factor of $\alpha_k = \dfrac{0.17}{d_k^{0.3}}$.

The simulated bed profile, bed material size, volume of sedimentation, and gradation of flushed sediment were compared with the surveyed values in the following sections.

Table 6.8 Four simulations of Xiaolangdi Reservoir from May 2003 to October 2006

Case of simulation	Flow routing	Density of bed sediment (values shown in Table 6.2)	
		In reservoir regime	In river regime
Steady_OP1	Quasi-steady	Operation No. 1	Operation No. 4
Steady_OP2		Operation No. 2	Operation No. 4
Unsteady_OP1	Truly unsteady	Operation No. 1	Operation No. 4
Unsteady_OP2		Operation No. 2	Operation No. 4

6.4.1 Thalweg Profile

Bed profiles were surveyed several times between 2003 and 2006. These surveyed profiles were compared with those computed by GSTARS4.

RMS and AGD were compared for four simulation cases, as shown in Table 6.9 (a) and (b), respectively. Simulations using sediment density of operation number 1, Steady_OP1 and Unsteady_OP1, have lower RMS and AGD than the other. However, simulations cases of "OP1" were conducted only for the comparison and density of deposited sediment in the reservoir should be operation number 2, "OP2". Steady results have lower RMS and AGD values of thalweg elevations than unsteady ones. The prediction of channel geometric changes by GSTARS4 steady and unsteady simulations should be evaluated by comparing not only thalweg elevation changes but also by cross section changes. Statistical

evaluations on the predicted cross section changes by using steady and unsteady simulations are included in section 6.4.2.

Fig. 6.11 shows comparisons between measured and simulated thalweg elevations. In Fig. 6.11 (a) ~ (d), the surveyed thalweg values are slightly lower than the simulated results near Xiaolangdi Dam because the effect of the sediment flushing gates was not considered. It was difficult to consider the effect of the low level flushing gates because the data related to the operation of these gates were not available, therefore the effects of low level outlets were not included in this study.

A comparison between operation number 1 and 2 reveals that the simulation results with operation number 2 generally have higher thalweg elevation than those with operation number 1, as shown in Figs. 6.11 (a) ~ (d). Because the sediment density of operation number 1 is lower than that of operation number 2, the simulated results with operation number 1 have lower bed elevation.

Table 6.9 (a) RMS of thalweg elevation

Case of simulation	RMS (m)					
	Time					Average
	OCT. 2003	MAY 2004	OCT. 2004	NOV. 2005	OCT. 2006	
Steady_OP1	4.95	4.08	6.46	3.87	4.13	4.70
Steady_OP2	4.99	4.15	6.42	3.83	4.55	4.79
Unsteady_OP1	5.93	5.48	6.24	3.57	5.04	5.25
Unsteady_OP2	6.28	5.90	6.42	4.24	6.04	5.78

Table 6.9 (b) AGD of thalweg elevation

Simulation	AGD					
	Time					Average
	OCT. 2003	MAY 2004	OCT. 2004	NOV. 2005	OCT. 2006	
Steady_OP1	1.020	1.016	1.027	1.016	1.015	1.019
Steady_OP2	1.020	1.016	1.027	1.016	1.018	1.020
Unsteady_OP1	1.020	1.017	1.024	1.013	1.017	1.018
Unsteady_OP2	1.022	1.020	1.025	1.018	1.022	1.021
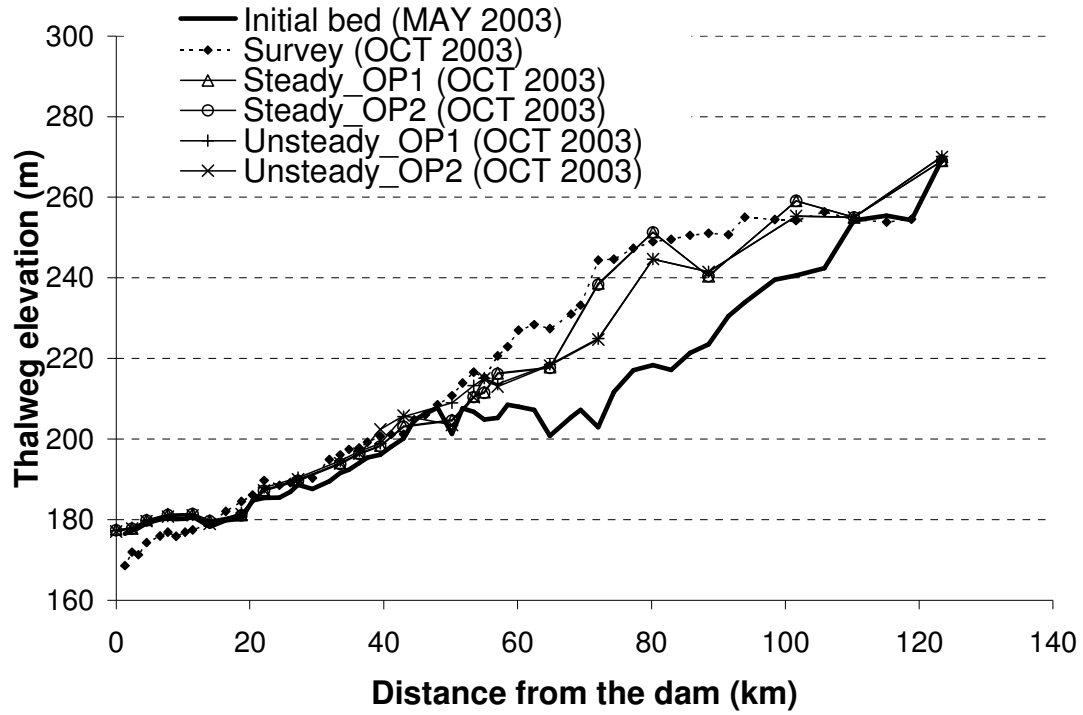
(a) October 2003
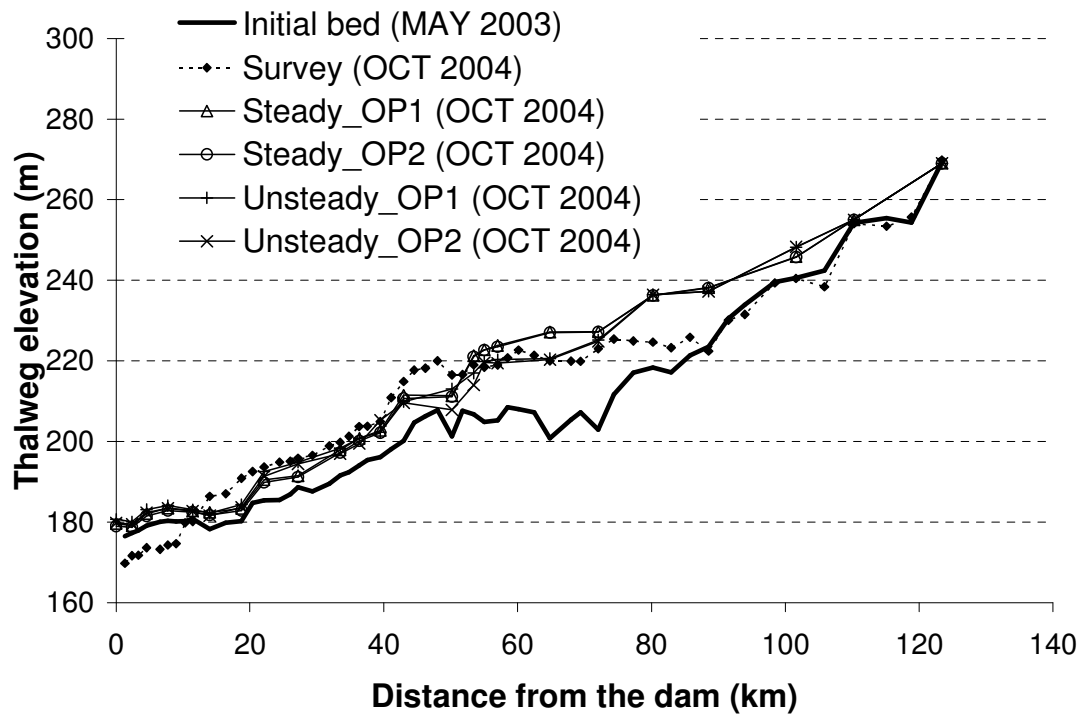
(b) October 2004

Figure 6.11 Comparison of surveyed and simulated thalweg elevations
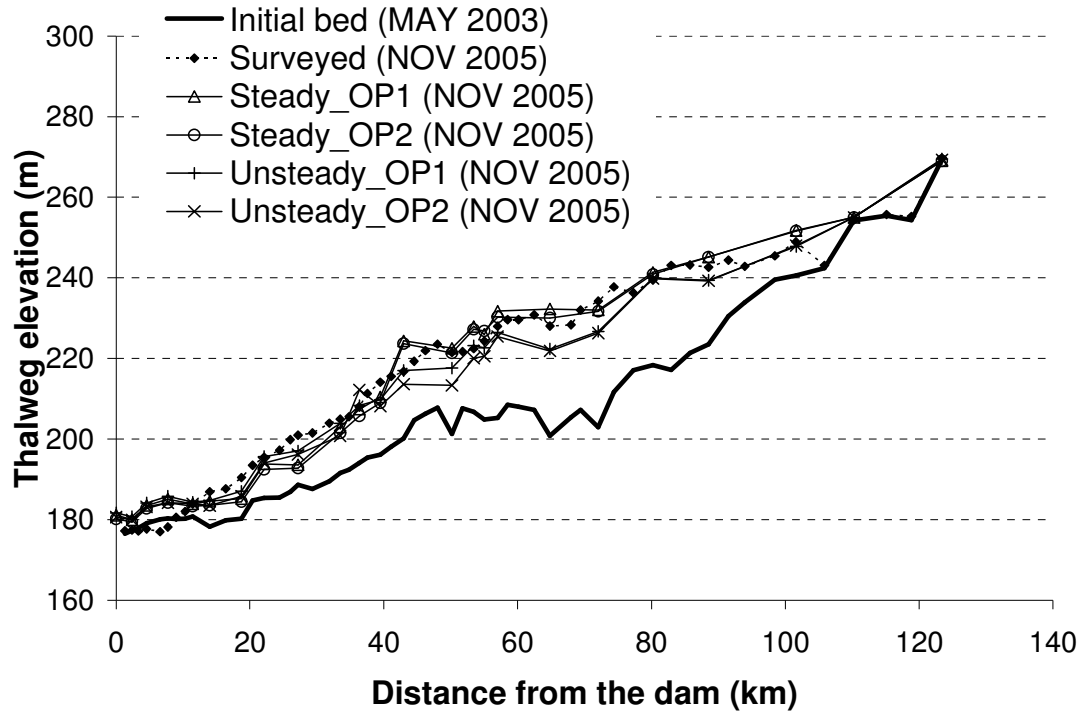
(c) November 2005
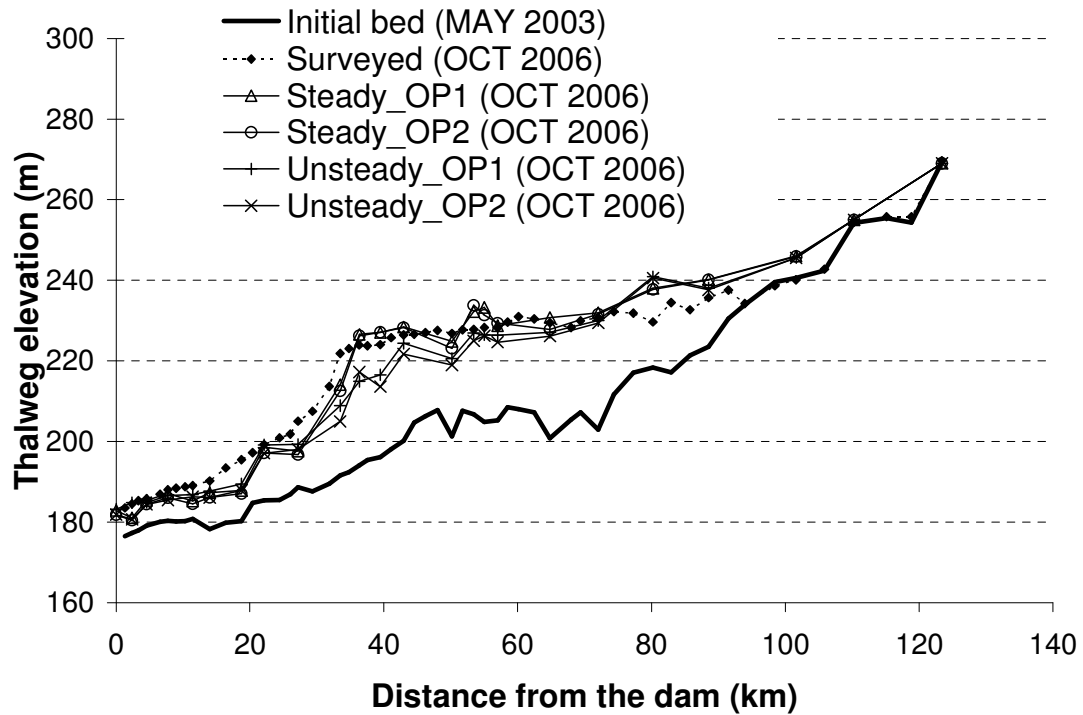
(d) October 2006

Figure 6.11 Continued

77

6.4.2 Cross Sectional Changes

Figs. 6.12 ~ 6.15 show comparisons of simulated and measured cross sections. Simulations results of steady flow reservoir operation type 1 (Steady_OP1) and unsteady flow operation type 1 (Unstead_OP1) are shown in Appendix A.

Results shown in Figs. 6.12 ~ 6.15 indicate that the steady and unsteady flow simulation results are generally in agreement with the measured results. However, the steady simulation predicts a narrowing of the river regime after October 2004. The unsteady effect in the river regime was not significant in 2003. The rate of water surface drop in 2003 was less than that of 2004, 2005, and 2006, as shown in Fig. 6.1. Water discharge from the upstream boundary in 2003 was the smallest from 2003 to 2006. Steady simulation results of October 2003 and May 2004 do not have a narrow of the cross section because the unsteady effect is small in 2003. However, the unsteady effect should be considered after May 2004 and the steady simulation predicts narrowing of the channel. Fig. 6.13 (a), (b), and (c) show the formation of a narrow channel for the steady simulation while the unsteady flow simulations predict a wide channel. A comparison of Figs. 6.12 (a) ~ (c) and Figs. 6.13 (a) ~ (c) shows scour pattern at the upper reach in October 2003 and October 2004. The unsteady flow simulation predicts more scour than the steady flow simulation results. Water discharge from the upstream boundary increases suddenly, as shown in Fig. 6.1, and variation of water stage and discharge follows loop-rating curve. The rising limb has more unit stream power, *VS*, than the falling limb because the former has higher friction slope and faster flow velocity. Therefore, both limbs have various sediment transport capacities. Unsteady simulation computes sediment transport capacities for both limbs. Sum of sediment transport capacities of

rising and falling limb from unsteady simulation is not the same as that computed from

steady simulation, because the sediment transport capacity is not liner to the unit stream

power, as shown in Eq. (3.15). The steady flow simulations show a narrowing of the river

regime after October 2004. Simulation results of the lower reach are better than those of

the upper reach. This is because upstream cross sections are directly influenced by the

discharged water and sediment from the Sanmenxia Reservoir. Scour and deposition in

the lower reaches, about 10 ~ 60 km above the Xiaolangdi dam, is less dependent on the

upstream condition. Figs. 6.13 (a), (b), and (c) show the scour due to drawdown flushing.

The unsteady flow simulations show similar results. The scour in the upper reach was

mainly caused by water discharged from the upstream Sanmenxia Reservoir. The trend

also can be found in Fig. 6.1. Because water and sediment discharge from Sanmenxia

Dam varies rapidly, the unsteady effect should be considered for this study area. The

predicted channel cross section changes in the reservoir regime, from Xiaolangdi Dam to

50 ~ 60 km above it, are close to measurements because the effect of water flow released

from the upstream dam attenuates as it goes downstream and the unsteady effects

decrease.

To evaluate the performance of both steady and unsteady simulation, RMS and AGD

were computed for each cross section by using Eqs, (6.7) and (6.8), respectively. Figs.

6.16 and 6.17 show comparison of statistical parameters of steady and unsteady

simulations, respectively. Steady simulation results of the lower reach are better than

those of the upper reach because the unsteady effect due to sudden release of water from

the upstream boundary diminished in the downstream direction, as shown in Fig. 6.16.

Fig. 6.16 (a) indicates that RMS values in October 2003 and May 2004 are all lower than

8 m along the study area. However, RMS values after October 2004, increased significantly in the upper reach, because the steady simulation predicted narrower channel. Similarly trend was also found for AGD values, as shown in Fig. 6.16 (b). Fig. 6.17 (a) and (b) show RMS and AGD of unsteady simulation and there is no increase of both parameters in the upper reach after October 2004.

Averaged values of RMS and AGD are summarized in Table 6.10 (a) and (b), respectively. As described above, RMS and AGD values were computed for every cross section at every time of comparison. Values shown at each line is the averaged RMS and AGD of all the cross sections. For example, values on line (1) of Table 6.10 (a) are the averages of RMS along the study area in October 2003. Before May 2004, steady simulation has lower RMS than unsteady by 0.2 ~ 0.4 m. However, steady simulation has higher RMS by 1.3 ~ 2.5 m after October 2004. Unsteady simulation has lower RMS. The same trend is found with AGD values, as summarized in Fig. 6.10 (b). Unsteady simulation has better prediction of cross section geometry changes, especially for the upper reach due to sudden inflow of water sediment from the upstream Sanmenxia reservoir, because unsteady flow simulation can compute sediment transport capacities of the rising and fall stages of the sudden inflow.
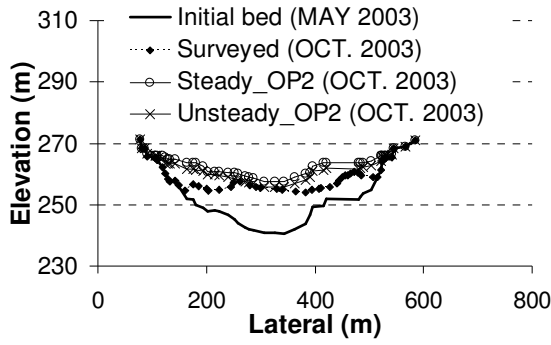
(a) 101.6 km above Xiaolangdi dam   (b) 80.2 km
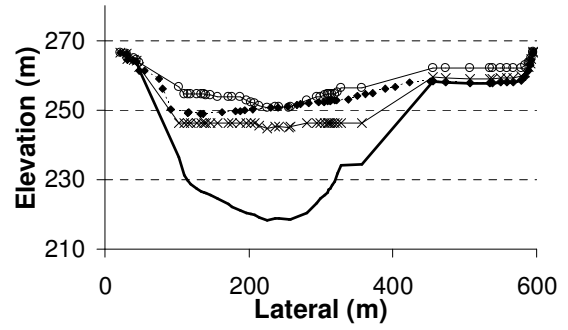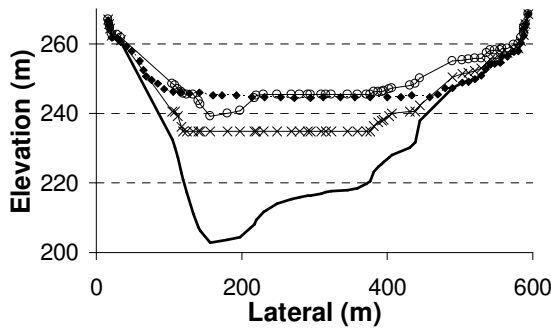
(c) 72.1km   (d) 57.0km
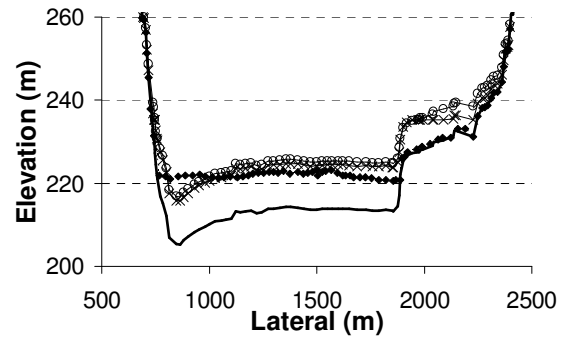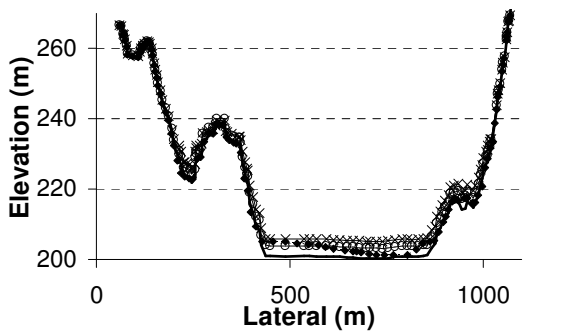
(e) 43.0 km   (f) 27.2 km
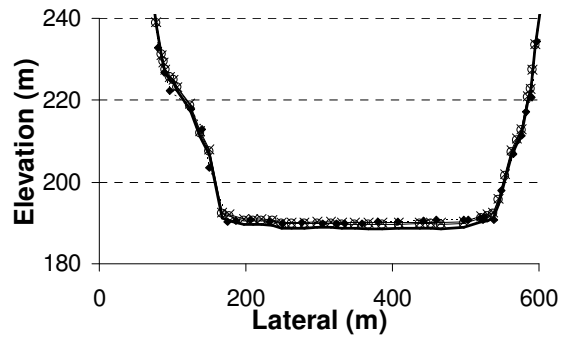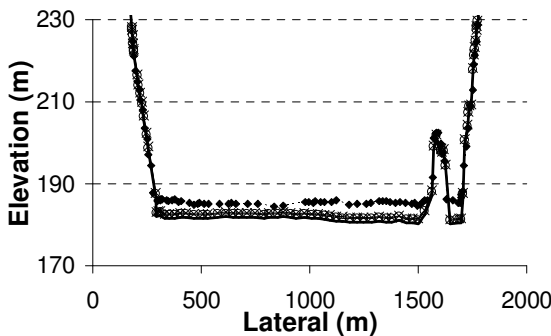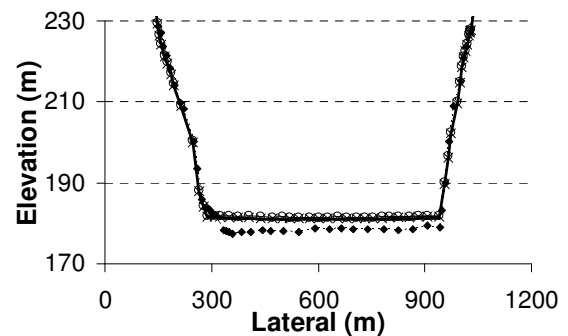
(g) 18.7 km   (h) 11.4 km

Figure 6.12 Comparisons between measured and GSTARS4 simulation results, October 2003

(a) 101.6 km above Xiaolangdi dam

(b) 80.2 km

(c) 72.1km

(d) 57.0km

(e) 43.0 km

(f) 27.2 km

(g) 18.7 km

(h) 11.4 km
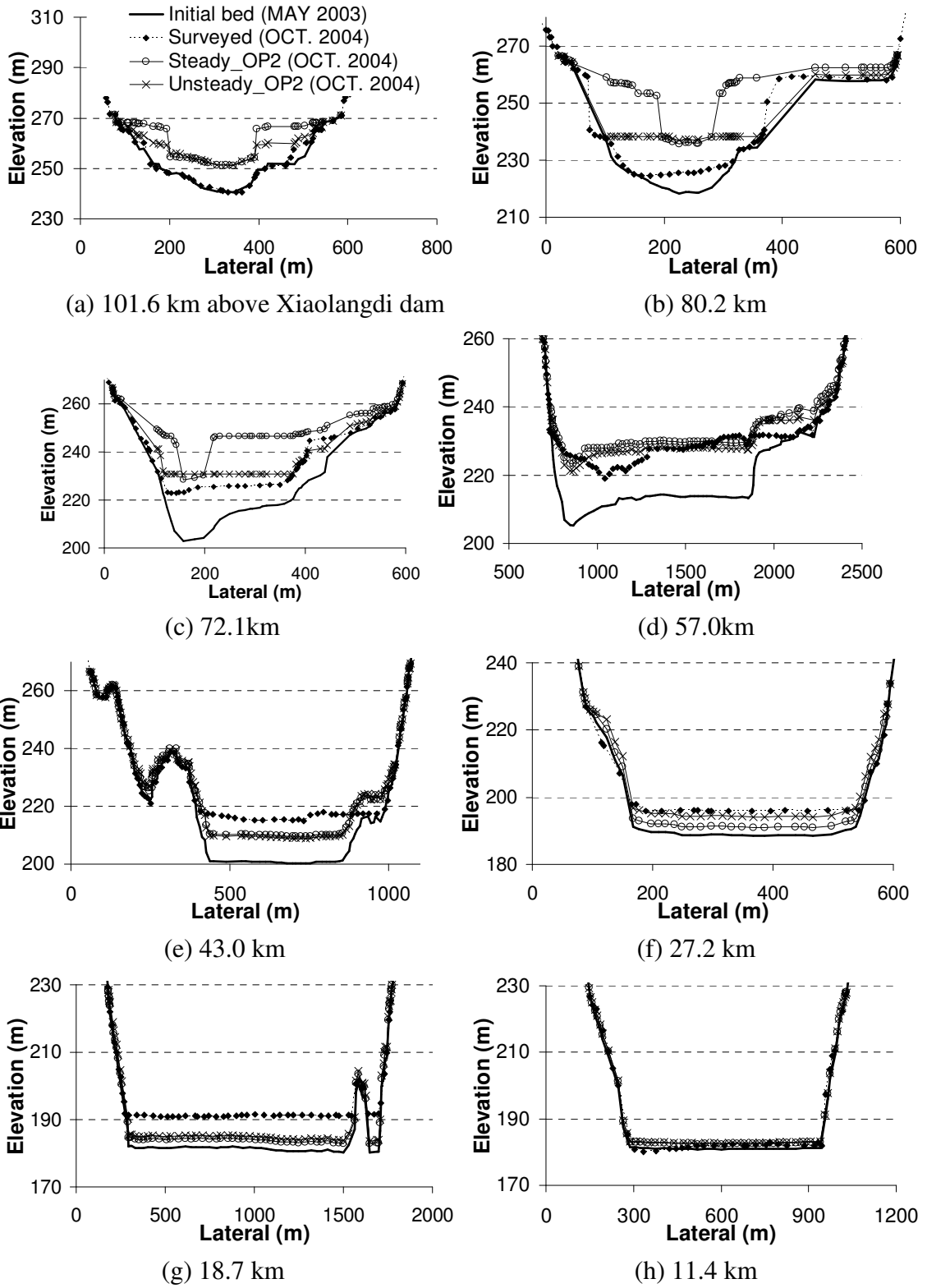
Figure 6.13 Comparisons between measured and GSTARS4 simulation results, October

2004
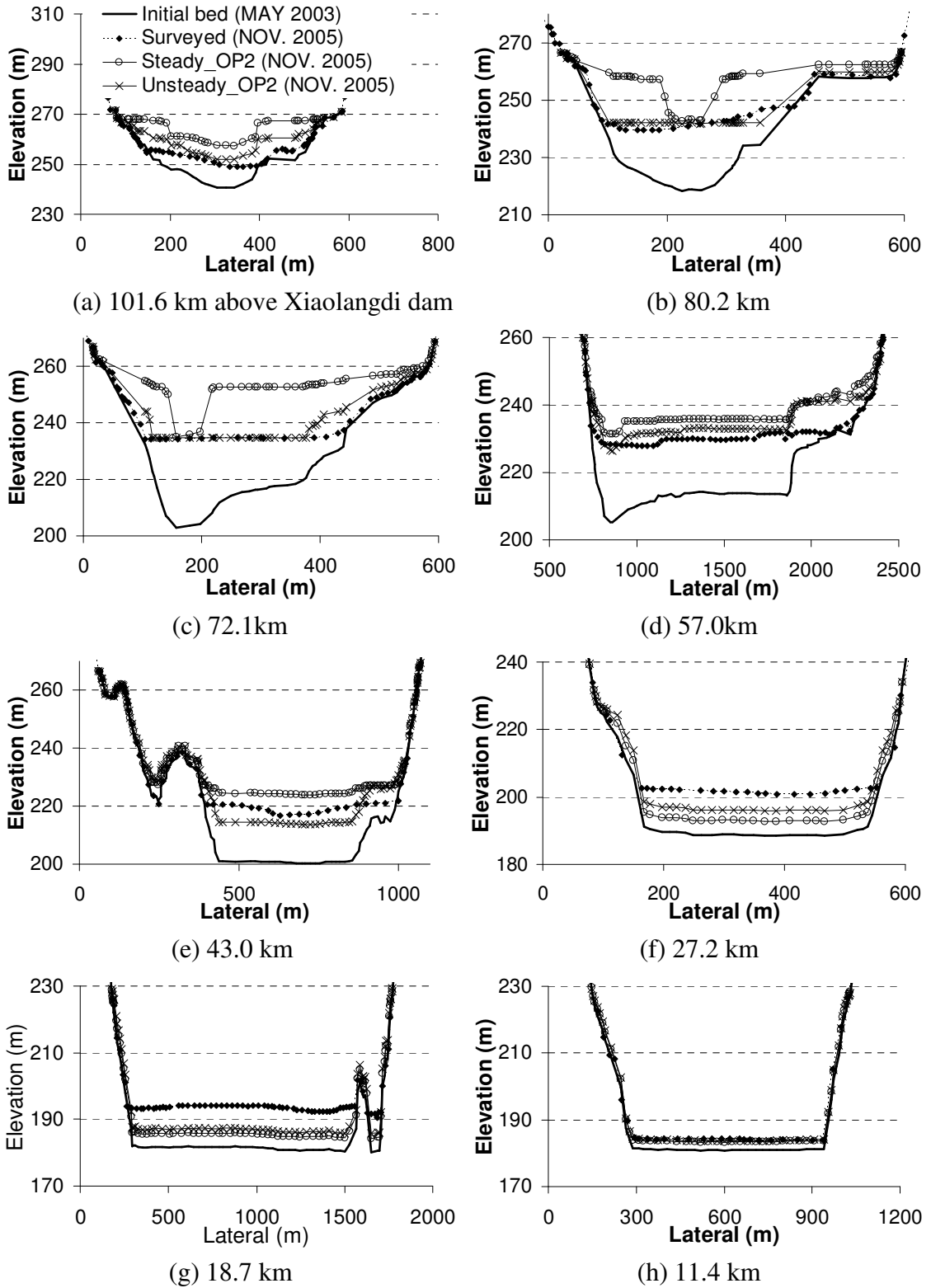
Figure 6.14 Comparisons between measured and GSTARS4 simulation results,

November 2005
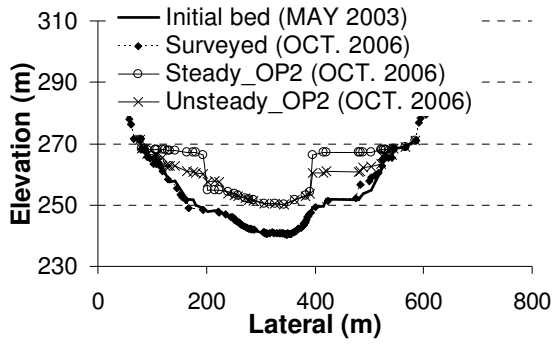
(a) 101.6 km above Xiaolangdi dam
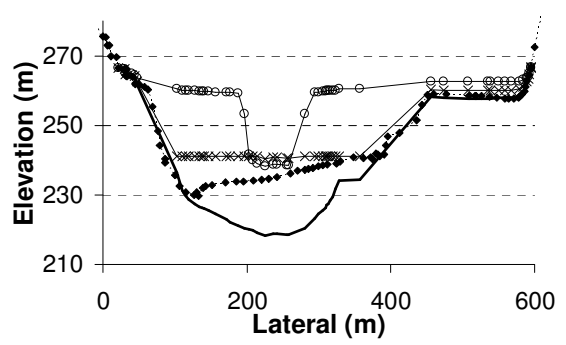
(b) 80.2 km
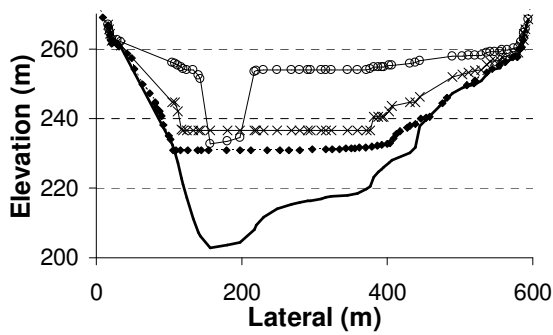
(c) 72.1km
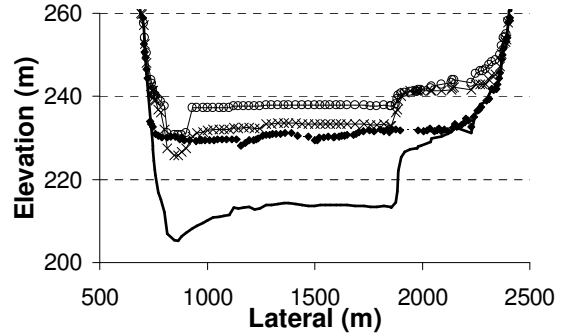
(d) 57.0km
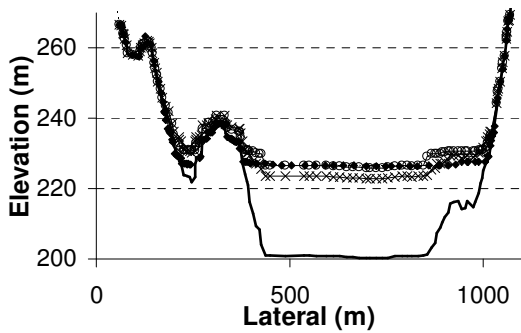
(e) 43.0 km
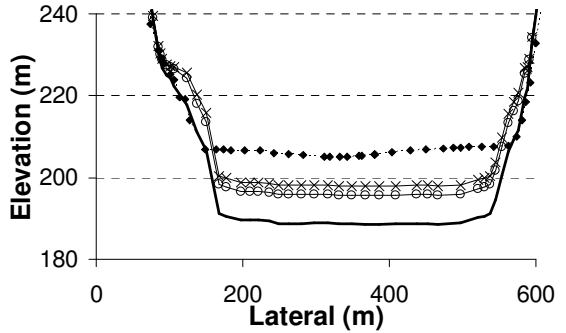
(f) 27.2 km
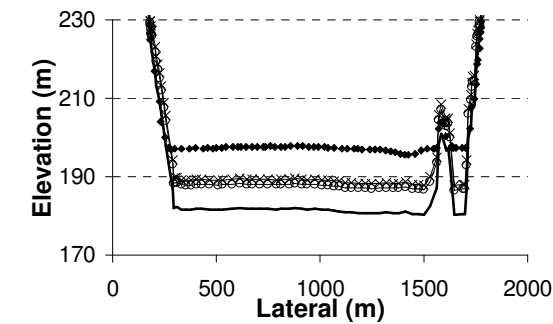
(g) 18.7 km
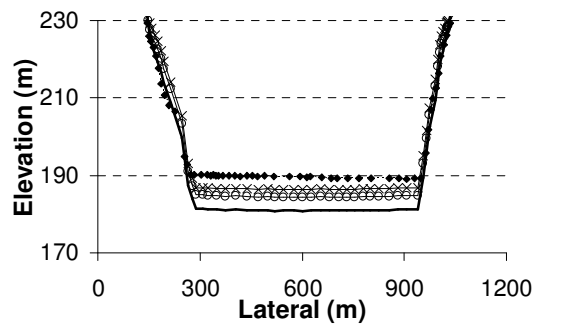
(h) 11.4 km

Figure 6.15 Comparisons between measured and GSTARS4 simulation results, October

2006

(a) RMS   (b) AGD
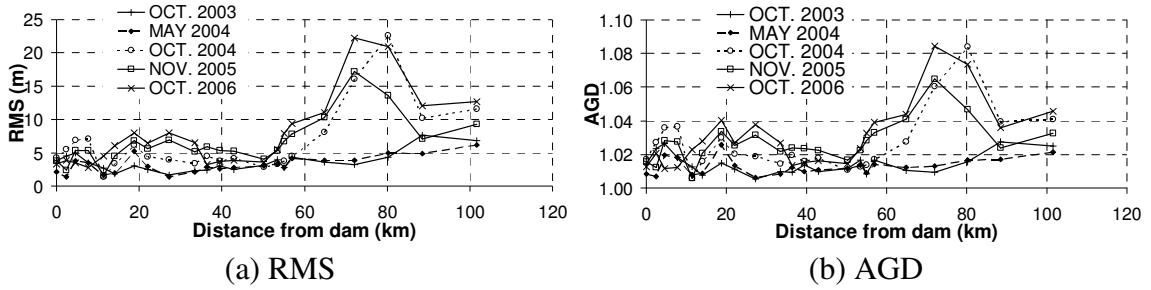
Figure 6.16 Comparison of goodness-of-fit between Steady_OP2 and measured results

(a) RMS   (b) AGD
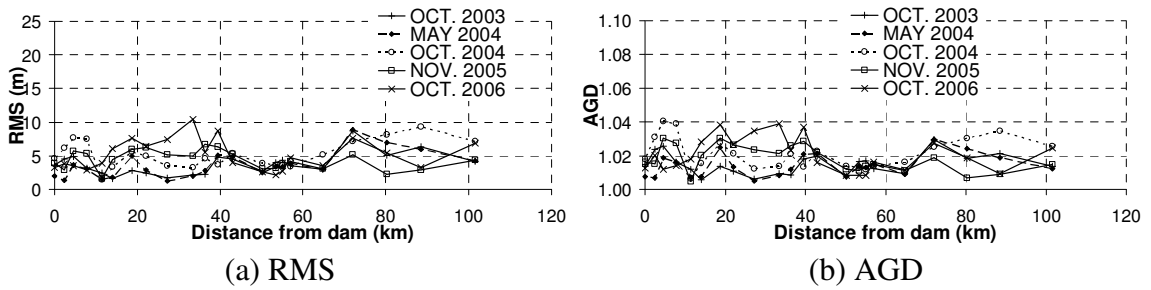
Figure 6.17 Comparison of goodness-of-fit between Unsteady_OP2 and measured results

Table 6.10 (a) Averaged RMS of cross section data

| Case of simulation | RMS (m) | | | | | |
| | Time | | | | | Overall (average of 1~5) |
	OCT. 2003 (1)	MAY 2004 (2)	OCT. 2004 (3)	NOV. 2005 (4)	OCT. 2006 (5)	
Steady_OP2	3.56	3.23	6.45	6.60	7.68	5.50
Unsteady_OP2	3.76	3.63	5.14	4.38	5.10	4.40

Table 6.10 (b) Averaged AGD of cross section data

| Case of simulation | AGD | | | | | |
| | Time | | | | | Overall (average of 1~5) |
	OCT. 2003 (1)	MAY 2004 (2)	OCT. 2004 (3)	NOV. 2005 (4)	OCT. 2006 (5)	
Steady_OP2	1.014	1.013	1.026	1.027	1.031	1.022
Unsteady_OP2	1.015	1.014	1.021	1.018	1.021	1.018

85

6.4.3 Bed Material Size

Fig. 6.18 shows comparisons between simulated and measured bed material sizes. The measured and simulated results of sediment size distributions generally decrease in the downstream direction. For the upper reach, the measured bed material size was mainly determined by the sediment release from the upstream Sanmenxia Reservoir. It takes time and distance for the sediment released from the Sanmenxia Reservoir to be fully mixed with the sediments in the Xiaolangdi Reservoir. This may explain why there are some discrepancies between the simulated results from GSTARS4 and the measured bed material size in the upper part of the study area, as shown in Fig. 6.18 (c) and 6.18 (e).

The Xiaolangdi Reservoir delta was formed at about 60 km to 80 km, where bed material size varies significantly, as shown in Figs 6.18 (b) ~ (e). At the toe of the delta or at about 60 km above the dam, sediment transport and mixing are active. The predicted bed material sizes with steady and unsteady simulations were evaluated by using RMS and AGD. Similar to Eq. (6.7) and (6.8), these parameters can be computed from the following equations.

(1) RMS

$$\text{RMS} = \left[\sum_{j=1}^{J} \left(d_{50,cj} - d_{50,mj} \right)^2 / J \right]^{1/2} \tag{6.9}$$

where $d_{50,c}$ and $d_{50,m}$ = computed and measured mean bed material size in mm, respectively. The unit of RMS for bed material size is in mm.

(2) AGD

$$\text{AGD} = \left[\prod_{j=1}^{J} R_j \right]^{1/J}, \quad R_j = \begin{bmatrix} d_{50,cj} / d_{50,mj} & \text{for } d_{50,cj} \geq d_{50,mj} \\ d_{50,mj} / d_{50,cj} & \text{for } d_{50,cj} < d_{50,mj} \end{bmatrix} \tag{6.10}$$

AGD for mean bed material size is a dimensionless parameter.

Comparison of RMS and AGD are summarized in Table 6.11 (a) and (b). Unsteady simulation has slightly lower average values of RMS and AGD than those for steady simulation. Typically, bed material is very fine and the size does not vary significantly in the reservoir regime regardless of the location. There is an abrupt change of bed material size near the reservoir delta and d_{50} in the river regime is much coarser than in the reservoir. Measured bed material size distribution in the study area has the same trend as described in section 6.1.2. Computed d_{50}, for steady and unsteady simulations, agrees with typical bed material size profile. Measured d_{50} profiles have some variations or oscillations even in the reservoir reach, as shown in Fig. 6.18 (b) ~ (e) and there is an abrupt change of measured d_{50}, around 100 km in Fig. 6.18 (c). It is possible that these uncommon variations of measured d_{50} profile were due to the difficulty of bed material measurements. These results indicate that GSTARS4 can be used to predict the variation of bed material size distribution along the study area for a combination of both river and reservoir regimes with RMS of 0.0151 ~ 0.0155 mm and AGD of 1.55 ~ 1.80 for the Xiaolangdi Reservoir.

Table 6.11 (a) RMS of mean bed material size

Case of simulation	RMS (mm)					
	Time					Average
	OCT. 2003	MAY 2004	OCT. 2004	APR. 2005	NOV. 2005	
Steady_OP2	0.0089	0.0148	0.0204	0.0104	0.0232	0.0155
Unsteady_OP2	0.0068	0.0173	0.0225	0.0069	0.0220	0.0151

Table 6.11 (b) AGD of mean bed material size

Case of simulation	AGD					
	Time					Average
	OCT. 2003	MAY 2004	OCT. 2004	APR. 2005	NOV. 2005	
Steady_OP2	1.35	1.62	1.88	2.05	2.12	1.80
Unsteady_OP2	1.28	1.40	1.96	1.56	1.54	1.55

(a) October 2003

(b) May 2004

(c) October 2004

(d) April 2005

(e) November 2005
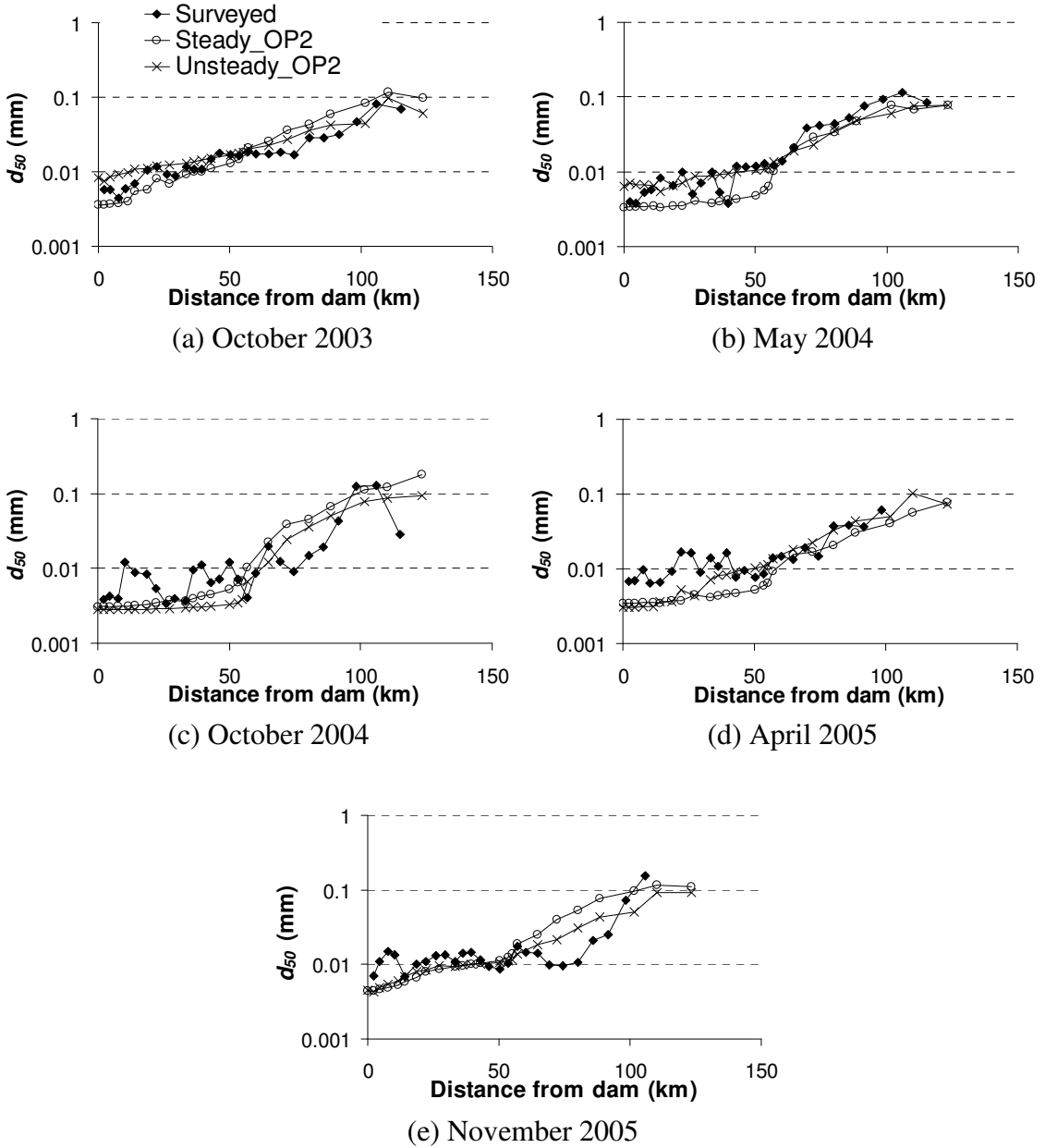
Figure 6.18 Comparisons of bed material size variations

6.4.4 Yearly Reservoir Sedimentation

The total amount of sedimentation in the Xiaolangdi Reservoir was computed with the following two methods. The first method compared sediment inflow and outflow. Sediment inflow into the Xiaolangdi Reservoir was computed by the product of water inflow and sediment concentration from the upstream Sanmenxia Reservoir. The amount of sediment flushed out of the Xiaolangdi Reservoir can also be computed as the product of outflow discharge and sediment concentration. The second method compares the surveyed reservoir volumes before and after each flushing. The reservoir volume was surveyed more than twice a year. These surveys were made at the beginning and end of each flushing. Therefore, the difference between the two sets of surveyed reservoir volumes give the total amount of sediment flushed out.

Table 6.12 and Fig. 6.19 show comparisons of sedimentation volume using three different methods. "Measured (in-out)" is based on the product of measured discharge and concentration at the upstream and downstream boundaries, i.e., Sanmenxia Dam and Xiaolangdi Dam. "Steady_OP2 (in-out)" and "Unsteady_OP2 (in-out) is based on the simulated discharge and concentration at the downstream boundary, Xiaolangdi Dam, using steady and unsteady flow simulations. "Measured reservoir change" is based on a comparison between the measured reservoir volume before and after flushing.

The results in Table 6.12 and Fig. 6.19 indicate that the simulated volume of sedimentation using GSTARS4 agrees reasonably well with measured results. The total volume of sedimentation in the Xiaolangdi Reservoir from May 2003 to October 2006 is

about 12×10^8 m^3. Both steady and unsteady simulations predicted the volumes of sedimentation are in the same order of magnitude. With the exception of the first year when the flow regime changed drastically from a river to a reservoir, the unsteady flow simulation agrees slightly better with the measured data than the steady flow simulation. Steady simulation slightly under estimates the total volume of sedimentation from 2004 because, the unsteady effect should be considered from 2004, as mentioned in section 6.4.2. Volume of sedimentation was measured for four years. Four measurement results were used to computed RMS and AGD for both steady and unsteady simulations.

(1) RMS

$$\text{RMS} = \left[\sum_{j=1}^{4} \left(V_{R,cj} - V_{R,mj} \right)^2 / 4 \right]^{1/2} \tag{6.11}$$

where $V_{R,c}$ and $V_{R,m}$ = computed and measured volume of sedimentation in m^3, respectively. The unit of RMS for the volume of sedimentation is in m^3 in this study.

(2) AGD

$$\text{AGD} = \left[\prod_{j=1}^{4} R_j \right]^{1/4}, \quad R_j = \begin{bmatrix} V_{R,cj} / V_{R,mj} & \text{for } V_{R,cj} \geq V_{R,mj} \\ V_{R,mj} / V_{R,cj} & \text{for } V_{R,cj} < V_{R,mj} \end{bmatrix} \tag{6.12}$$

The goodness-of-fit evaluation between measured and simulated volume of sedimentation are summarized in Table 6.13. The ratio between RMS and total volume of sedimentation was computed as

$$\text{Ratio} = \frac{\text{RMS}}{\text{Surveyed total volume of sedimentation } (=12.2 \times 10^8 \text{ m}^3)} \tag{6.13}$$

The ratio between RMS and measured total volume of sedimentation in the Reservoir, 12.2×10^8 m^3, is less than 5% for both steady and unsteady simulations. Because steady

simulation has lower RMS but higher AGD, both steady and unsteady simulations are good for predicting volume of sedimentation.

Although the simulated volume of sedimentation using GSTARS4 are reasonably accurate, more studies and field observations should be made before the model can be applied for long-term prediction with confidence under different reservoir operation plans.

Table 6.12 Comparison of measured and simulated sedimentation volume

Year	Sedimentation Volume ($\times 10^8$ m^3)			
	Measured (in-out)	Measured reservoir volume change	Steady_OP2 (in-out)	Unsteady_OP2 (in-out)
2003	6.1	4.80	6.3	7.3
2004	1.0	0.55	0.5	1.3
2005	3.3	3.35	2.6	3.4
2006	1.8	3.43	1.1	1.7
Total	12.2	12.1	10.5	13.6
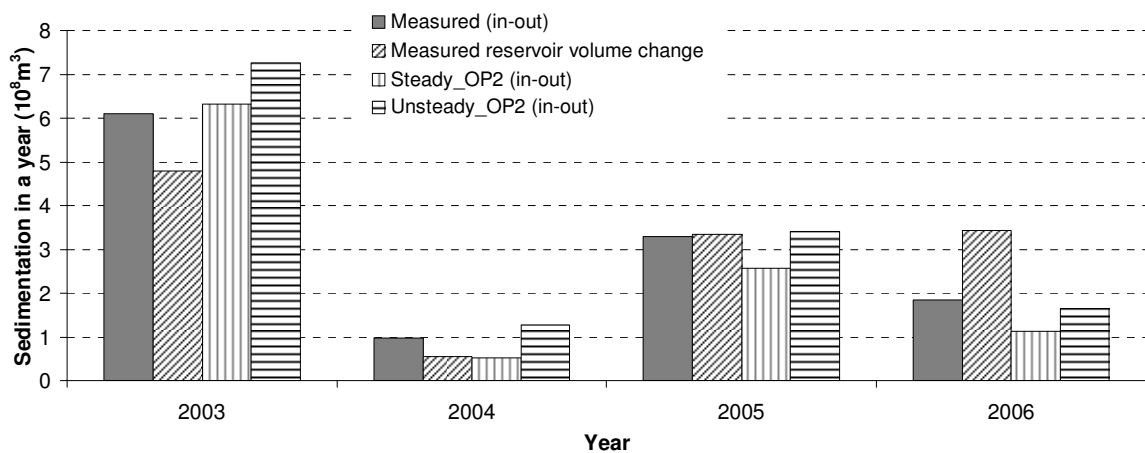
Figure 6.19 Measured and simulated sedimentation volumes

Table 6.13 Comparison of measured and simulated sedimentation volume

Simulations case	RMS	Ratio (RMS/measured sedimentation)	AGD
Steady_OP2	5.69×10^7 m^3	4.67 %	1.42
Unsteady_OP2	6.08×10^7 m^3	4.98 %	1.16

6.4.5 Gradation of Flushed Sediment

Gradation of flushed sediment is important for the study of flushing impacts downstream. Figs. 6.20 (a) ~ (d) show gradations of incoming sediment from the upstream reservoir and flushed sediment out of the Xiaolangdi Reservoir. "Measured in" stands for sediment input from the upstream boundary and is used as the upstream boundary condition. "Measured out" is based on the measurement of sediment concentration at Xiaolangdi Dam. "Steady_OP2 out" and "Unsteady_OP2 out" are based on the simulated results with operation type 2 with steady and unsteady schemes, respectively.

The sediment input from the upstream reservoir is coarser than that flushed out of the Xiaolangdi Reservoir. One of the objectives of the Xiaolangdi Reservoir operation is to regulate sedimentation volume and sediment size distribution. It is desirable to flush fine sediment rather than coarse materials so flushed sediments can be transported to the sea. Steady and unsteady simulations do not show any significant difference in the gradation of flushed sediment. Simulated gradation of flushed sediment both with steady and unsteady is coarser than the measured data, especially in years 2004 and 2005. The gradation of flushed sediment is affected by the shape and location of the outlet. In the Xiaolangdi Reservoir, deposited sediment was flushed through a low level outlet. However, the low level outlet was not considered, because required field data were not available. This study focuses on the general trend along the 120 km reach of study during 3.5 years of operation with a 1D model. Simulation of sediment scour and transport near the low level outlet may require a 2D or 3D model.
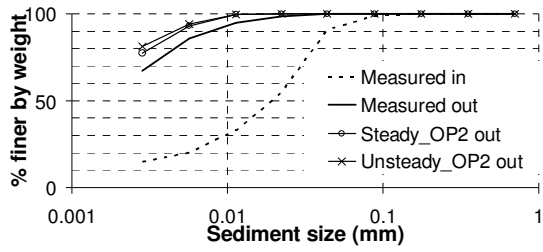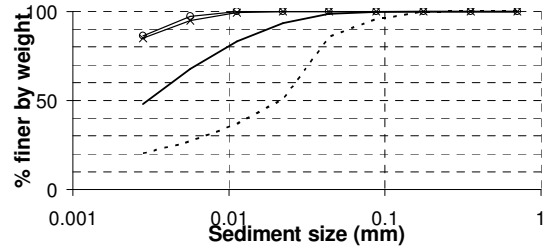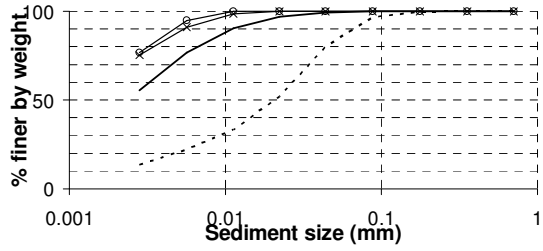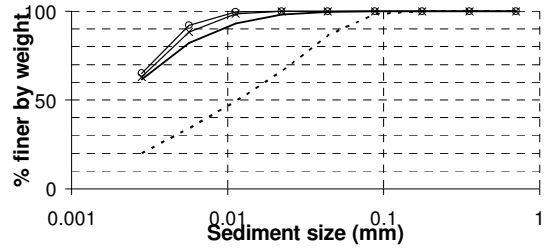
Figure 6.20 Comparisons of incoming and flushed sediment gradation

CHAPTER 7. SUMMARY

7.1 Summary and Conclusions

The GSTARS4 model uses an uncoupled scheme to simulate flow and channel adjustments. GSTARS4 is based mainly on GSTARS3. GSTARS3 can be applied to most reservoir sedimentation studies. However, flow and sediment transport mechanisms in the Xiaolangdi Reservoir are very complicated and some of the assumptions made in the GSTARS3 model may not be valid to fully simulate sedimentation and drawdown flushing processes of the Xiaolangdi Reservoir. Development of the GSTARS4 model can be divided into two categories. One is the addition of unsteady flow routing and the other one is the revision of sediment routing. GSTARS3 can simulate the flow with steady or quasi-steady schemes. The more advanced unsteady flow scheme adopted from the SRH-1D model was modified and further improved and included in the GSTARS4 model for fully unsteady flow simulations.

Due to the high sediment concentration in the study reach, time step Δt and distance between cross sections Δx should be determined carefully to assure stable computational results. If the rate of change of the channel bed is not small enough compared to the water depth within a time step of computation, it is possible that the computed results may not be stable. Stability criteria for GSTARS steady and unsteady simulations were derived in chapter 5 and applied to determine Δt and Δx for the Xiaolangdi Reservoir simulation.

The study reach is about 120 km long from the downstream boundary, Xiaolangdi Dam, to the upstream boundary, Sanmenxia Dam. Incoming water and sediment discharges from the upstream Sanmenxia Reservoir were used as the upstream boundary conditions in the numerical simulation. Sedimentation process and water flow in the Xiaolangdi Reservoir are directly affected by water and sediment released from the Sanmenxia Reservoir. In the upstream reach, just downstream of the Sanmenxia Reservoir, the channel flow is in the river regime. In the downstream reach, where back water effects apply, it is in the reservoir regime. Complexity of the simulation arises from the study area consisting of two regimes, a river and reservoir regime. One major difference between the two regimes is the density of sediment deposited on the bed. GSTARS4 can use various densities of deposited sediment in the study area. Site-specific coefficients, such as Manning's n and recovery factor were calibrated and determined for the Xiaolangdi Reservoir.

GSTARS4 was applied to simulate and predict the Xiaolangdi Reservoir variations of longitudinal profile, cross section, bed material size, and the amount of sedimentation between May 2003 ~ October 2006. The goodness-of-fit of both steady and unsteady simulations were evaluated by computing two statistical parameters, RMS and AGD. Application of the GSTARS4 model to simulate the Xiaolangdi Reservoir sedimentation and flushing processes produced the following results:

1) The simulated longitudinal bed profiles along the study reach, for steady and unsteady simulations, are generally in good agreement with surveyed profiles, RMS (4.79 m for steady and 5.78 for unsteady) and AGD (1.020 for steam and 1.021 for unsteady). Especially in the lower reach of study area, computed profiles are in good agreement with the measured ones.

2) Evaluation of overall goodness-of-fit of cross section geometry indicated that the unsteady simulation predicted the cross section geometry closer than the steady simulation for entire 120 km of study area. In the reservoir regime, steady and unsteady routing predicted almost the same cross section and the predictions are in good agreement with the measured channel geometry. Both steady and unsteady simulations have RMS (less than 10 m) and AGD (less than 1.04) in the reservoir regime. However, unsteady routing predicts more reasonable channel cross sectional shape than the steady flow simulation in the upstream reach the river regime. In the upstream reaches, the steady simulation has increased RMS (from about 5 to 22 m) and AGD (from 1.02 to 1.08) after October 2004, 1.5 year of routing. The unsteady effects in the upper reach are more significant than in the lower reach. The release of sediments and water from the upstream Sanmenxia Reservoir can have a significant influence on the cross section profile and bed material size distribution in the upper study reach near the upstream Sanmenxia dam.

3) Simulated bed material size using GSTARS4 steady and unsteady simulations indicates that predicted bed material follows typical reservoir sedimentation pattern with finer material in the reservoir and coarser material above the

reservoir delta. Unsteady simulation has slightly better result of prediction of d_{50} than steady simulation, because the former has RMS of 0.0151 mm and AGD of 1.55, while 0.0155 mm and 1.80 for the latter.

4) The ratio between RMS and surveyed total volume of sedimentation is less than 5 % for steady and unsteady simulations.

5) The simulated and measured gradations of flushed sediment are encouraging because the Xiaolangdi Reservoir can store coarser materials and flush finer sediments to the downstream Yellow River, reducing the possibility of downstream deposition.

6) The simulated results using GSTARS4 are in general agreement with measured results between 2003 and 2006. However, this does not necessarily mean that the model can be used with confidence for long term simulation of 10, 20, or 30 years without further verifications. The erosion and sedimentation processes of the Xiaolangdi Reservoir are complex, and require long term observations of the reservoir's operations and their impacts on reservoir sedimentation.

7.2 Contributions

The studies in this dissertation have advanced the technology of numerical modeling of reservoir sedimentation and flushing in the following areas:

1) GSTARS4 was developed by modifying GSTARS3 and SRH-1D to simulate steady and unsteady flow sedimentation and flushing processes in reservoirs.

2) Stability criteria for GSTARS4 modeling of sediment transport and channel geometric changes was derived mathematically.

3) The procedure for the numerical simulation of reservoir sediment erosion, transport, and deposition was developed using the Xiaolangdi Reservoir field data. Data, required for boundary condition and calibration of coefficients, such as Manning's *n* and recovery factor, for reservoir sedimentation and flushing simulation, were determined.

7.3 Recommendations for Future Studies

This study focused on the general trend of scour and deposition along a 120 km reach of the Xiaolangdi Reservoir in 3.5 years using the 1D model GSTARS4, developed for one dimensional long term and long reach simulation.2D or 3D models should be considered to simulate sediment scour and transport near the low level outlet.

It is desirable to have a long term simulation with a master plan of reservoir operation. Long term observation of the Xiaolangdi Reservoir operation is important to understand the long term reservoir sedimentation process. Long term simulation in the Xiaolangdi Reservoir verified with field observation with different operational plans may be a good case study for the reservoir sedimentation model.

Optimization of flushing efficiency may be valuable for future implementation of drawdown flushing. Flushing efficiency may be improved by increasing the flow rate or duration of flushing. However, the more water used for flushing, the less water resources would be left. Therefore, it is better to have an optimized flushing efficiency by carefully scheduling the flow rate and the duration of flushing.

REFERENCES

Ackers, P., and White, W.R. (1973). "Sediment transport: new approach and analysis," *Journal of the Hydraulic Division*, ASCE, Vol. 99, No. HY11, pp. 2041-2060.

Armanini, A., and Di Sivio, G. (1988) "A one-dimensional model for the transport of a sediment mixture in non-equilibrium condition." *Journal of Hydraulic Research*, Vol.26, No.3, pp. 275-292.

Ashida, K., and Michiue, M. (1970). "Study on suspended sediment (1)," *Annals DPRI*, No. 13B, pp. 233-242. (In Japanese.)

Atkinson, E. (1996). *Feasibility of flushing sediment from reservoirs*, Report OD 137, HR Wallingford, UK.

Chang, H. H., (1988). *Fluvial Processes in River Engineering*, John Wiley and Sons, New York.

Chang, H. H., Harrison, L. L., Lee, W., and Tu, S., (1996). "Numerical modeling for sediment-pass-though reservoirs," *Journal of Hydraulic Engineering*, ASCE, Vol. 122, No. 7, pp. 381-388.

Chen, D., Acharya, K., and Stone, M. (2010) "Sensitivity Analysis of Nonequilibrium Adaptation Parameters for Modeling Mining-Pit Migration." *Journal of Hydraulic Engineering*, ASCE, Vol.136, No.10, pp.806-811.

De Vries, M. (1971). *Solving River Problems by Hydraulic and Mathematical Models*, Delft Hydraulic Laboratory, Delft, The Netherlands.

DuBoys, M.P. (1879). "Le Rhône et les rivières à lit affouillable," *Annals de Ponts et Chaussée*, Vol. 18, No. 5, pp. 141-195 (In French).

Engelund, F., and Hansen, E. (1972). *A monograph on sediment transport in alluvial streams,* Teknish Forlag, Technical Press, Copenhagen, Denmark.

Fan, J. (1986). "Turbid density currents in reservoirs," *Water Int.*, Vol. 11, No. 3, pp. 107-116.

Fan, J., and Morris, G. L. (1992a). "Reservoir Sedimentation. I: Delta and Density Current Deposits." *Journal of Hydraulic Engineering*, ASCE, Vol. 118, No. 3, pp. 354-369.

Fan, J., and Morris, G. L. (1992b). "Reservoir Sedimentation. II: Reservoir Desiltation and Long-Term Storage Capacity." *Journal of Hydraulic Engineering*, ASCE, Vol. 118, No. 3, pp. 370-383.

Han, Q. (1980). "A Study on the Nonequilibrium Transportation of Suspended Load," *Proceedings of the International Symposium on River Sedimentation*, Beijing, China, pp. 793-802. (In Chinese.).

Han, Q. (2003). *Reservoir sedimentation*, Science Publication, Beijing (in Chinese).

Han, Q. (2006). "Diffusion Equation Boundary Condition and Recovery Coefficient," *Journal of Changsha University of Science and Technology,* Vol. 3, No. 3, pp. 7-19. (in Chinese).

Han, Q., and He, M. (1990). "A Mathematical Model for Reservoir Sedimentation and Fluvial Processes," *International Journal of Sediment Research*, vol. 5, no. 2, IRTCES, pp. 43-84.

Henderson, F.M. (1966). *Open channel flow*, MacMillan Book Company, New York, NY.

Huang, J. V., and Greimann B. (2007) *User's Manual for SRH-1D V2.0 (Sedimentation and River Hydraulics – One Dimension, Version 2.0)*, Technical Service Center, U.S. Bureau of Reclamation, Denver, Colorado.

Hwang, J. S. (1985). "The study and planning of reservoir desilting in Taiwan," *Water International*, Vol. 10, pp. 7-13.

IRTCES (1985). *Lecture notes of the training course on reservoir sedimentation*, International Research and Training Center on Erosion and Sedimentation, Sediment Research Laboratory of Tsinghua University, Beijing, China.

Julien, P. Y. (1998). *Erosion and Sedimentation*, Cambridge University Press, Cambridge, UK.

Julien, P. Y. (2002). *River Mechanics*, Cambridge University Press, New York.

Laursen, E.M.(1958). "The total sediment load of streams," *Journal of the Hydraulic Division*, ASCE, Vol. 84, No. 1, pp. 1530-1–1530-36.

Madden, E., (1993). *Modified Laursen method for estimating bed-material sediment load*, USACE-WES, Contract Report HL-93-3.

Mahmood, K. (1987). "Reservoir sedimentation: impact, extent and mitigation," World Bank Technical Paper, No. 71.

Meyer-Peter, E., and Müller, R. (1948). "Formula for bed-load transport," *Proceeding of the Int. Assoc. for Hydraulic Research*, 2nd Meeting, Stockholm.

Molinas, A., and Yang, C. T. (1986). *Computer Program User's Manual for GSTARS (Generalized Stream Tube model for Alluvial River Simulation)*, Technical Service Center, U.S. Bureau of Reclamation, Denver, Colorado.

Morris, G. L., and Hu, G., (1992). "HEC-6 modeling of sediment management in Loíza Reservoir, Puerto Rico" Hydraulic Engineering: Saving A Threatened Resource - in Search of Solutions, *Proceedings of the Hydraulic Engineering Sessions at Water Forum '9*2, ASCE, pp. 630-635.

Morris, G. L. and Fan, J., (1997). R*eservoir Sedimentation Handbook: Design and Management of Dams, Reservoir, and Watersheds for Sustainable Use*, McGraw Hill, New York.

Parker, G. (1990). "Surface based bedload transport relationship for gravel rivers," *Journal of Hydraulic Research*, Vol. 28, No. 4, pp. 417-436.

Simões, F. J. M. and Yang, C. T. (2006). "Sediment Modeling for Rivers and Reservoirs," Chapter 5 *Erosion and Sedimentation Manual*, U.S. Bureau of Reclamation, Technical Service Center, Denver Colorado.

Simões, F. J. M. and Yang, C. T. (2008). "GSTARS Computer Models and Their Applications, Part II: Applications," *International Journal of Sediment Research,* Vol. 23, No. 4, pp. 299 – 315, Beijing, China.

Toffaleti, F.B. (1969). "Definitive computations of sand discharge in rivers," *Journal of the Hydraulic Division*, ASCE, Vol. 95, No. HY1, pp. 225-246.

U.S. Army Corps of Engineers (1991). *HEC-6 Scour and Deposition in Rivers and Reservoirs, User's Manual*, Hydrologic Engineering Center, Davis, California.

U.S. Bureau of Reclamation (1987). *Design of Small Dams, 3rd edition*, Denver, Colorado.

Walling, D. E (1984). "Muddy waters move mountains," *The Geographical Magazine*, pp. 262-267.

Wang, Z. (1999). "Experimental study on scour rate and river bed inertia", *Journal of Hydraulic Research*, Vol.37, No.1, pp.17-37.

White, W. R. (2001). *Evacuation of sediments from reservoirs*, Thomas Telford Publishing, London.

White, W. R. and Bettess, R. (1984). "The feasibility of flushing sediments through reservoir," *Proceedings of the Syposium 'Challenges in African Hydrology and Water Resources'* Harare.

Yang, C. T. (1973). "Incipient Motion and Sediment Transport," J*ournal of the Hydraulics Division*, ASCE, Vol. 99, No. HY10, Proceeding Paper 10067, pp. 1679-1704.

Yang, C. T. (1979). "Unit Stream Power Equations for Total Load," *Journal of Hydrology*, Vol.40, pp. 123-138.

Yang, C. T. (1984). "Unit stream power equation for gravel," *Journal of the Hydraulic Division, ASCE*, Vol. 110, No. HY12, pp. 1783-1797.

Yang, C. T. (1996). *Sediment Transport: Theory and Practice*, McGraw-Hill Companies, Inc., New York (reprint by Krieger Publishing Company, 2003).

Yang, C. T. (2010). "Discussion of "Sediment Transport Modeling Review – Current and Future Developments" by A. N. Papanicolaou, M. Elhakeem, G. Krallis, S. Prakash, and J. Edinger," *Journal of Hydraulic Engineering*, ASCE, Vol. 136, No. 8, pp. 552-555

Yang, C. T., and Song, C.C.S. (1979). "Theory of Minimum Rate of Energy Dissipation," *Journal of the Hydraulics Division*, ASCE, Vol. 105, No. HY7, pp. 769-784.

Yang, C. T., and Simões, F. J. M. (2002). *User's Manual for GSTARS3 (Generalized Sediment Transport model for Alluvial River Simulation version 3.0)*, Technical Service Center, U.S. Bureau of Reclamation, Denver, Colorado.

Yang, C.T., Simões, F. J. M. (2008). "GSTARS Computer Models and Their Application, part I : Theoretical Development," *International Journal of Sediment Research* , Vol. 23, No. 3, pp. 197-211.

Yang, C. T., and Marsooli, R. (2010). "Recovery Factor for Non-equilibrium Sedimentation Processes," *International Journal of Hydraulic Research*, Vol. 48, No. 3, pp. 409-413.

Yang, C. T., and Ahn, J. (2011). *User's Manual for GSTARS4 (Generalized Sediment Transport model for Alluvial River Simulation version 4.0)*, Colorado State University, Fort Collins, Colorado.

Yang, C. T., Molinas, A., and Wu, B. (1996). "Sediment Transport in the Yellow River," *Journal of Hydraulic Engineering*, ASCE, vol.122, no.5, pp. 237-244.

Yang, C. T., Huang, J. V., and Greimann, B. (2005) *User's Manual for GSTAR-1D 1.0 (Generalized Sediment Transport for Alluvial Rivers – One Dimension, Version 1.0),* Technical Service Center, U.S. Bureau of Reclamation, Denver, Colorado.

Yellow River Conservancy Comminsion (2004). *The Great Yellow River*, Yellow River Conservancy Press, China.

Zhang, Q. (1980). "Diffusion Process of Sediment in Open Channel and Its Application," *Journal of Sediment Research*, 1980, summer, pp.37-52.

Zhou, J. and Lin, B. (1995). "2-D Mathematical Model for Suspended Sediment," *Journal of Basic Science and Engineering,* Vol. 3, No. 1, pp.77-97.

Zhou, J. and Lin, B. (1998). "One-Dimensional Mathmatical Model for Suspended Sediment by Lateral Integration," *Journal of Hydraulic Engineering,* ASCE, Vol. 124, No. 7, pp.712-717.

Zhou, J, Spork, V., Koehgeter, J., and Gouve, G. (1997). "Bed Conditions of Non-Equilibrium Transport of Suspended Sediment," *International Journal of Sediment Research,* Vol. 12, No.3, pp.241-247.

APPENDIX A

Simulated Steady Flow Reservoir Operation Type 1 (Steady_OP1), Unsteady Flow

Reservoir Operation Type 1 (Unsteady_OP1), and Measured Cross Section Geometry
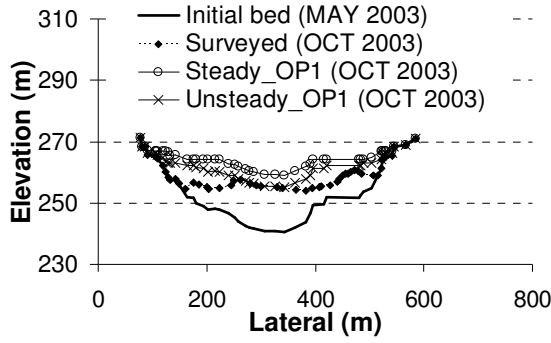
(a) 101.6 km above the Xiaolangdi Dam
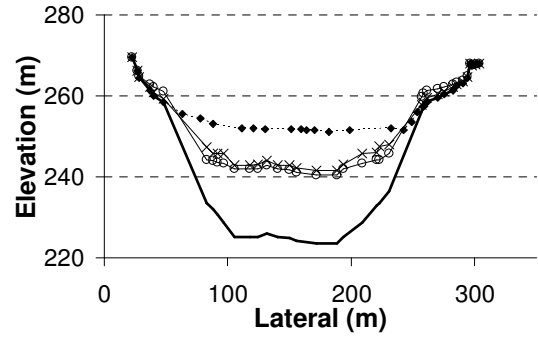
(b) 88.5 km
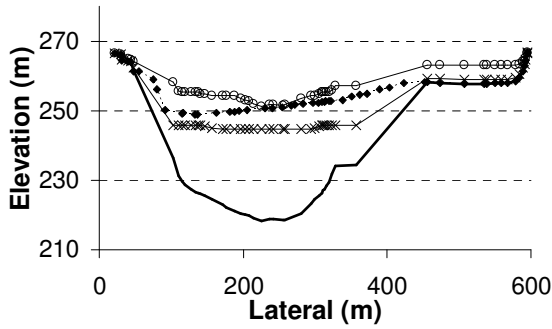
(c) 80.2 km
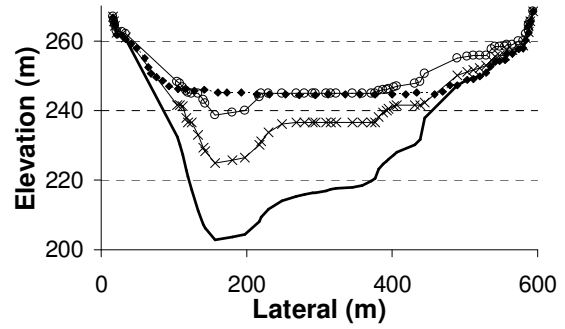
(d) 72.1 km
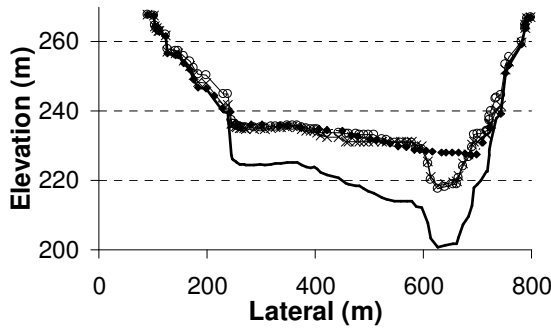
(e) 64.8 km
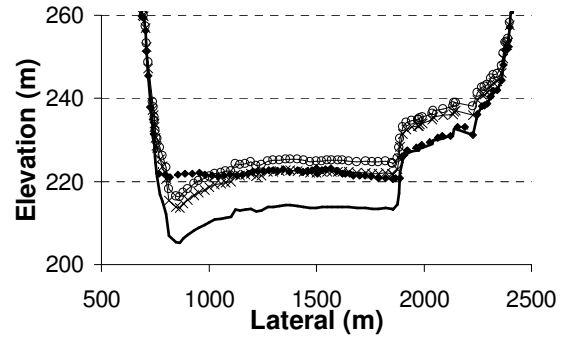
(f) 57.0 km
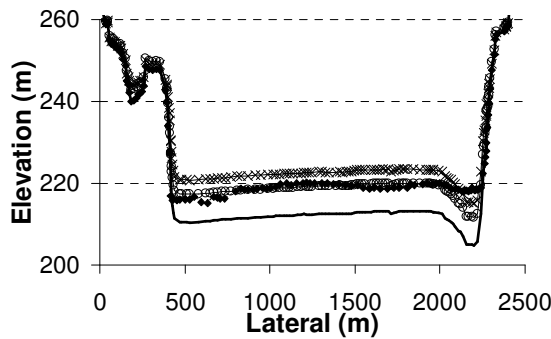
(g) 55.0 km
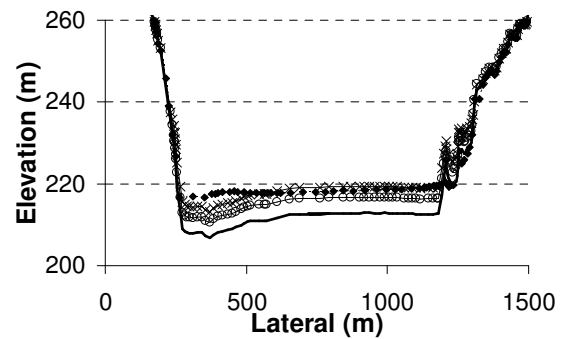
(h) 53.4 km

Figure A.1 Comparison of measurement and GSTARS4 simulation (Steady_OP1 and

Unsteady_OP1), in October 2003
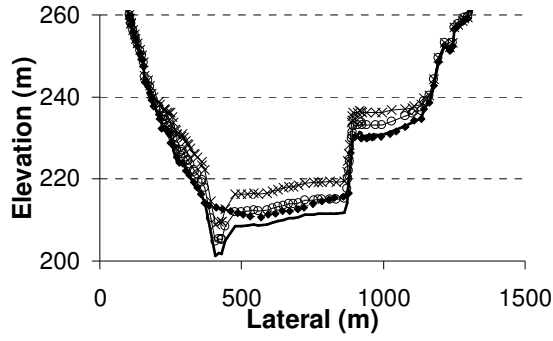
(i) 50.2 km
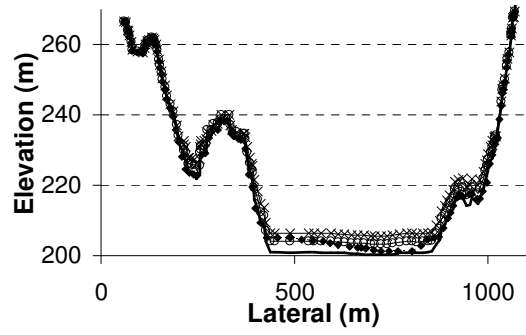
(j) 43.0 km
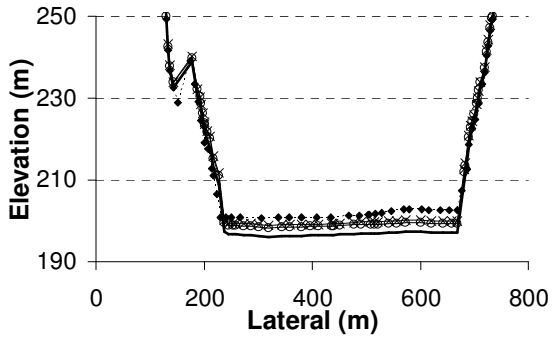
(k) 39.5 km
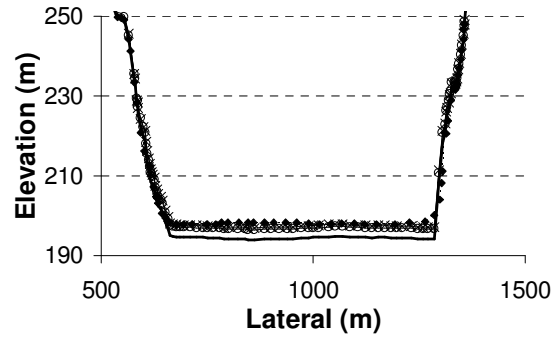
(l) 36.3 km
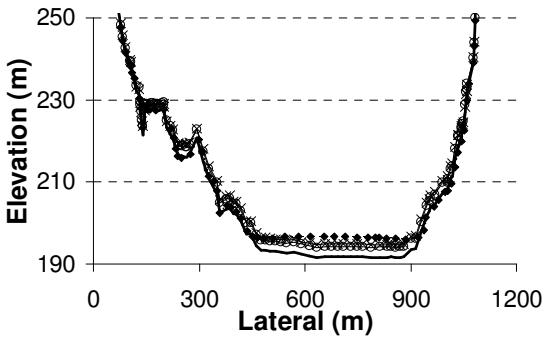
(m) 33.5 km
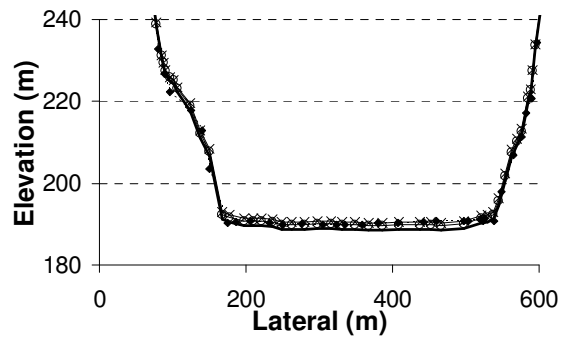
(n) 27.2 km
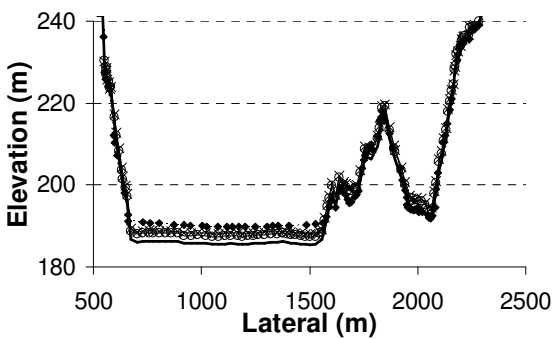
(o) 22.1 km
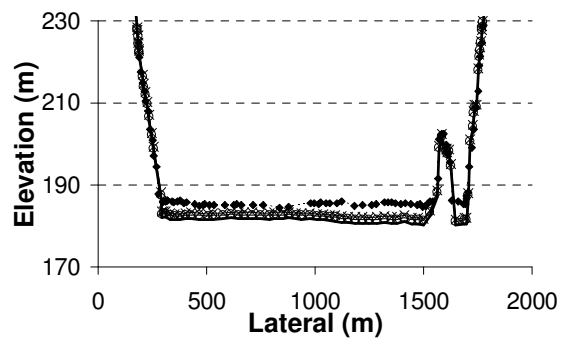
(p) 18.7 km

Figure A.1 Continued

110
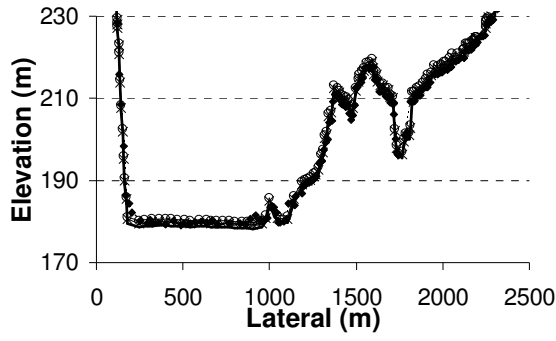
(q) 14.0 km
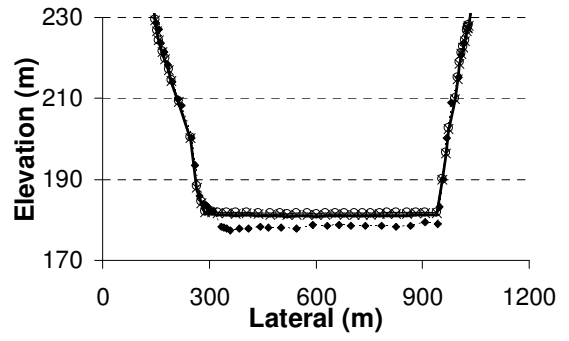
(r) 11.4 km
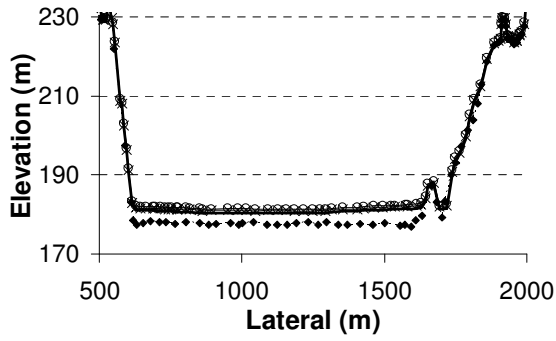
(s) 7.7 km
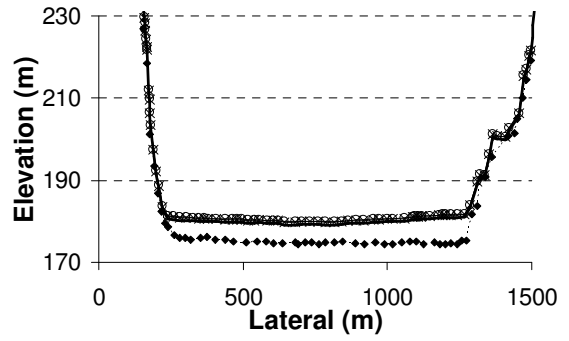
(t) 4.6 km
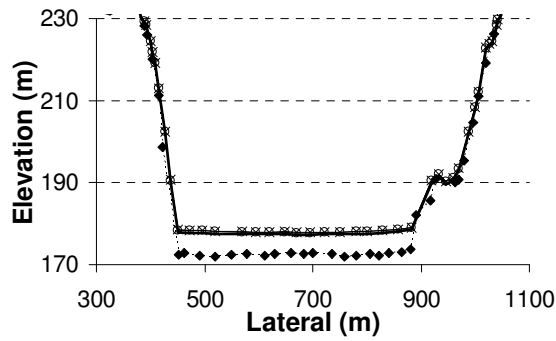
(u) 2.4 km
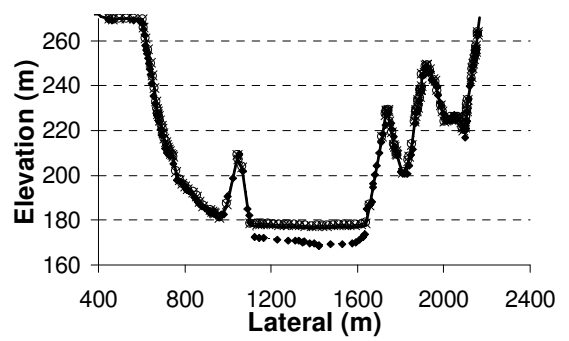
(v) 1.0 km

Figure A.1 Continued
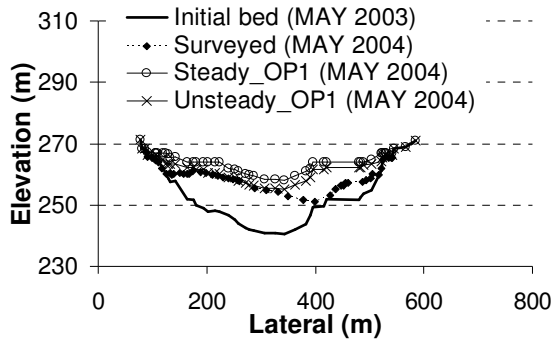
111

(a) 101.6 km above the Xiaolangdi Dam
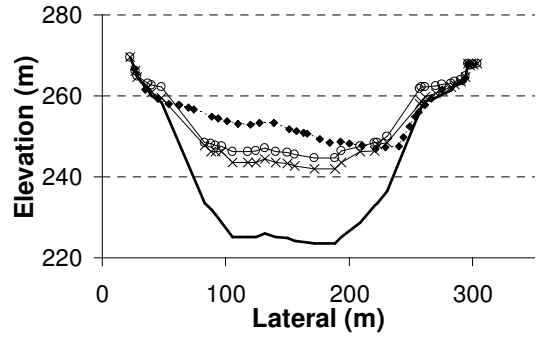
(b) 88.5 km
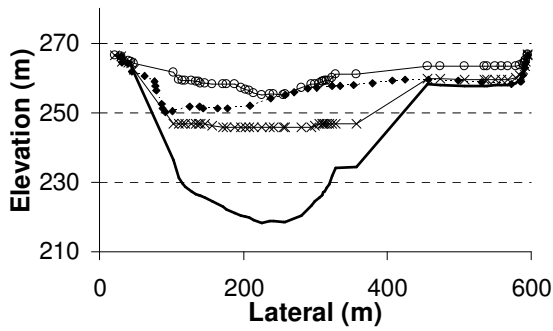
(c) 80.2 km
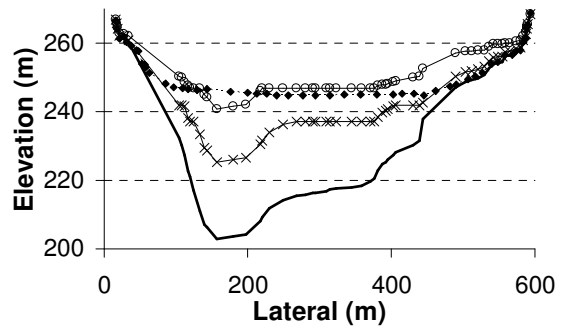
(d) 72.1 km
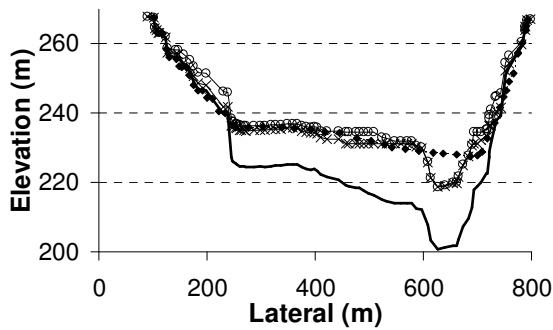
(e) 64.8 km
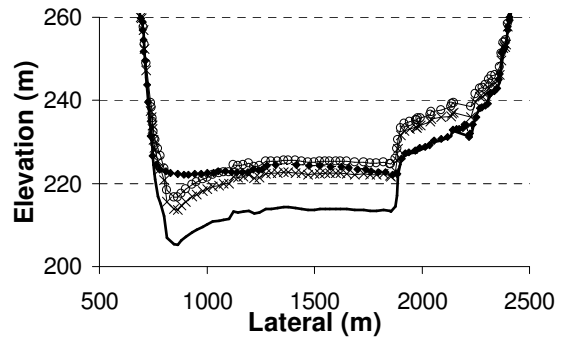
(f) 57.0 km
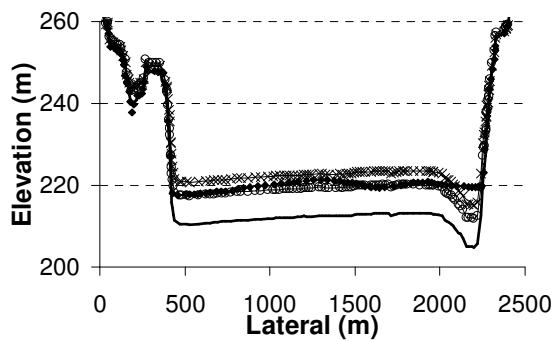
(g) 55.0 km
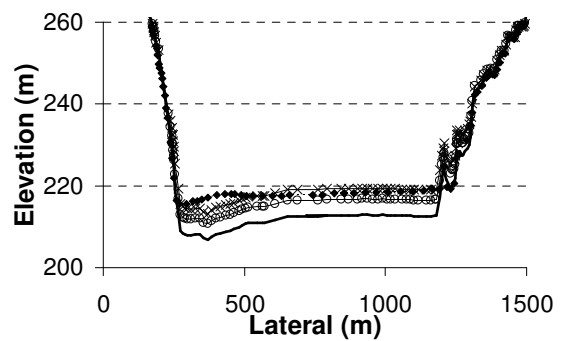
(h) 53.4 km

Figure A.2 Comparison of measurement and GSTARS4 simulation (Steady_OP1 and Unsteady_OP1), in May 2004

112
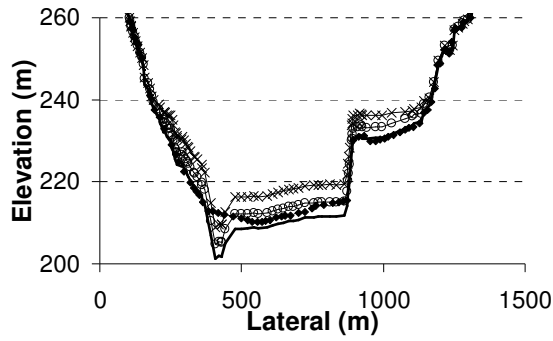
(i) 50.2 km
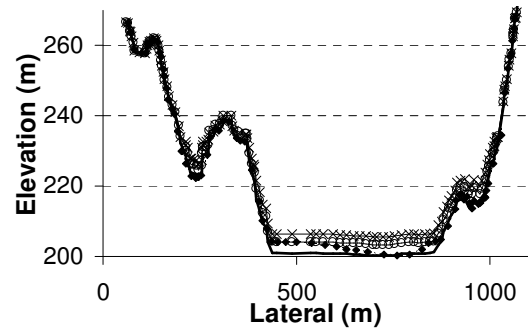
(j) 43.0 km
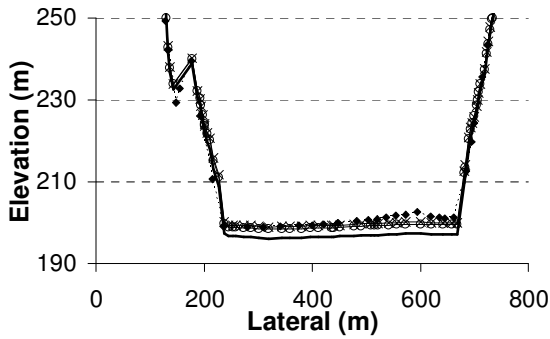
(k) 39.5 km
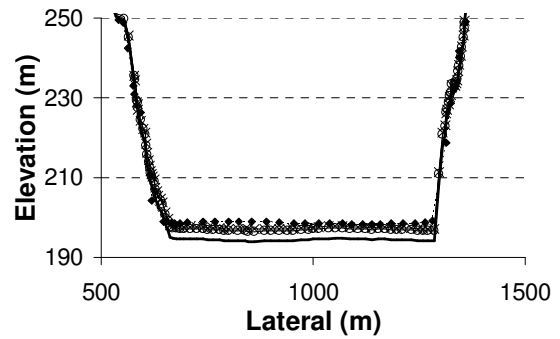
(l) 36.3 km
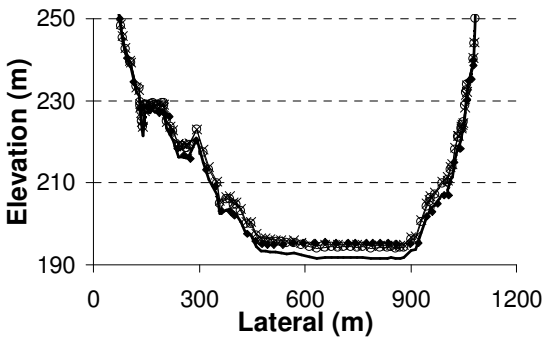
(m) 33.5 km
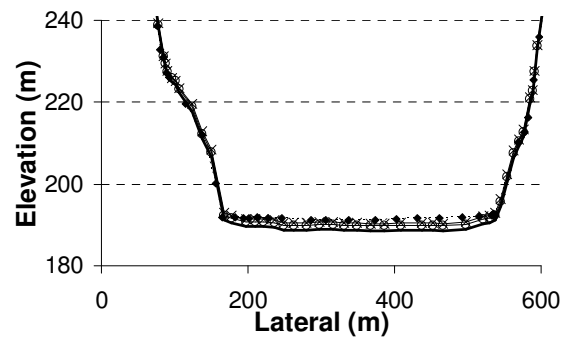
(n) 27.2 km
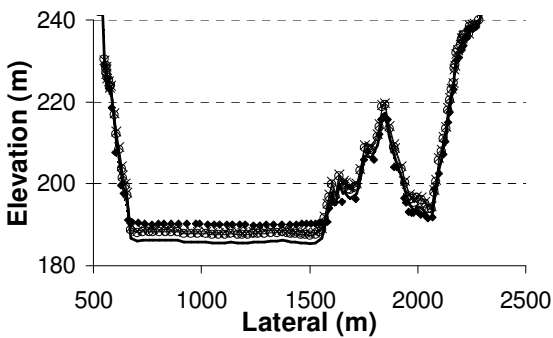
(o) 22.1 km
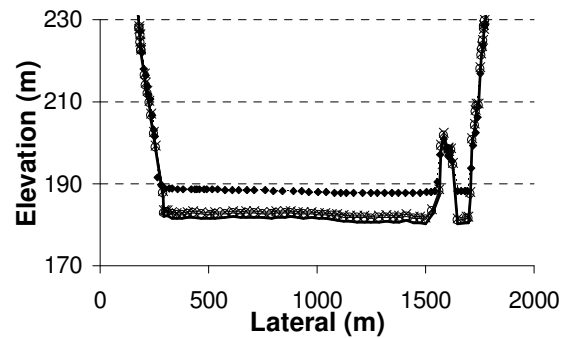
(p) 18.7 km

Figure A.2 Continued

113
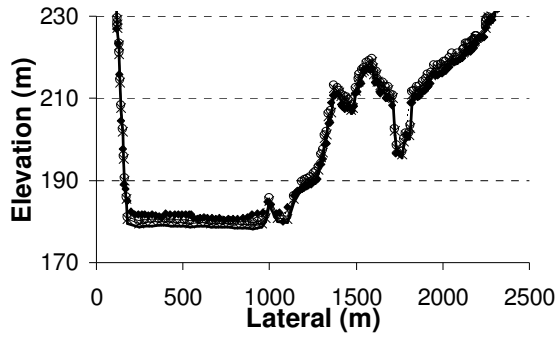
(q) 14.0 km

(r) 11.4 km

(s) 7.7 km

(t) 4.6 km

(u) 2.4 km

(v) 1.0 km

Figure A.2 Continued
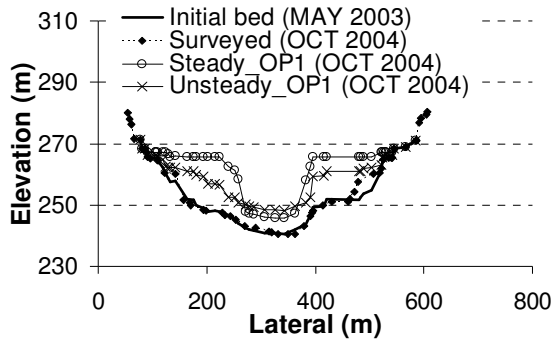
114

(a) 101.6 km above the Xiaolangdi Dam
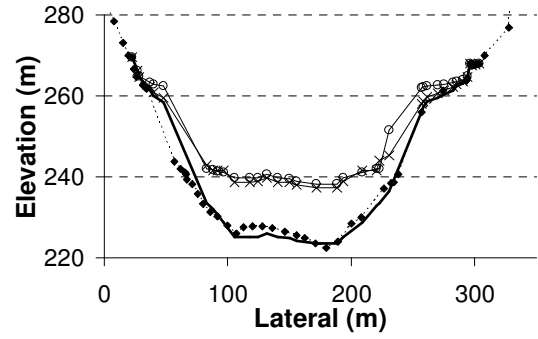
(b) 88.5 km
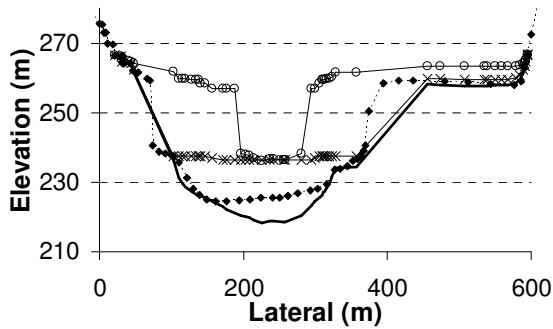
(c) 80.2 km
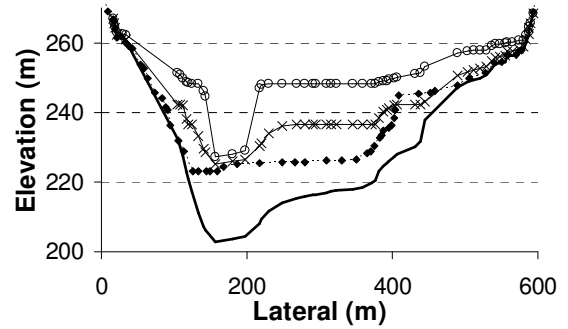
(d) 72.1 km
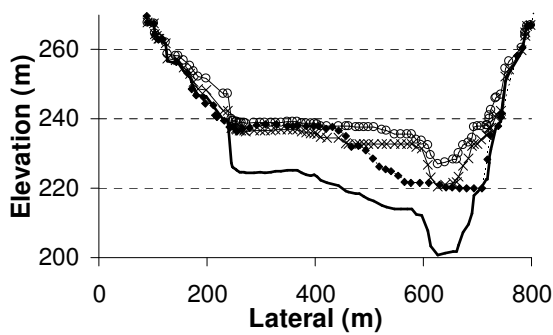
(e) 64.8 km
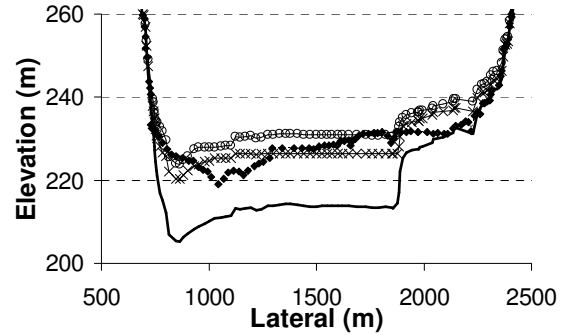
(f) 57.0 km
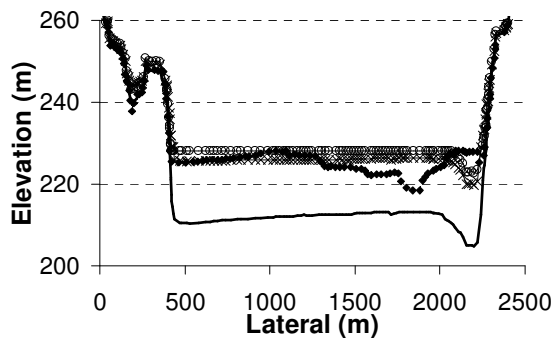
(g) 55.0 km
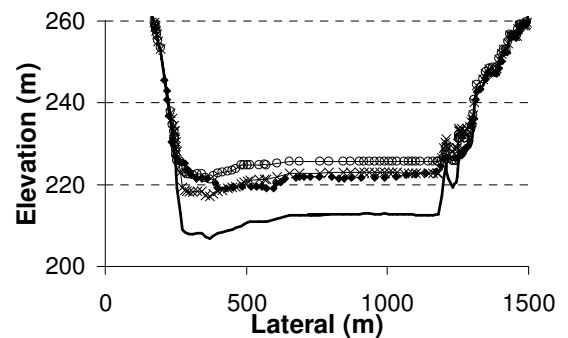
(h) 53.4 km

Figure A.3 Comparison of measurement and GSTARS4 simulation (Steady_OP1 and Unsteady_OP1), in October 2004
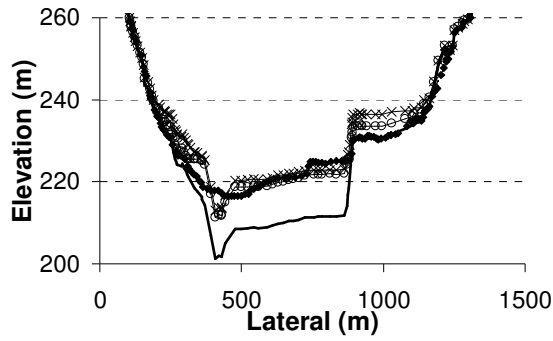
(i) 50.2 km
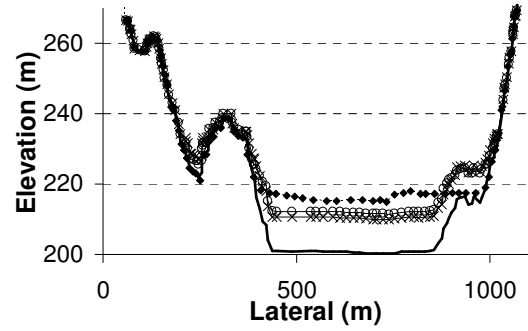
(j) 43.0 km
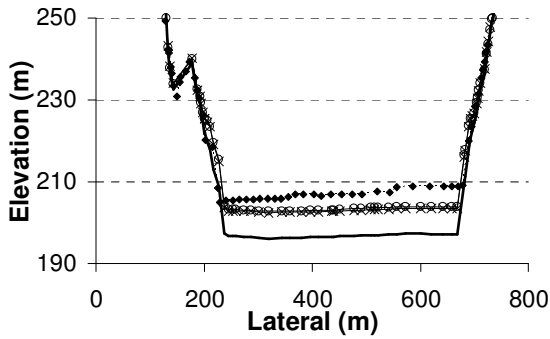
(k) 39.5 km
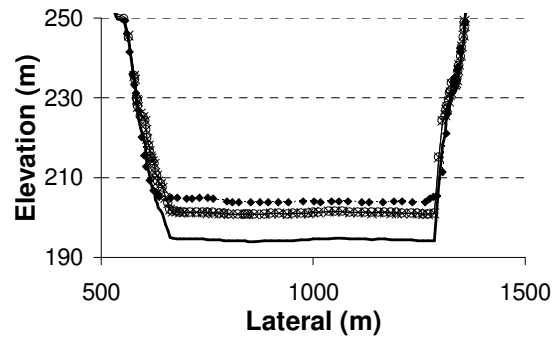
(l) 36.3 km
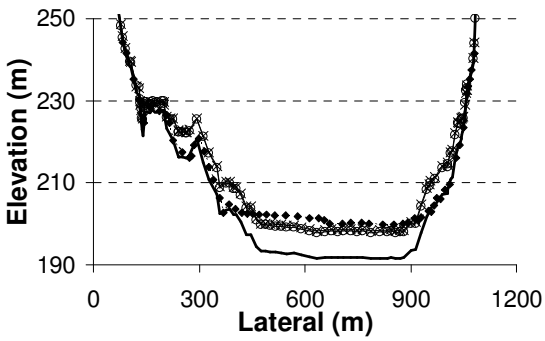
(m) 33.5 km
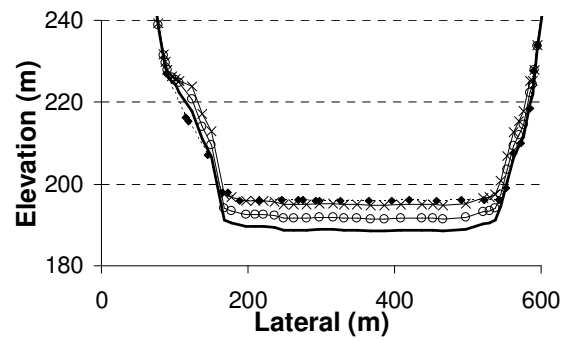
(n) 27.2 km
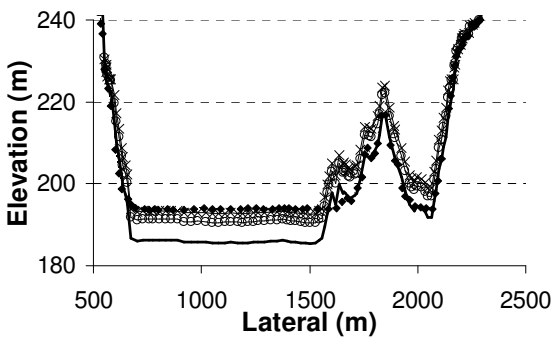
(o) 22.1 km
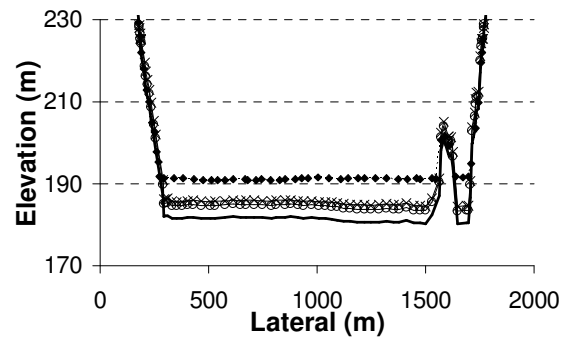
(p) 18.7 km

Figure A.3 Continued
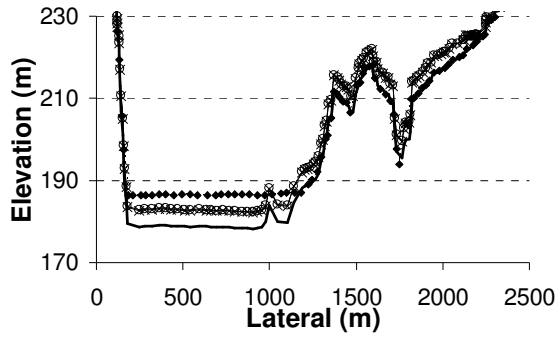
(q) 14.0 km
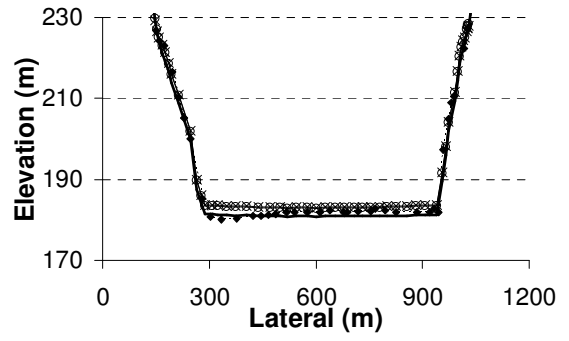
(r) 11.4 km
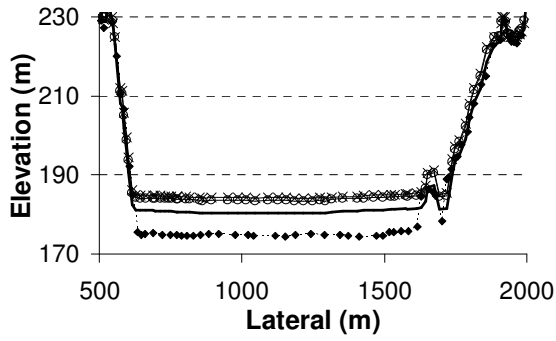
(s) 7.7 km
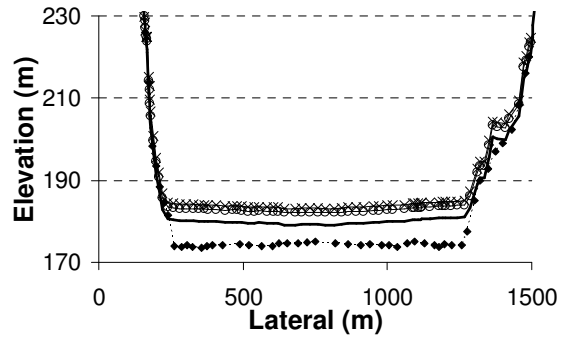
(t) 4.6 km
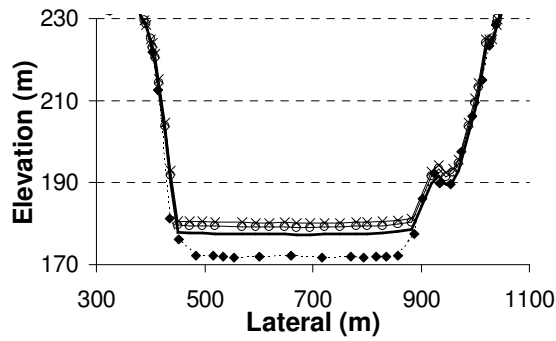
(u) 2.4 km
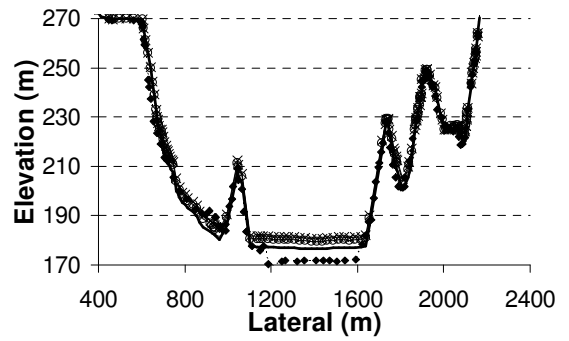
(v) 1.0 km

Figure A.3 Continued

117
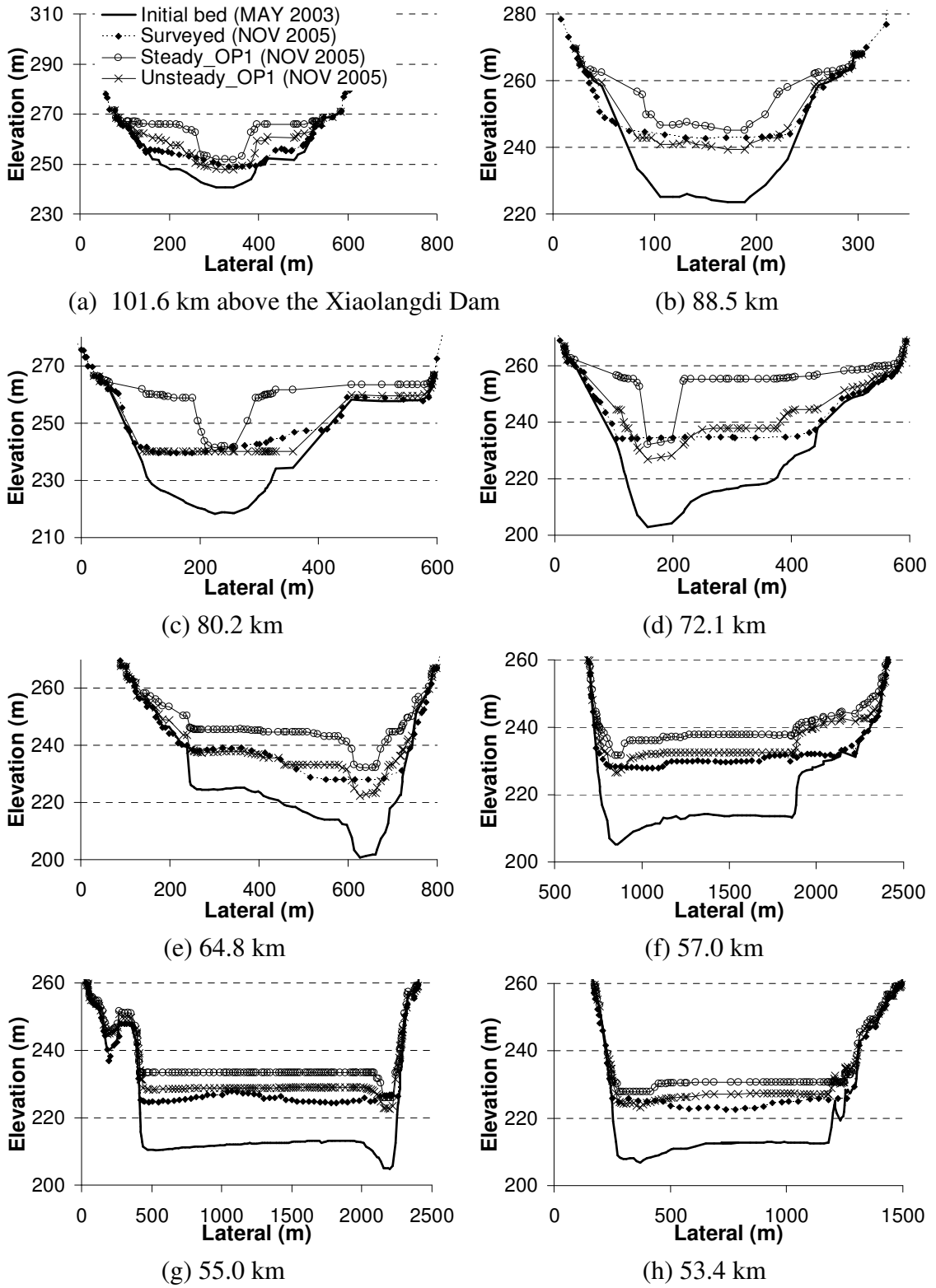
Figure A.4 Comparison of measurement and GSTARS4 simulation (Steady_OP1 and Unsteady_OP1), in November 2005
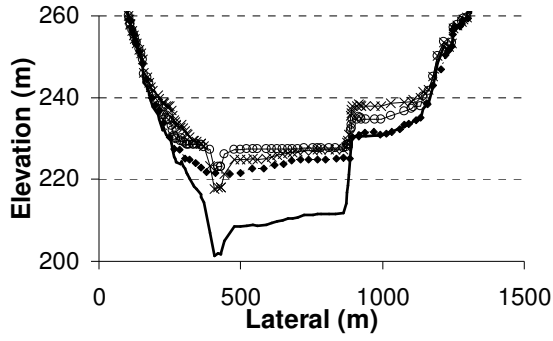
(i) 50.2 km
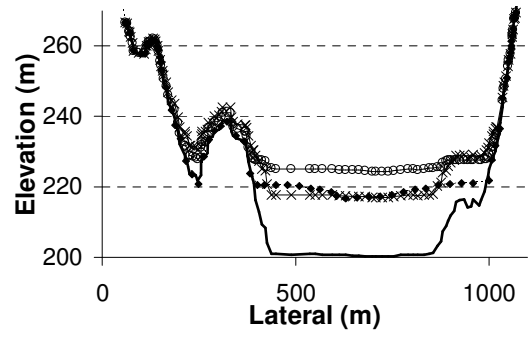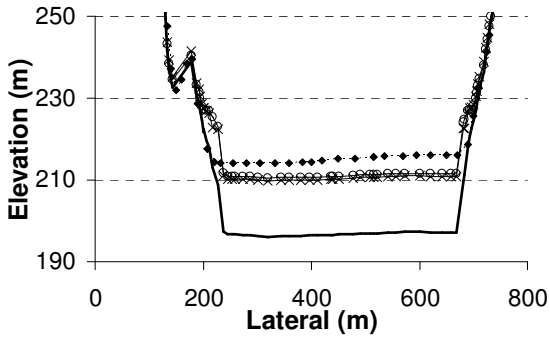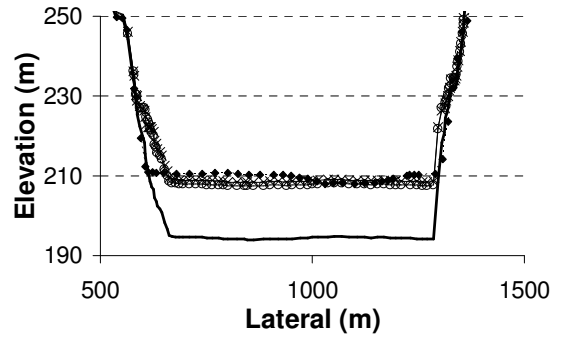
(j) 43.0 km
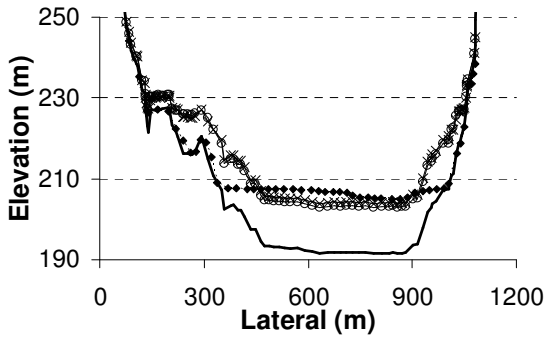
(k) 39.5 km
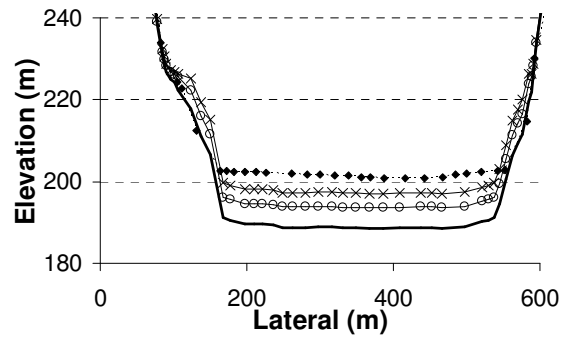
(l) 36.3 km
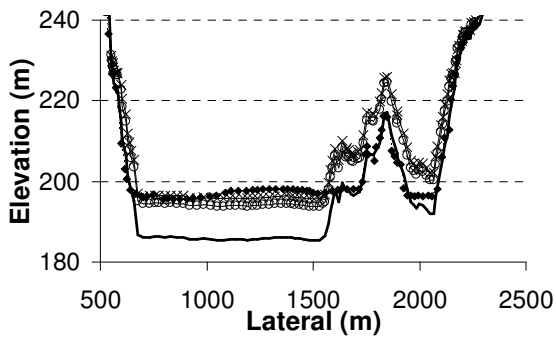
(m) 33.5 km
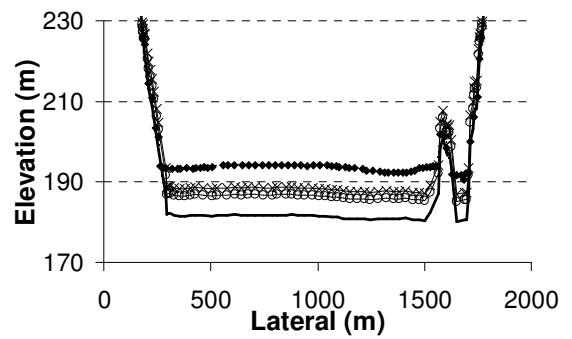
(n) 27.2 km

(o) 22.1 km

(p) 18.7 km

Figure A.4 Continued
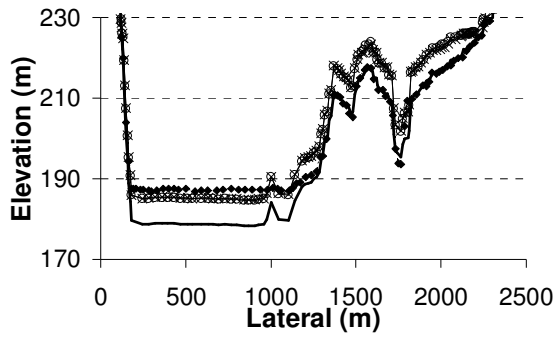
(q) 14.0 km
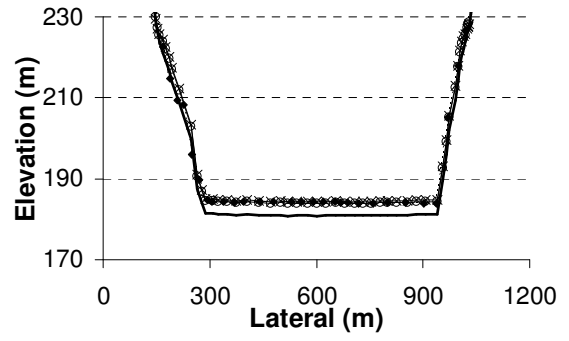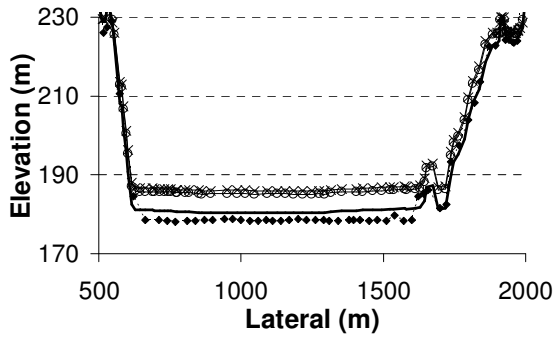
(r) 11.4 km

(s) 7.7 km
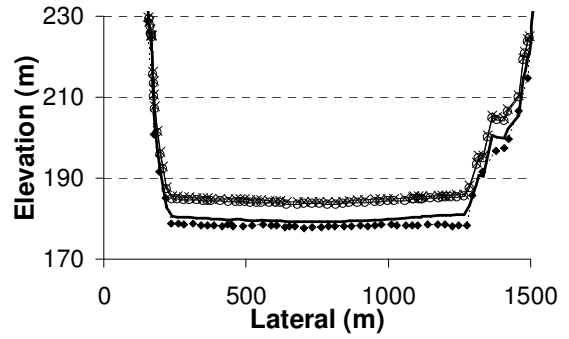
(t) 4.6 km
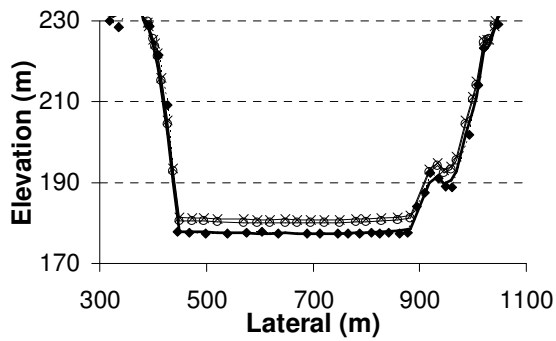
(u) 2.4 km
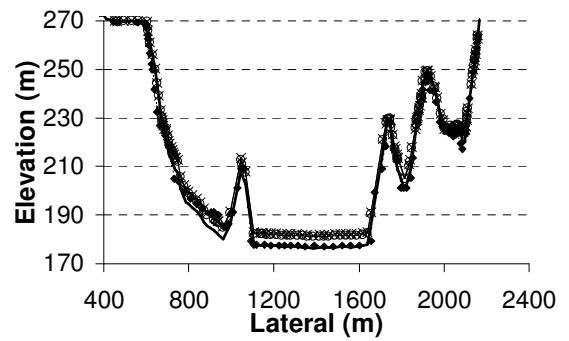
(v) 1.0 km

Figure A.4 Continued

120
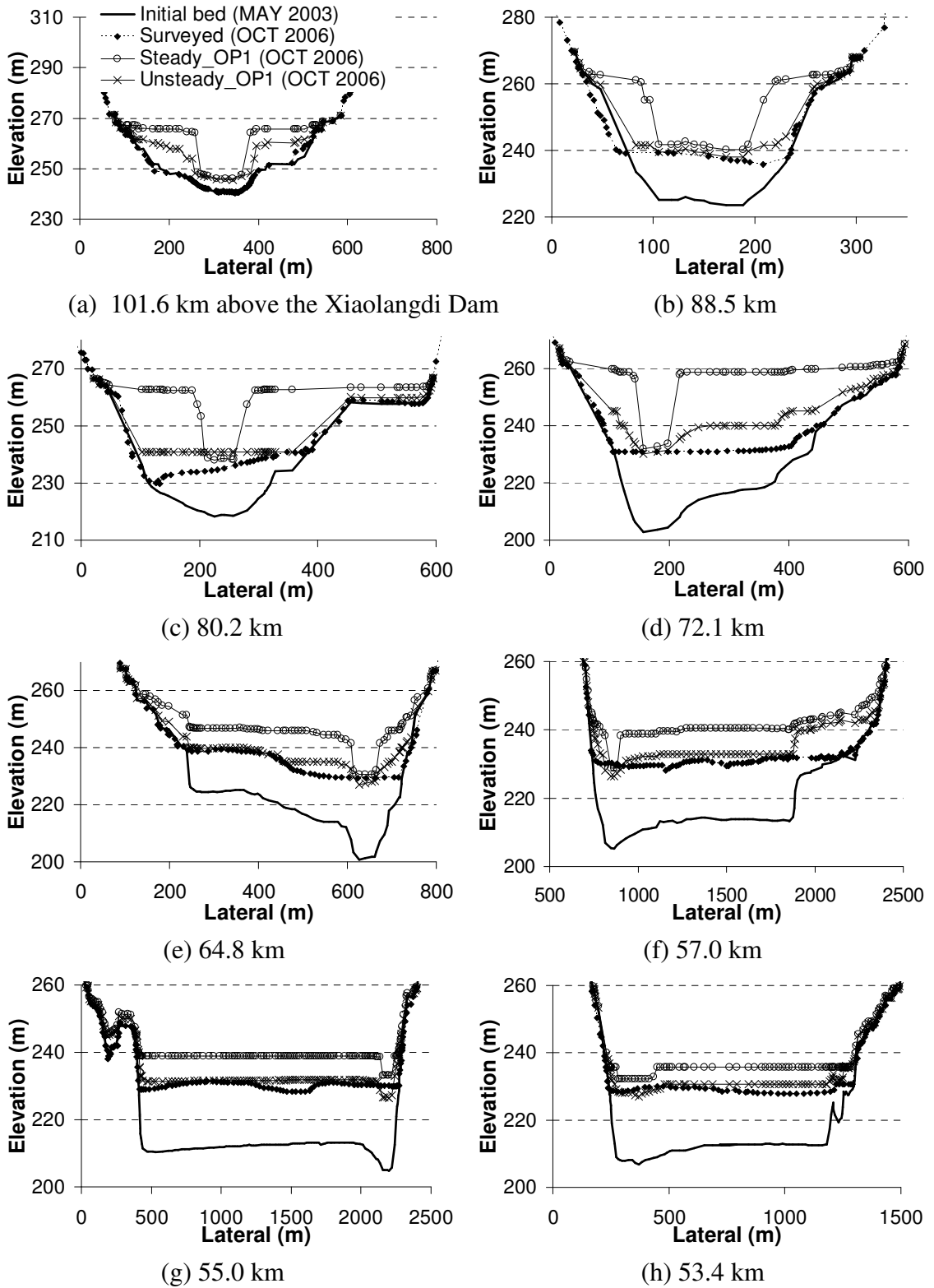
Figure A.5 Comparison of measurement and GSTARS4 simulation (Steady_OP1 and Unsteady_OP1), in October 2006

121
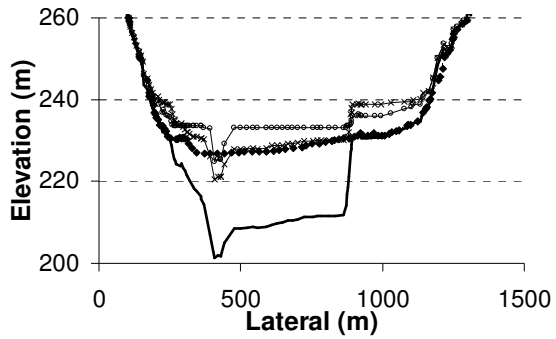
(i) 50.2 km
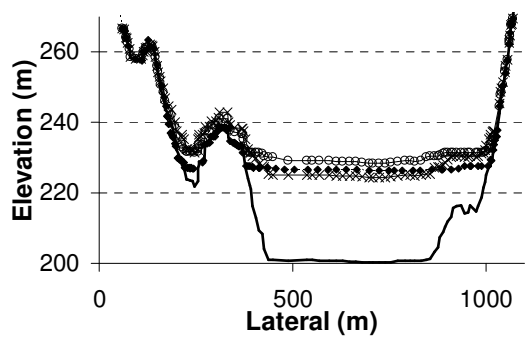
(j) 43.0 km

(k) 39.5 km

(l) 36.3 km

(m) 33.5 km

(n) 27.2 km

(o) 22.1 km

(p) 18.7 km

Figure A.5 Continued
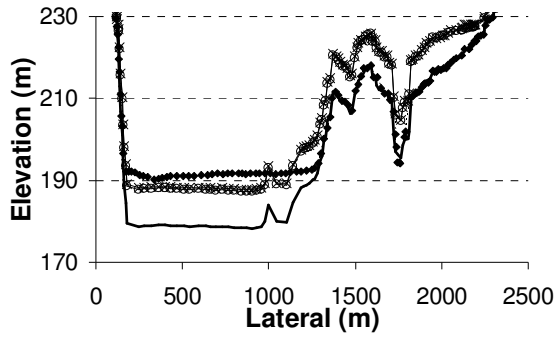
(q) 14.0 km
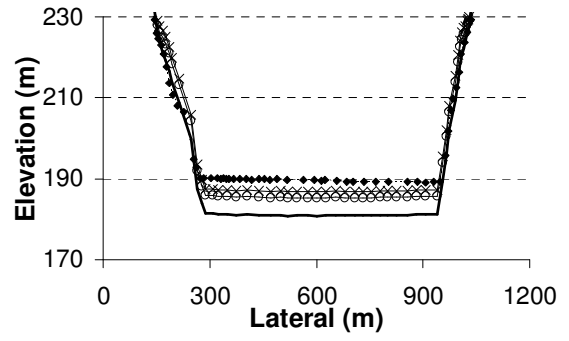
(r) 11.4 km
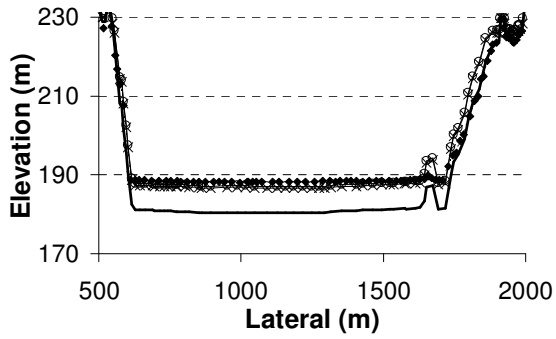
(s) 7.7 km
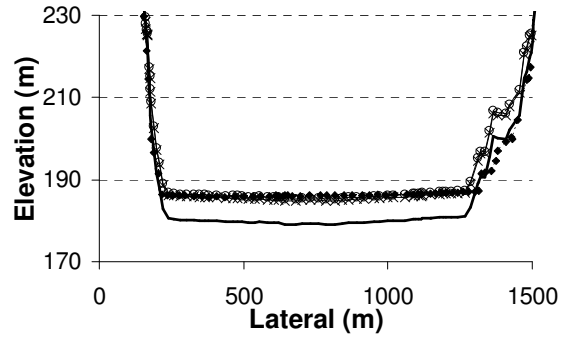
(t) 4.6 km
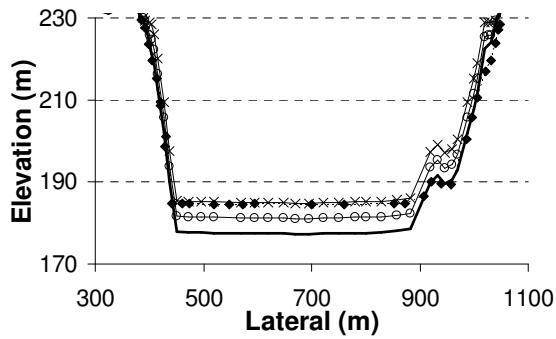
(u) 2.4 km
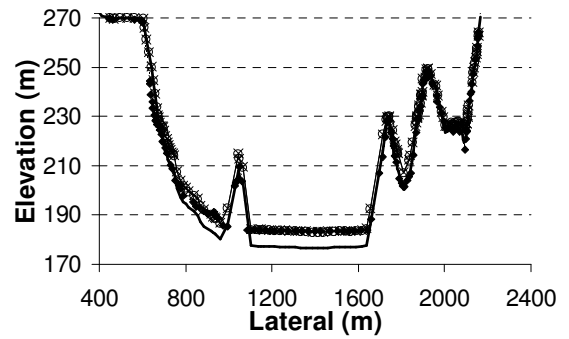
(v) 1.0 km

Figure A.5 Continued

123

APPENDIX B

Simulated Steady Flow Reservoir Operation Type 2 (Steady_OP2), Unsteady Flow

Reservoir Operation Type 2 (Unsteady_OP2), and Measured Cross Section Geometry
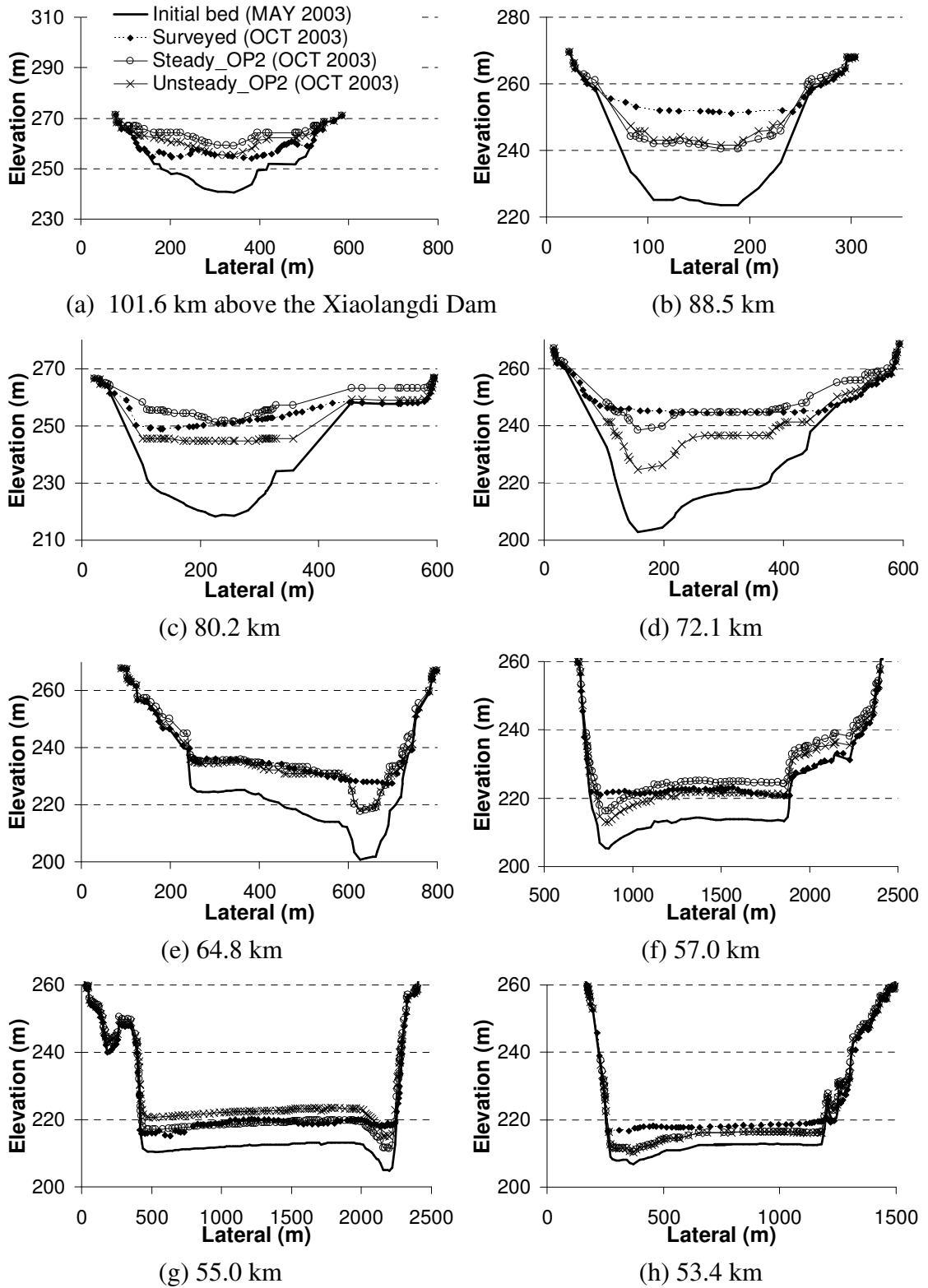
Figure B.1 Comparison of measurement and GSTARS4 simulation (Steady_OP2 and Unsteady_OP2), in October 2003
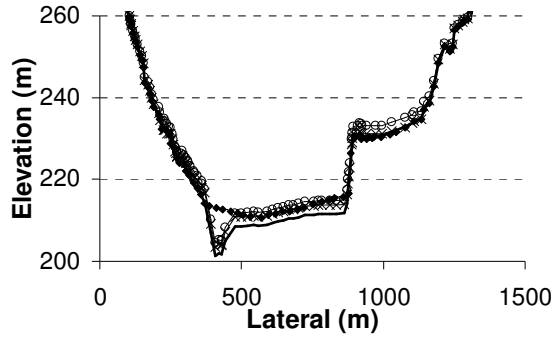
(i) 50.2 km
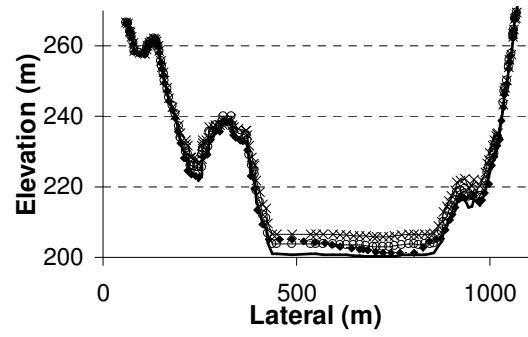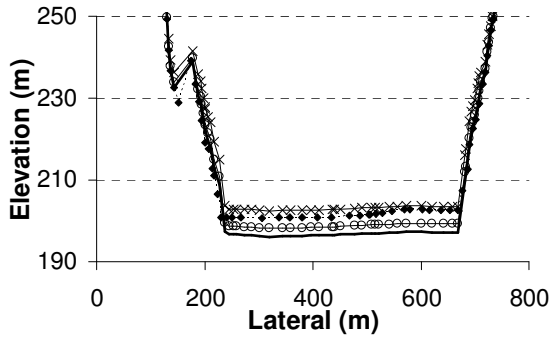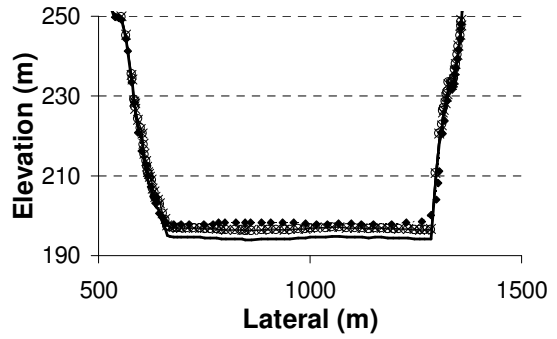
(j) 43.0 km
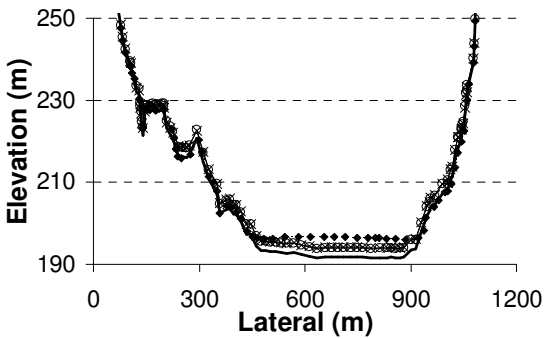
(k) 39.5 km
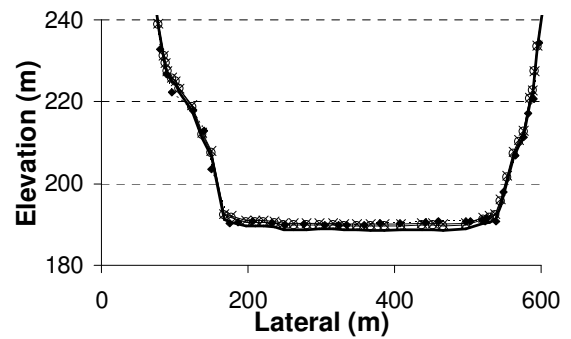
(l) 36.3 km
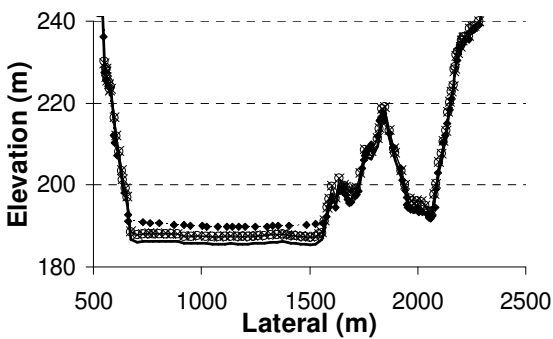
(m) 33.5 km
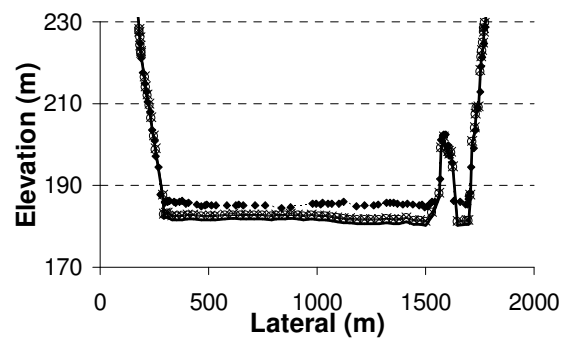
(n) 27.2 km

(o) 22.1 km

(p) 18.7 km

Figure B.1 Continued

126
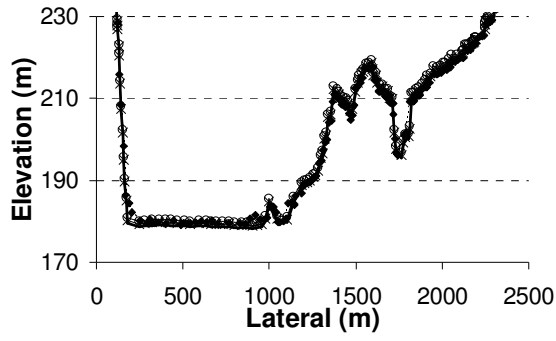
(q) 14.0 km
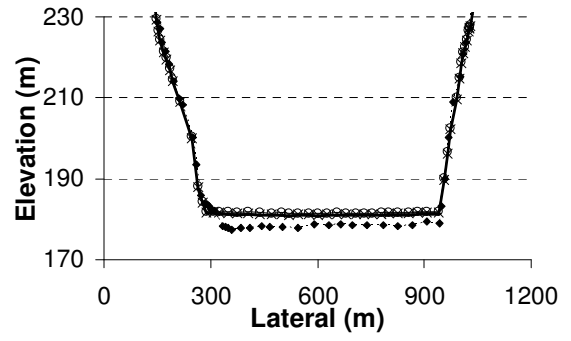
(r) 11.4 km
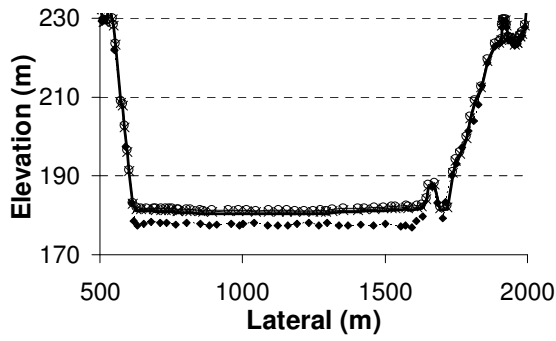
(s) 7.7 km
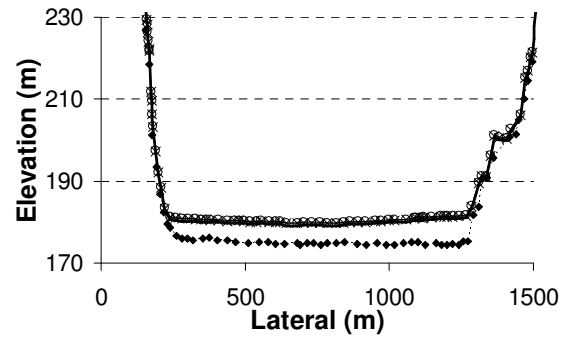
(t) 4.6 km
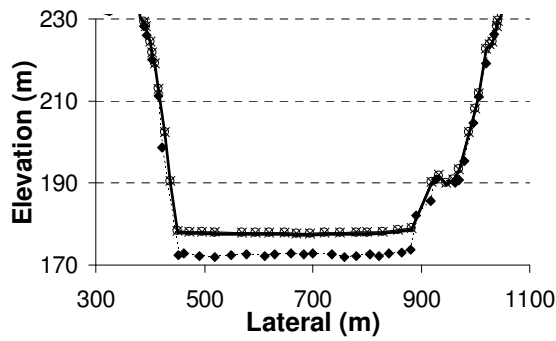
(u) 2.4 km
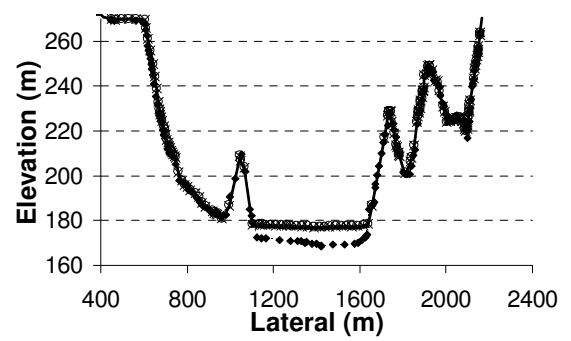
(v) 1.0 km

Figure B.1 Continued

127
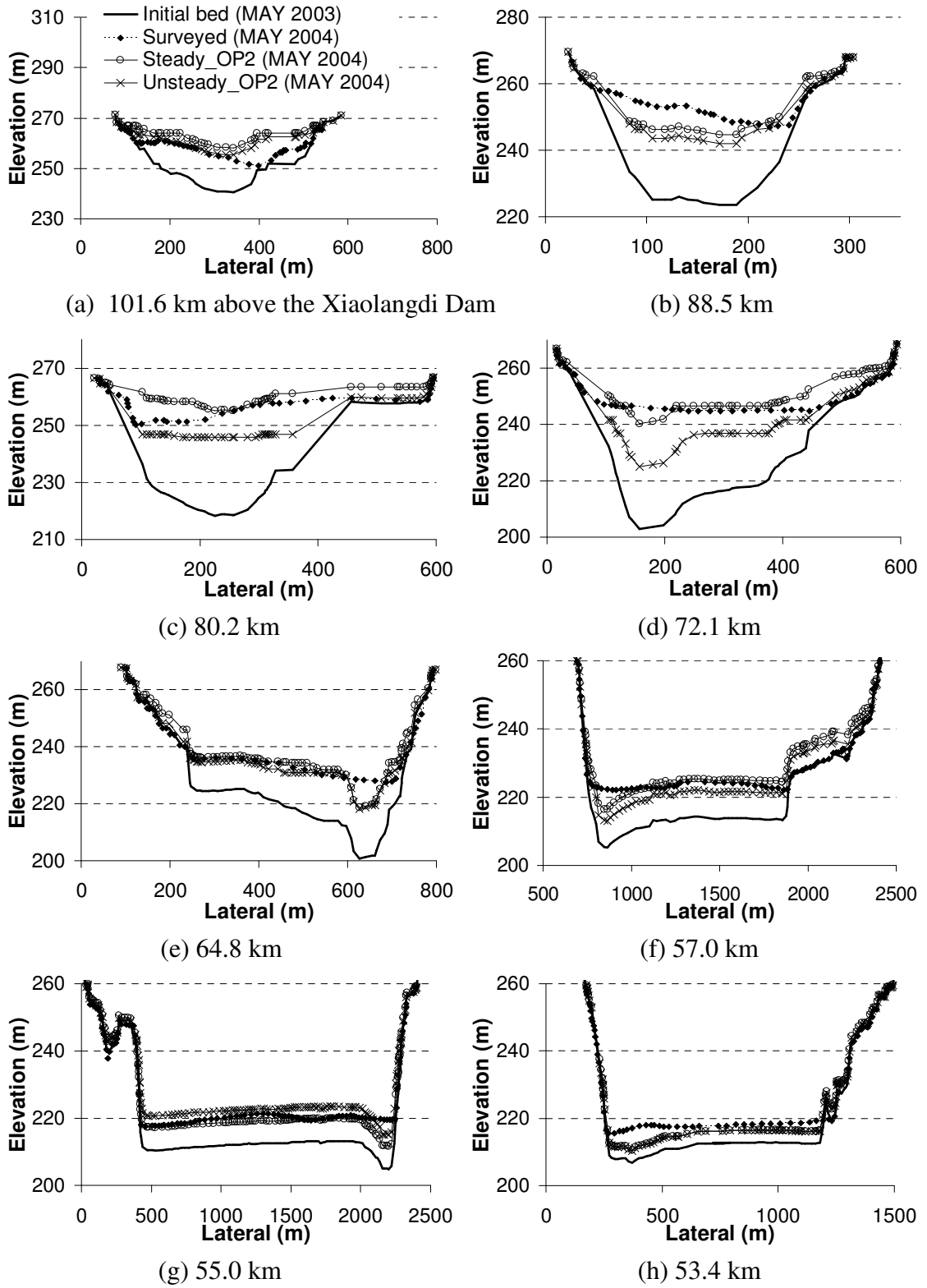
Figure B.2 Comparison of measurement and GSTARS4 simulation (Steady_OP2 and Unsteady_OP2), in May 2004
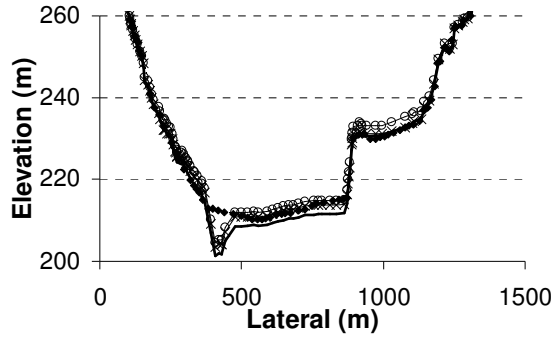
(i) 50.2 km
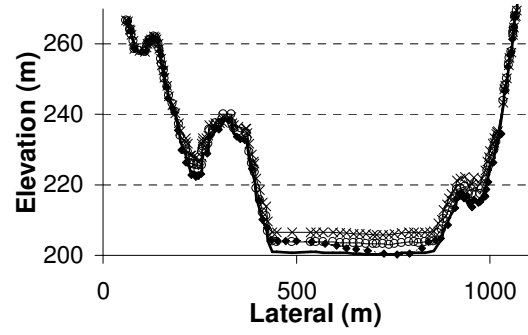
(j) 43.0 km
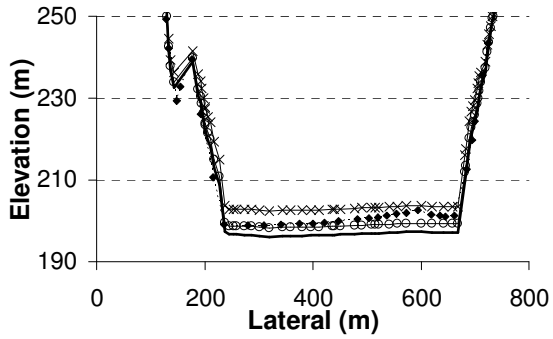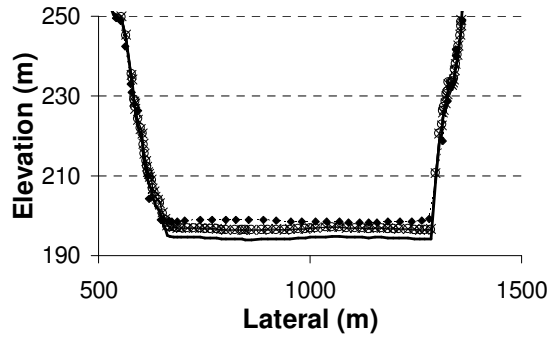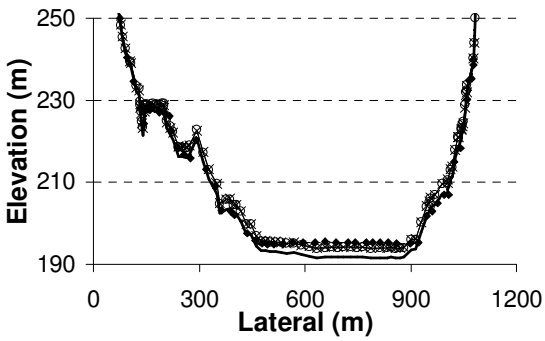
(k) 39.5 km
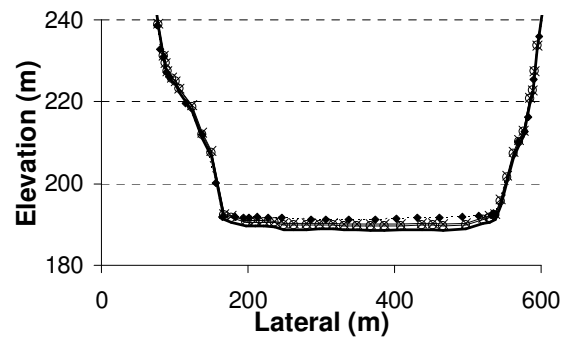
(l) 36.3 km
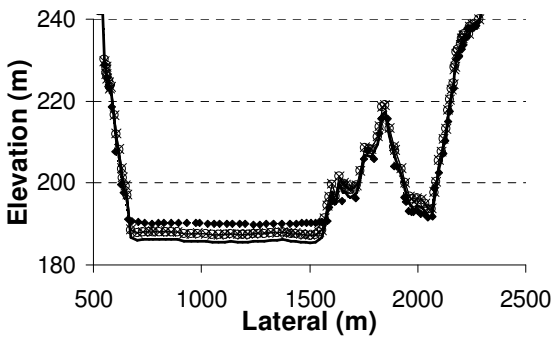
(m) 33.5 km

(n) 27.2 km

(o) 22.1 km

(p) 18.7 km

Figure B.2 Continued

(q) 14.0 km

(r) 11.4 km

(s) 7.7 km

(t) 4.6 km

(u) 2.4 km

(v) 1.0 km
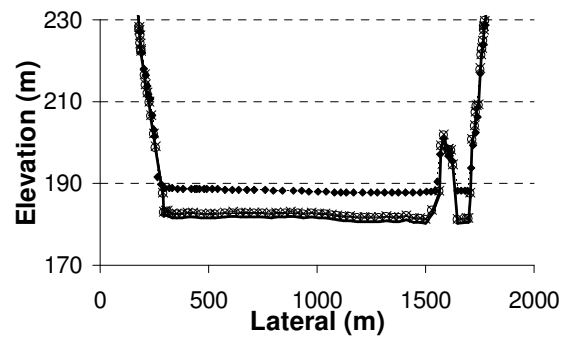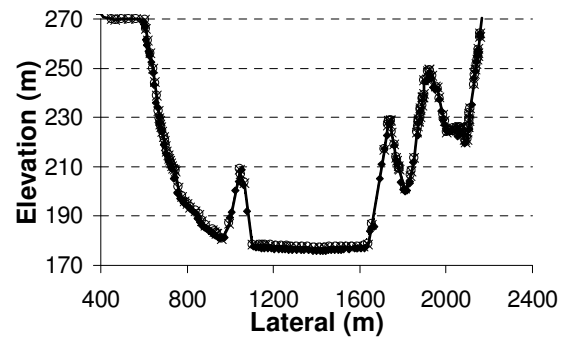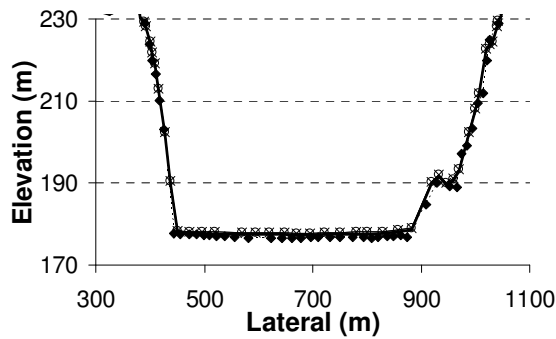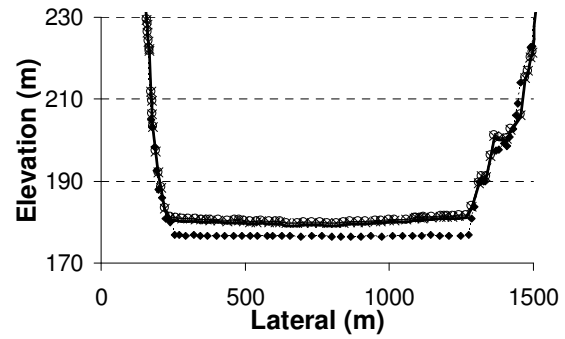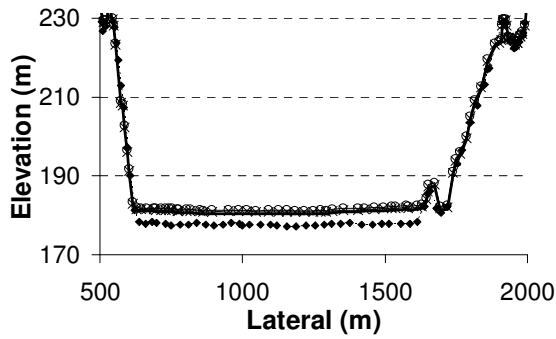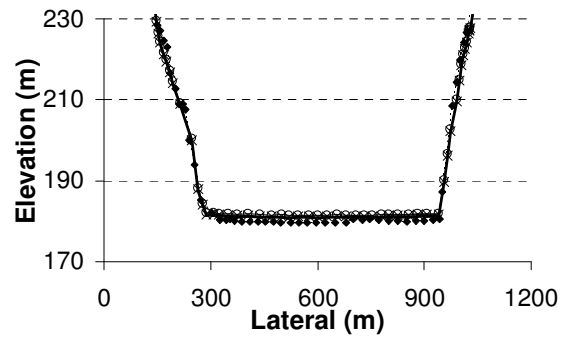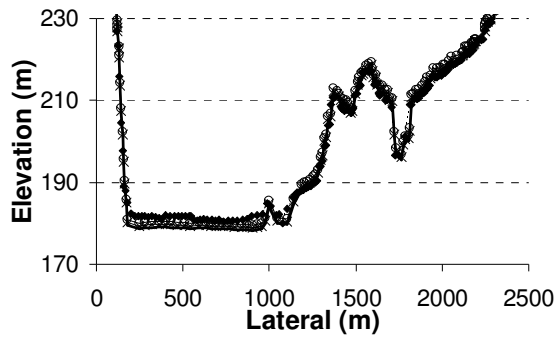
Figure B.2 Continued
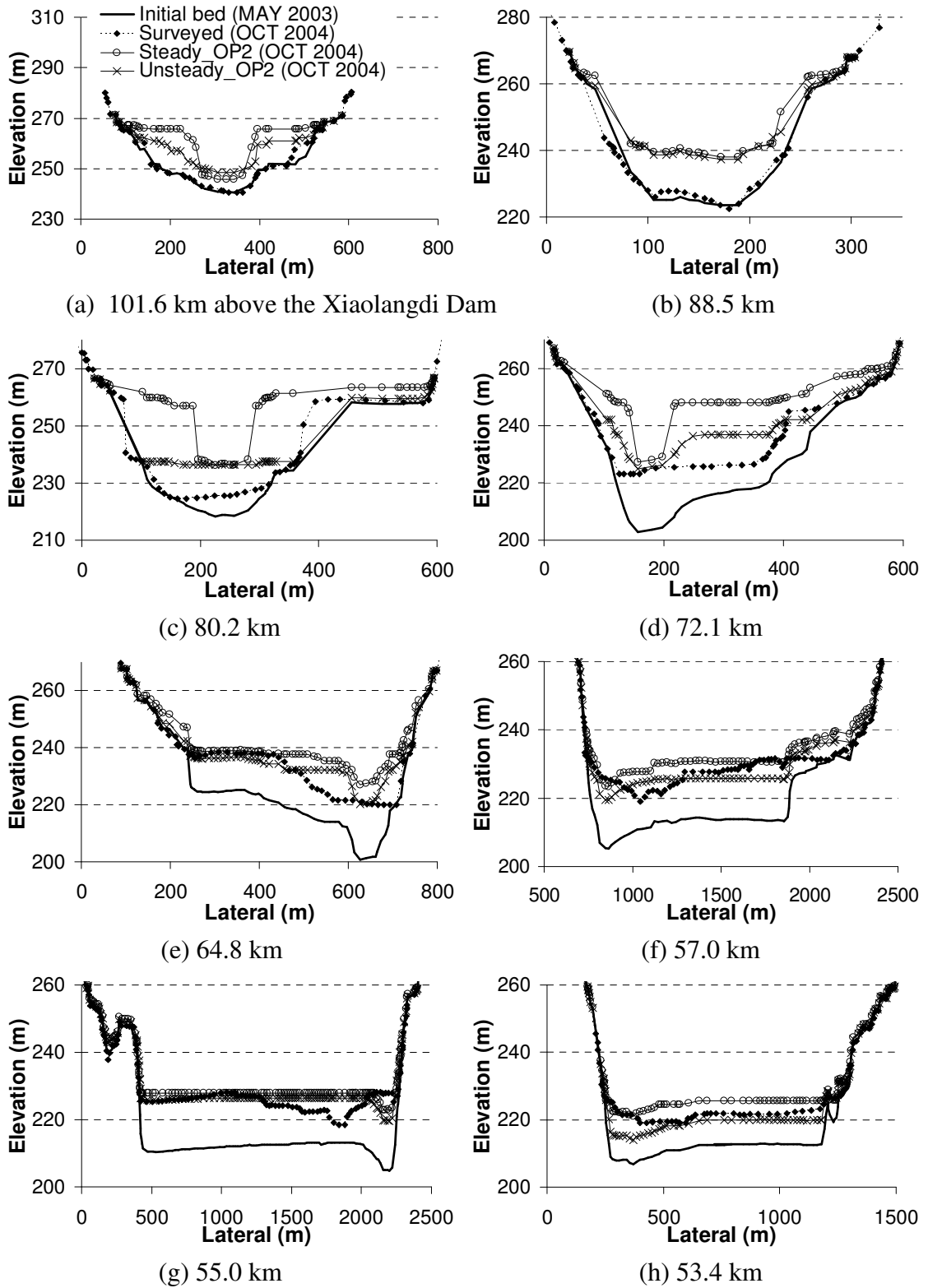
Figure B.3 Comparison of measurement and GSTARS4 simulation (Steady_OP2 and Unsteady_OP2), in October 2004

131
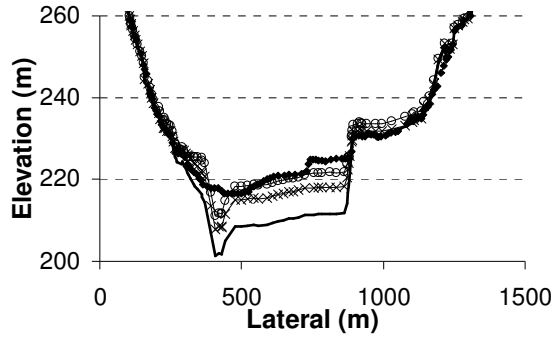
(i) 50.2 km
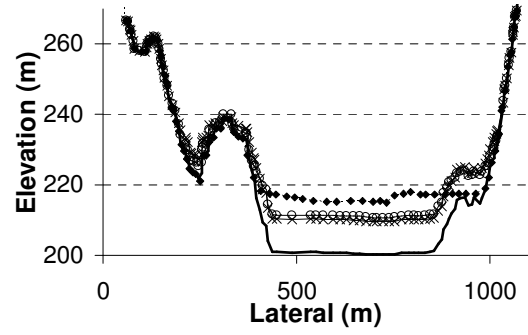
(j) 43.0 km

(k) 39.5 km

(l) 36.3 km

(m) 33.5 km

(n) 27.2 km

(o) 22.1 km

(p) 18.7 km

Figure B.3 Continued

132
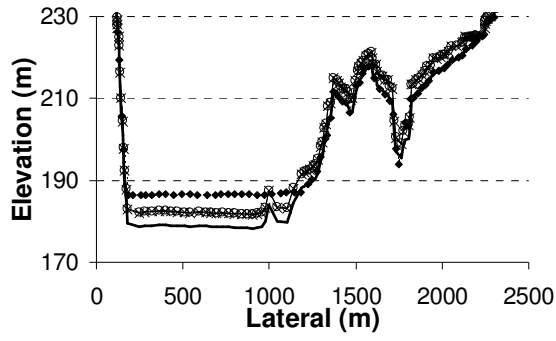
(q) 14.0 km

(r) 11.4 km

(s) 7.7 km

(t) 4.6 km

(u) 2.4 km

(v) 1.0 km

Figure B.3 Continued
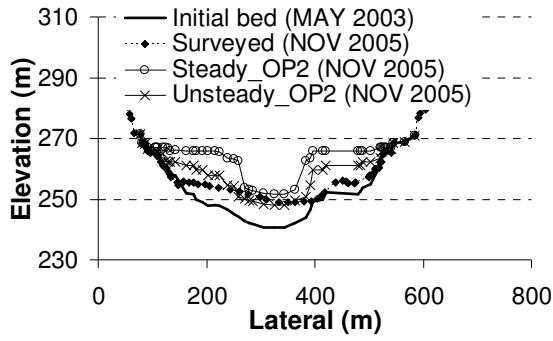
133

(a) 101.6 km above the Xiaolangdi Dam
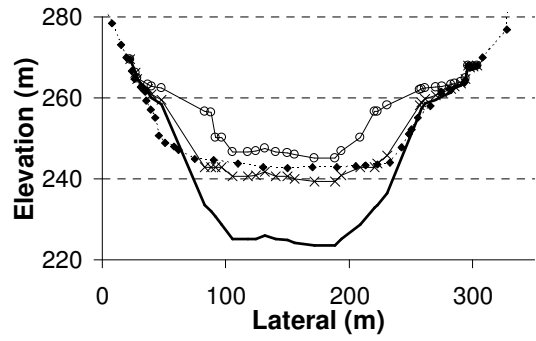
(b) 88.5 km
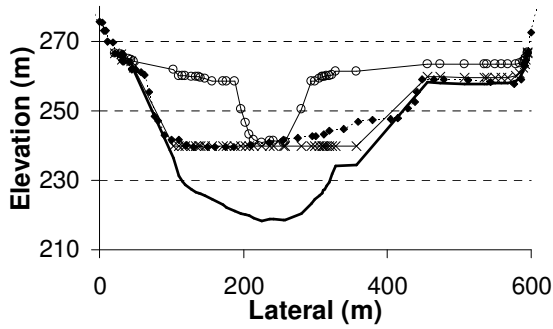
(c) 80.2 km
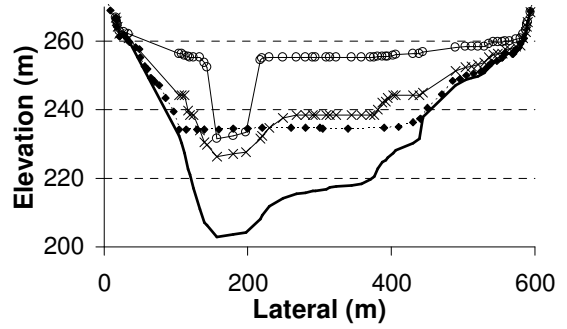
(d) 72.1 km
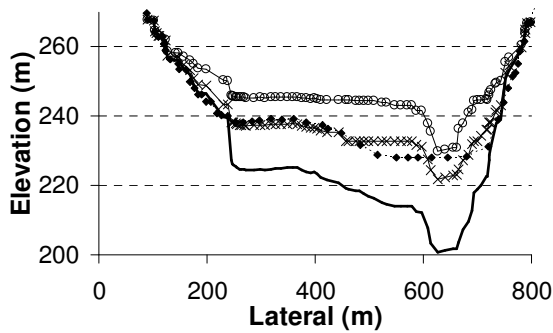
(e) 64.8 km
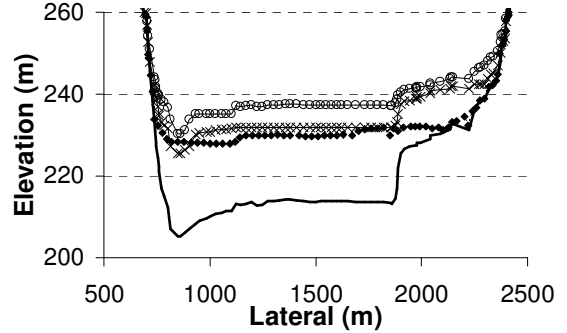
(f) 57.0 km
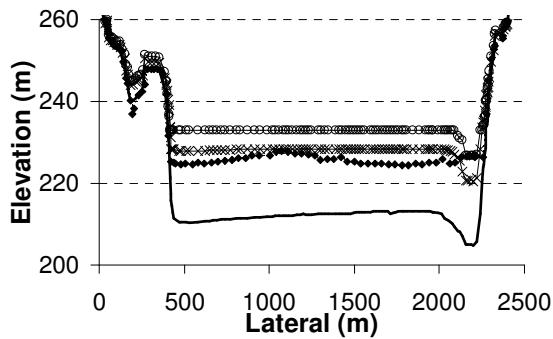
(g) 55.0 km
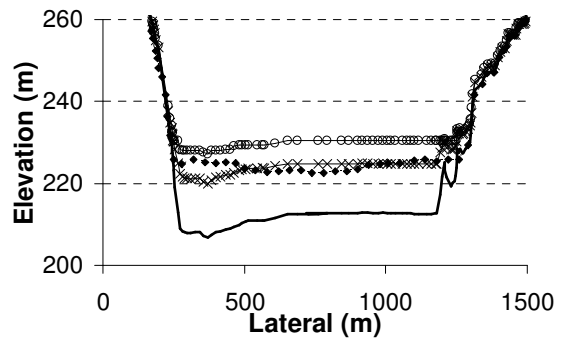
(h) 53.4 km

Figure B.4 Comparison of measurement and GSTARS4 simulation (Steady_OP2 and Unsteady_OP2), in November 2005
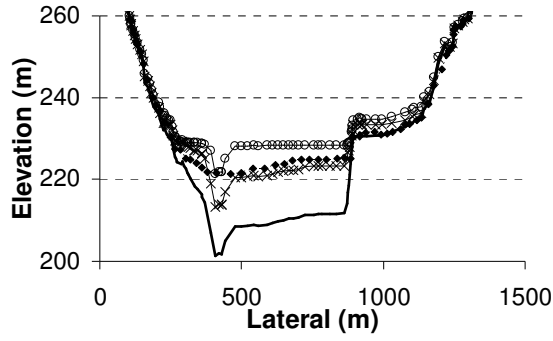
(i) 50.2 km
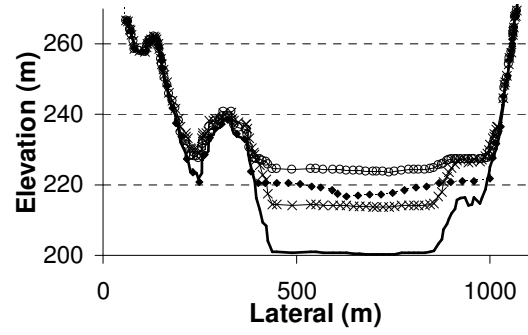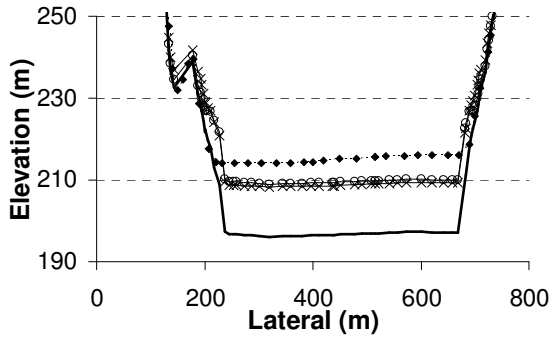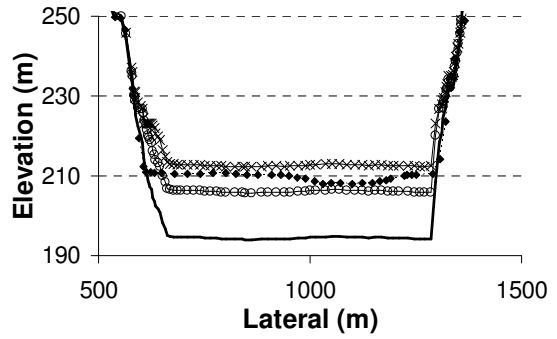
(j) 43.0 km
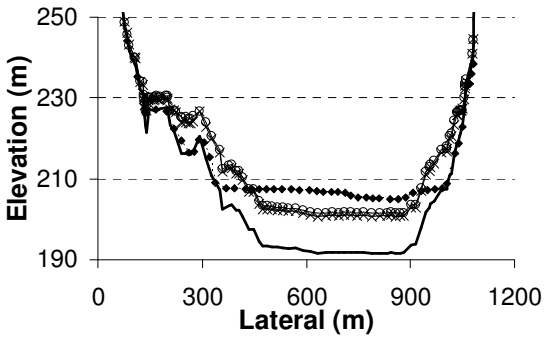
(k) 39.5 km
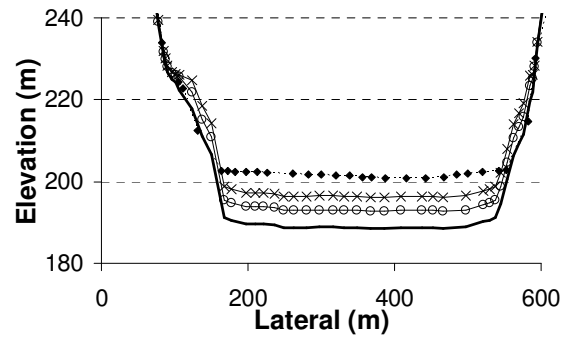
(l) 36.3 km
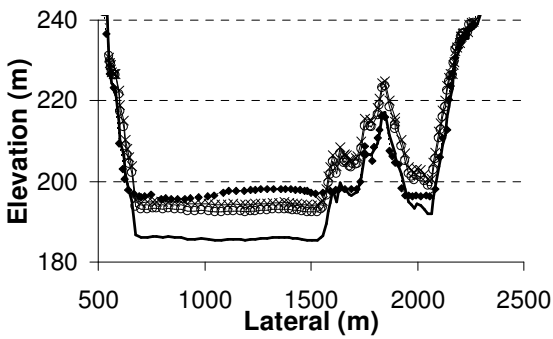
(m) 33.5 km
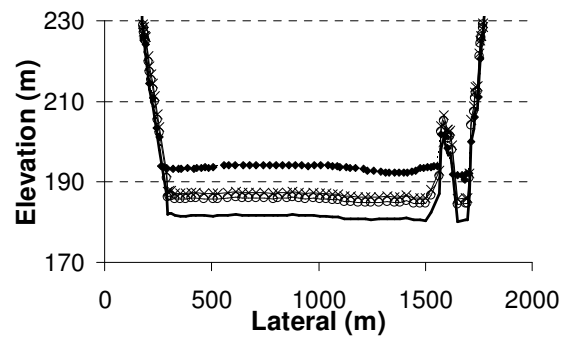
(n) 27.2 km

(o) 22.1 km

(p) 18.7 km

Figure B.4 Continued
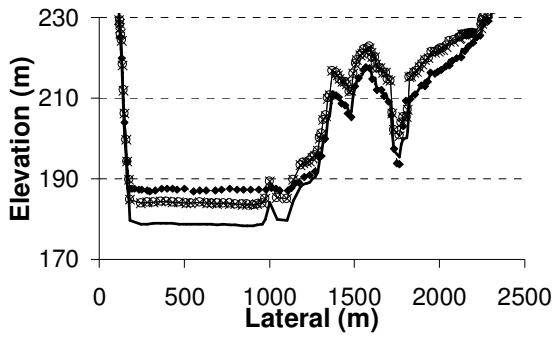
(q) 14.0 km
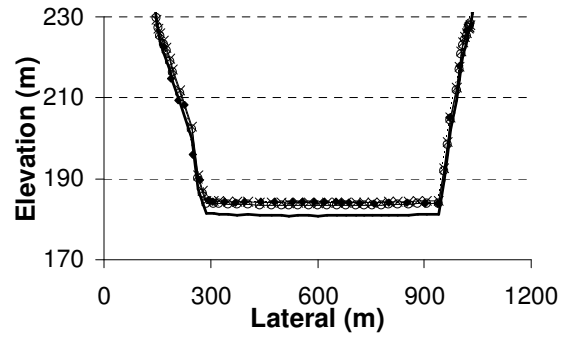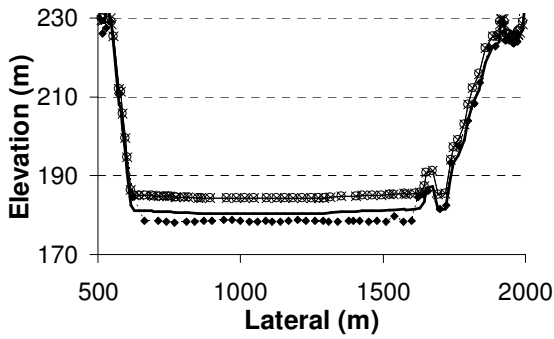
(r) 11.4 km

(s) 7.7 km
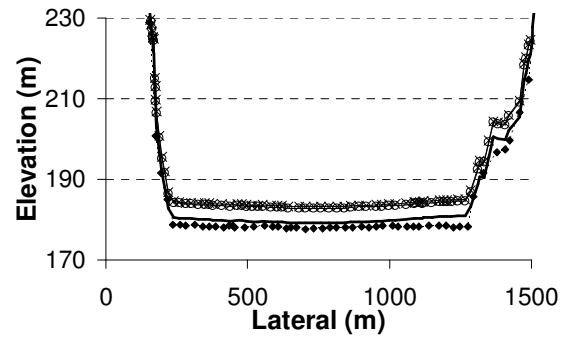
(t) 4.6 km
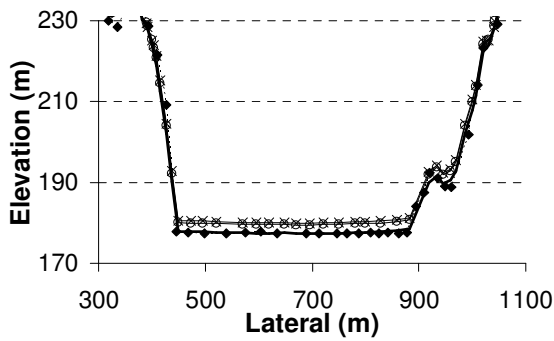
(u) 2.4 km
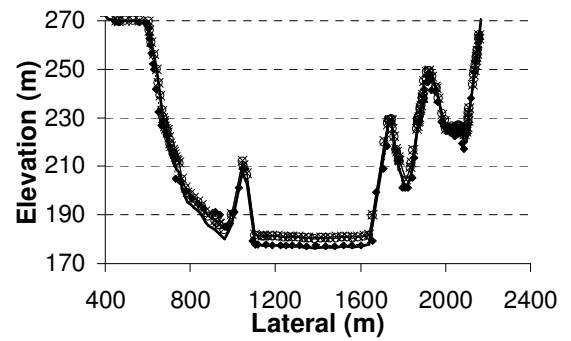
(v) 1.0 km

Figure B.4 Continued

136
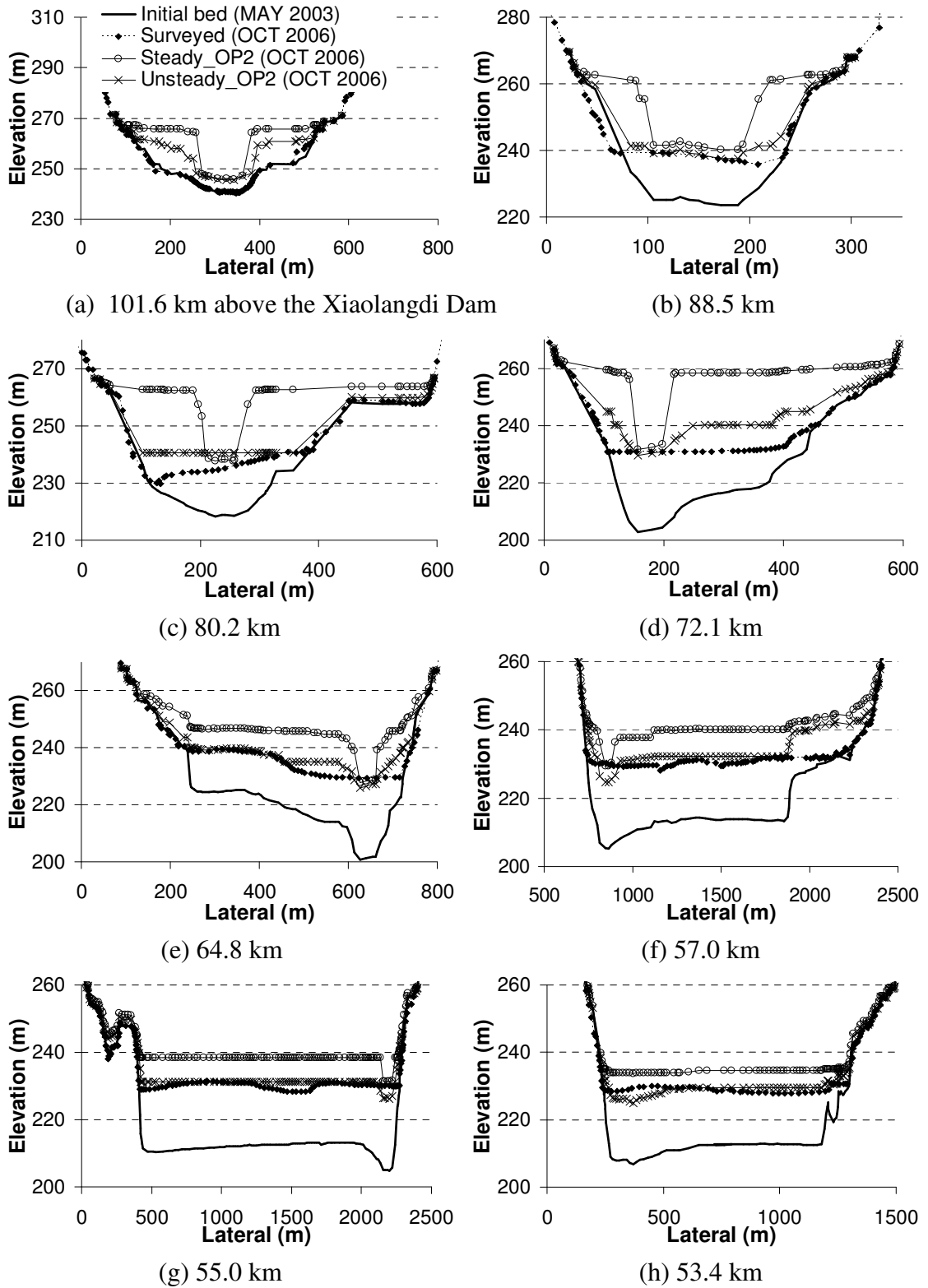
Figure B.5 Comparison of measurement and GSTARS4 simulation (Steady_OP2 and Unsteady_OP2), in October 2006
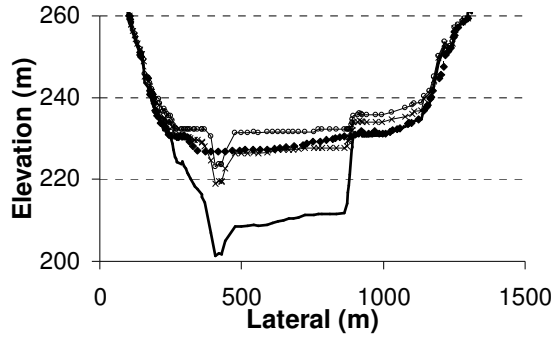
(i) 50.2 km
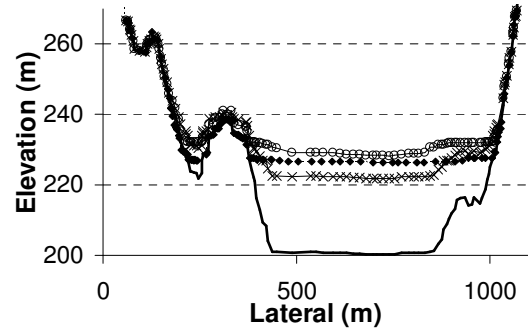
(j) 43.0 km
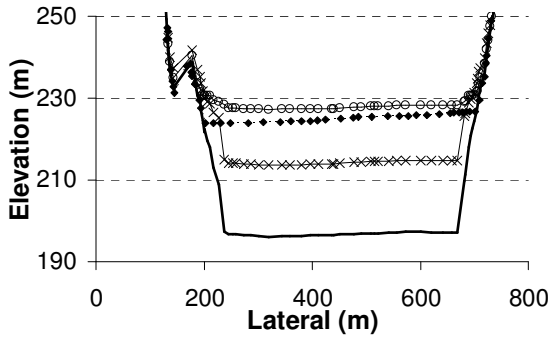
(k) 39.5 km
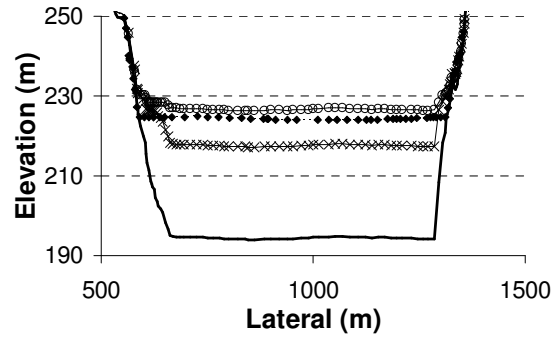
(l) 36.3 km
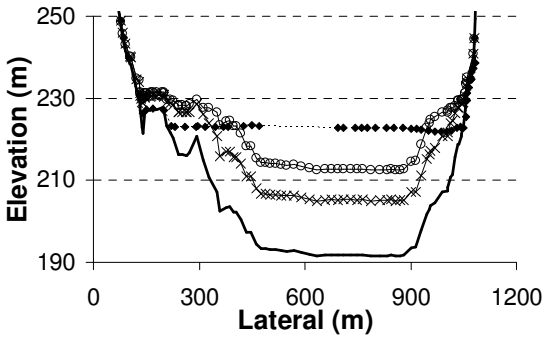
(m) 33.5 km
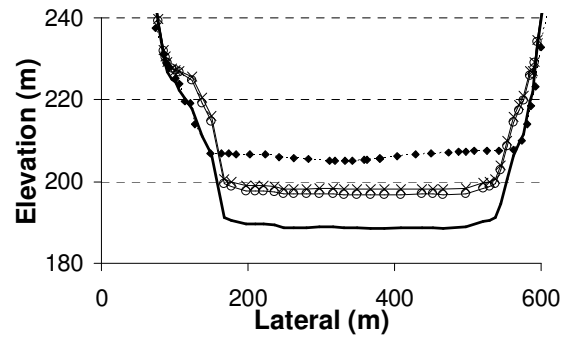
(n) 27.2 km
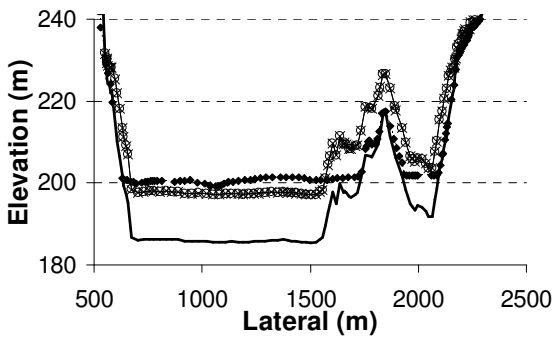
(o) 22.1 km
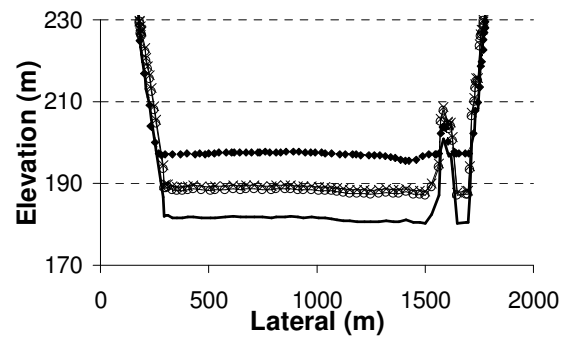
(p) 18.7 km

Figure B.5 Continued

138
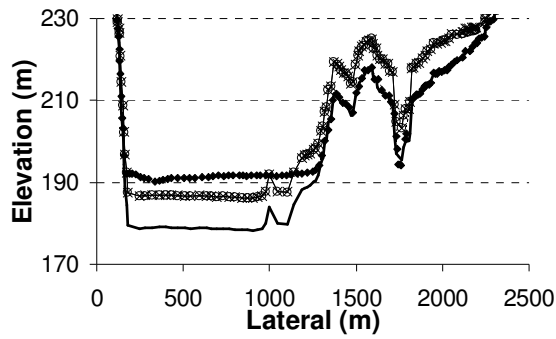
(q) 14.0 km
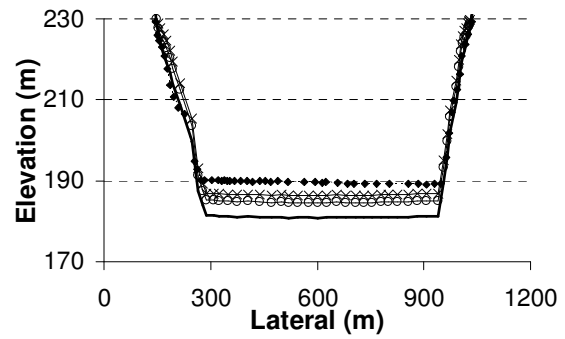
(r) 11.4 km
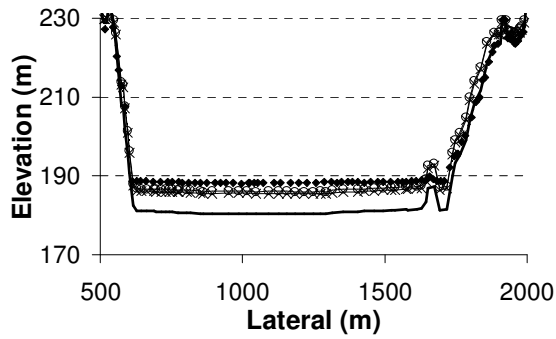
(s) 7.7 km
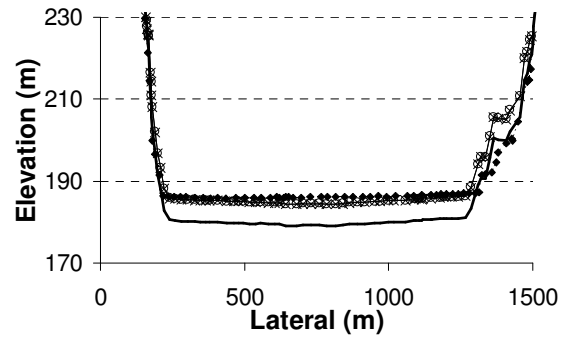
(t) 4.6 km
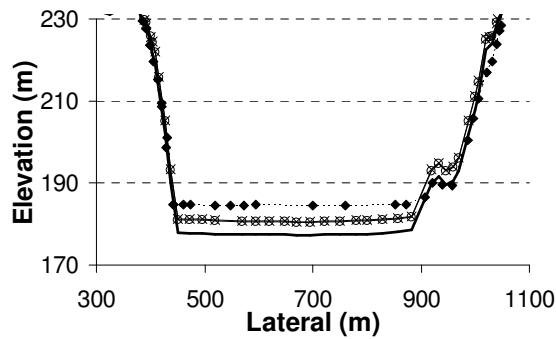
(u) 2.4 km

(v) 1.0 km

Figure B.5 Continued

139